

Chulalongkorn University

Chula Digital Collections

Chulalongkorn University Theses and Dissertations (Chula ETD)

2020

Patient-specific organ dose calculated by dose tracking software based on monte carlo simulation in pediatric abdominal CT

Yuparak Innan
Faculty of Medicine

Follow this and additional works at: <https://digital.car.chula.ac.th/chulaetd>



Part of the [Radiation Medicine Commons](#), and the [Radiology Commons](#)

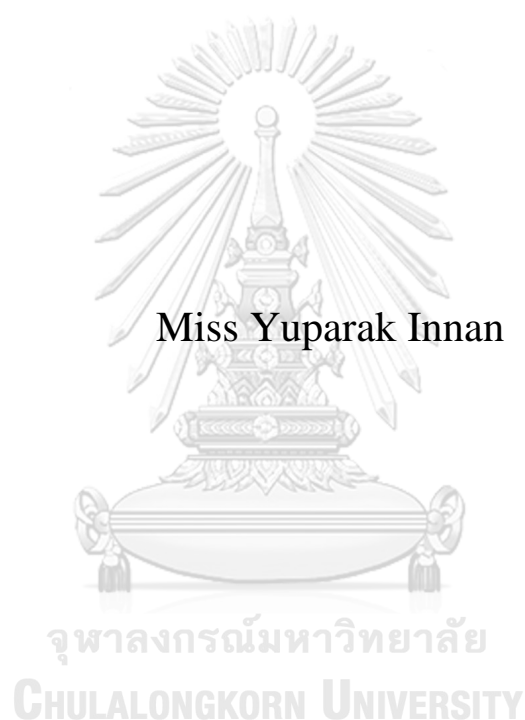
Recommended Citation

Innan, Yuparak, "Patient-specific organ dose calculated by dose tracking software based on monte carlo simulation in pediatric abdominal CT" (2020). *Chulalongkorn University Theses and Dissertations (Chula ETD)*. 246.

<https://digital.car.chula.ac.th/chulaetd/246>

This Thesis is brought to you for free and open access by Chula Digital Collections. It has been accepted for inclusion in Chulalongkorn University Theses and Dissertations (Chula ETD) by an authorized administrator of Chula Digital Collections. For more information, please contact ChulaDC@car.chula.ac.th.

Patient-specific organ dose calculated by dose tracking software
based on Monte Carlo simulation in pediatric abdominal CT



A Thesis Submitted in Partial Fulfillment of the Requirements
for the Degree of Master of Science in Medical Physics
Department of Radiology
FACULTY OF MEDICINE
Chulalongkorn University
Academic Year 2020
Copyright of Chulalongkorn University

การคำนวณปริมาณรังสีจำเพาะที่อวัยวะด้วยวิธีมอนติคาร์โลจากโปรแกรมติดตามปริมาณรังสี
ในการตรวจเอกซเรย์คอมพิวเตอร์ช่องท้องของผู้ป่วยเด็ก



น.ส.ยุภารักษ์ อินแนน

วิทยานิพนธ์นี้เป็นส่วนหนึ่งของการศึกษาตามหลักสูตรปริญญาวิทยาศาสตรมหาบัณฑิต
สาขาวิชาฟิสิกส์การแพทย์ ภาควิชารังสีวิทยา
คณะแพทยศาสตร์ จุฬาลงกรณ์มหาวิทยาลัย
ปีการศึกษา 2563
ลิขสิทธิ์ของจุฬาลงกรณ์มหาวิทยาลัย

Thesis Title	Patient-specific organ dose calculated by dose tracking software based on Monte Carlo simulation in pediatric abdominal CT
By	Miss Yuparak Innan
Field of Study	Medical Physics
Thesis Advisor	Assistant Professor KITIWAT KHAMWAN, Ph.D.

Accepted by the FACULTY OF MEDICINE, Chulalongkorn University in
Partial Fulfillment of the Requirement for the Master of Science

..... Dean of the FACULTY OF
MEDICINE
(Professor SUTTIPONG WACHARASINDHU, M.D.)

THESIS COMMITTEE

..... Chairman
(Associate Professor ANCHALI KRISANACHINDA,
Ph.D.)

..... Thesis Advisor
(Assistant Professor KITIWAT KHAMWAN, Ph.D.)

..... External Examiner
(Professor Kosuke Matsubara, Ph.D.)



จุฬาลงกรณ์มหาวิทยาลัย
CHULALONGKORN UNIVERSITY

ยุทธักษ์ อินเนน : การคำนวณปริมาณรังสีจำเพาะที่อวัยวะด้วยวิธีมอนติคาร์โลจากโปรแกรมติดตามปริมาณรังสี ในการตรวจเอกซเรย์คอมพิวเตอร์ช่องท้องของผู้ป่วยเด็ก.
(Patient-specific organ dose calculated by dose tracking software based on Monte Carlo simulation in pediatric abdominal CT) อ.ที่ปรึกษาหลัก : ผศ. ดร.กิตติวัฒน์ คำวัน

งานวิจัยนี้มีวัตถุประสงค์เพื่อประเมินการคำนวณปริมาณรังสีจำเพาะที่อวัยวะด้วยวิธีจำลองมอนติคาร์โลจากโปรแกรมติดตามปริมาณรังสีเรดิเมทริกซ์ในการตรวจเอกซเรย์คอมพิวเตอร์ช่องท้องของผู้ป่วยเด็กในโรงพยาบาลพระรามเก้า ตรวจสอบความถูกต้องของปริมาณรังสีจำเพาะบุคคลที่อวัยวะที่คำนวณด้วยโปรแกรมติดตามปริมาณรังสีโดยใช้ชุดวัดรังสีแบบแก้ว โดยใส่เข้าไปในตำแหน่งอวัยวะที่ต้องการตรวจสอบในหุ่นจำลองแอนเดรอสันแนโคแฟนทอม เก็บข้อมูลแบบย้อนหลังในผู้ป่วยเด็กที่ได้รับการตรวจเอกซเรย์คอมพิวเตอร์ช่องท้อง ทั้งหมด 164 การสแกน (78 คน) อายุตั้งแต่ 0 ถึง 15 ปี ซึ่งเป็นผู้ป่วยที่ได้รับการตรวจเอกซเรย์คอมพิวเตอร์แบบสแกนครั้งเดียว ค่าความต่างศักย์หลอดเอกซเรย์ อยู่ระหว่าง 80 ถึง 135 kVp ซึ่งถูกปรับค่าตามขนาดและอายุของผู้ป่วย เวลาหมุนของหลอดเอกซเรย์ 0.35-0.5 วินาที ผู้ป่วยทั้งหมดได้รับการตรวจด้วยเทคนิคการปรับเปลี่ยนปริมาณรังสีแบบอัตโนมัติ ปริมาณรังสีจำเพาะที่อวัยวะ และปริมาณรังสียังผลถูกคำนวณด้วยวิธีมอนติคาร์โลจากโปรแกรมติดตามปริมาณรังสีเรดิเมทริกซ์ โดยการคำนวณได้จากการจับคู่ข้อมูลอายุผู้ป่วยให้เหมาะสมกับหุ่นจำลองคอมพิวเตอร์สไลซ์โคแฟนทอม ค่าประมาณรังสีจำเพาะ SSDE ถูกคำนวณจากขนาดเส้นผ่านศูนย์กลางของผลของตัวผู้ป่วย ความแตกต่างระหว่างปริมาณรังสีจำเพาะที่อวัยวะที่คำนวณโดยใช้ชุดวัดรังสีแบบแก้วและคำนวณด้วยวิธีมอนติคาร์โลจากโปรแกรมติดตามปริมาณรังสี มีค่าตั้งแต่ร้อยละ 8.88 ถึงร้อยละ 51.85 ค่าเฉลี่ยปริมาณรังสีจำเพาะที่อวัยวะที่มีค่าสูงที่สุด 5 อันดับแรก ได้แก่ ไต กระเพาะอาหาร กระเพาะปัสสาวะ ส่วนบนของลำไส้ใหญ่ และม้าม ในกลุ่มผู้ป่วยอายุ 15 ปี มีค่าเท่ากับ 18.44, 17.07, 16.74, 16.47 และ 16.14 มิลลิเกรย์ ตามลำดับ ค่าเฉลี่ยปริมาณรังสียังผลในเด็กแรกเกิด 1, 5, 10 และ 15 ปี เท่ากับ 2.24, 3.23, 4.05 และ 8.46 มิลลิซีเวิร์ต ตามลำดับ ค่าเฉลี่ยค่าประมาณรังสีจำเพาะขนาด SSDE เท่ากับ 2.72, 4.52, 6.15, 2.28 และ 14.21 มิลลิเกรย์ ตามลำดับ งานวิจัยนี้สรุปได้ว่า ค่าเฉลี่ยปริมาณรังสีจำเพาะที่อวัยวะและค่าปริมาณรังสียังผลในกลุ่มผู้ป่วยเด็กสามารถประเมินได้อย่างมีประสิทธิภาพโดยใช้โปรแกรมติดตามปริมาณรังสี ค่าปริมาณรังสียังผล และค่า SSDE ขึ้นอยู่กับน้ำหนักตัวของผู้ป่วยมากกว่าอายุของผู้ป่วย



สาขาวิชา ฟิสิกส์การแพทย์

ปีการศึกษา 2563

ลายมือชื่อ

นิติ

ลายมือชื่อ อ.ที่ปรึกษา

หลัก

6270015730 : MAJOR MEDICAL PHYSICS

KEYWORD: DOSE TRACKING SOFTWARE MONTE CARLO SIMULATION
EFFECTIVE DOSE (ED) SIZE -SPECIFIC DOSE ESTIMATES (SSDE)
ORGAN DOSES

Yuparak Innan : Patient-specific organ dose calculated by dose tracking software based on Monte Carlo simulation in pediatric abdominal CT. Advisor: Asst. Prof. KITIWAT KHAMWAN, Ph.D.

This study aimed to determine the patient-specific organ doses using Radimetrics dose tracking software in pediatric abdominal CT at Praram9 Hospital. The organ doses were measured using the anthropomorphic Rando phantom inserted with radiophotoluminescent glass dosimeters (RPLGDs) to verify the organ doses calculated by Radimetrics program. The retrospective data were collected from pediatric abdominal CT 164 studies (78 patients), age range 0-15 years-old, who underwent single phase abdominal CT at Praram9 Hospital. The tube voltages ranged between 80 and 135 kVp were adjusted according to the size and age of patients, and rotation time 0.35-0.5 sec. All patients were acquired using the automatic exposure control (AEC) protocol. The organ and effective doses (ED) calculations were calculated based on the Monte Carlo simulation internally determined by Radimetrics in accordance with patient age derived from stylized computational phantom models. The size-specific dose estimates (SSDE) were calculated based on the effective diameter method. The %difference of the organ doses compared between glass dosimeters and Radimetrics ranged from 8.88-51.58%. Five highest average organ doses were found in kidneys, stomach, urinary bladder, upper large intestine, and spleen for 15-yr patients, with the values of 18.44, 17.07, 16.74, 16.47 and 16.14 mGy, respectively. The average ED for abdominal CT in newborn, 1, 5, 10 and 15-yr were 2.24, 3.23, 4.05, 4.46 and 8.46 mSv, respectively. Average SSDE were 2.72, 4.52, 6.15, 2.28 and 14.21 mGy, respectively. In conclusion, patient-specific organ, and effective doses from 0 through 15-years-old can be determined effectively using dose tracking software. As the various sizes of pediatric patients, the patient ED and SSDE were correlated with patient's body weight rather than the patient age.

จุฬาลงกรณ์มหาวิทยาลัย
CHULALONGKORN UNIVERSITY

Field of Study: Medical Physics
Academic Year: 2020

Student's Signature
Advisor's Signature

ACKNOWLEDGEMENTS

I would like to thankfulness and deepest appreciation to my advisor Asst. Prof. Kitiwat Khmawan, Ph.D. Division of Nuclear Medicine, Department of Radiology, Faculty of Medicine, Chulalongkorn University, Bangkok, Thailand, for his invaluable, helpful, comments, suggestion, constructive direction, motivation and polishing of the thesis writing to improve English expression.

I would like to greatly grateful to Associate Professor Anchali Krisanachinda, Ph.D., Department of Radiology, Faculty of Medicine, Chulalongkorn University, Chairman of thesis defense for her kind suggestion, invaluable advice, constructive comments, and support in equipment in this research. Deeply thanks Professor Kosuke Matsubara, Ph.D., Kanazawa University, Japan, the external examiners of thesis defense for his invaluable suggestion and constructive comments in this research.

I would like to express my thankfulness to Associate Professor Sivalee Suriyapee, Chief Physicist and Lecturer Sornjarod Oonsiri, Ph.D., Physicist at Division of Radiation Oncology, Department of Radiology, Faculty of Medicine, Chulalongkorn University, for their invaluable guidance, constructive direction, sharing useful experience, and support in radiation dose measurement equipment in this research.

I would like extremely grateful all to Board of Directors of at Praram9 Hospital for their kind helpful, contributing and assistance in collecting data and doing research.

I would like to thank Mr. Jaroonroj Wongnil, Imaging Department manager and Ms. Hataipat Jantawong, Imaging-CT and MRI manager, Bumrungrad International Hospital, Bangkok, Thailand for their guidance on CT scanner, kindly support, and useful advice for quality control.

I am greatly grateful for all teachers, lecturers and staff at Master of Science Program in Medical Imaging, Faculty of Medicine, Chulalongkorn University for their suggestions and teaching during Medical Imaging. Finally, I am heartfelt thankful to my family for their invaluable encouragement, entirely care, financial support and understanding during the entire course of the study.

Yuparak Innan

TABLE OF CONTENTS

	Page
ABSTRACT (THAI)	iii
ABSTRACT (ENGLISH).....	iv
ACKNOWLEDGEMENTS.....	v
TABLE OF CONTENTS.....	vi
LIST OF TABLES.....	ix
LIST OF FIGURES	xii
LIST OF ABBREVIATIONS.....	xv
CHAPTER I INTRODUCTION.....	1
1.1 Background and Rationale.....	1
1.2 Research objective	2
1.3 Definitions	3
CHAPTER II REVIEW OF RELATED LITERATURE	4
2.1 Theory.....	4
2.1.1 Overview of Computed Tomography.....	4
2.1.2 Principle of CT.....	4
2.1.3 Components of Computed Tomography Scanner	7
2.1.4 The dosimetry in computed tomography.....	14
2.1.5 Abdominal computed tomography	18
2.1.6 Radio-photoluminescence Glass Dosimeter (RPLGD).....	20
2.2 Review of related literature	21
CHAPTER III RESEARCH METHODOLOGY	28
3.1 Research design	28
3.2 Research design model	28
3.3 Conceptual framework.....	29
3.4 Research question	29

3.5 Key words	29
3.6 Materials	29
3.6.1 Materials	29
3.6.2 Materials for QC.....	33
3.7 Methods	38
3.8 Outcome measurements	44
3.9 Statistical analysis.....	44
3.10 Sample size determination	44
3.11 Target population.....	45
3.11.1 Inclusion criteria.....	45
3.11.2 Exclusion criteria.....	45
3.12 Ethic consideration	45
CHAPTER V RESULTS	46
4.1 Quality control of the multidetector computed tomography canner: Toshiba Aquilion ONE and Siemens Somatom Sensation	46
4.2 Verification of organ doses: Radimetrics Program.....	46
4.3 Patient data and radiation dose determined from abdominal CT examination..	49
4.3.1 Patient characteristics of abdominal CT examination	49
4.3.2 Patient radiation dose	50
4.4 Factors affecting organ doses in pediatric patients.....	59
4.4.1 Correlation between age and patient-specific organ dose	59
4.4.2 Correlation between body weight and patient-specific organ dose.....	60
4.4.3 Correlation between gender and patient-specific organ dose.....	64
4.5 Local diagnostic reference level (LDRL) for pediatrics abdominal CT at Praram9 Hospital	66
CHAPTER IV DISCUSSION AND CONCLUSIONS	68
5.1 Discussion.....	68
5.2 Conclusions.....	77
REFERENCES	78
APPENDICES	81

Appendix A: Data record form	82
Appendix B: Quality Control of MDCT system.....	86
Appendix C: Quality Control of MDCT system.....	99
Appendix D: The Approval of Institutional Review Board.....	113
VITA	118



LIST OF TABLES

Table	Page
2.1 Normalised Values of Effective Dose per Dose Length Product for Adults Over Various Regions.....	16
2.2 Organ conversion factors for selected radiography procedures.....	18
2.3 f_{size} determination for patients with different BMI, LAT and AP dimensions and effective diameter.....	21
2.4 Comparison of major organ doses for the organs completely included in the abdomen/pelvis scan as derived by empirical correlation with patient abdominal circumference (Turner et al.)	25
2.5 Comparison of effective doses normalized to dose length product (DLP) (mSv/mGy cm) as given by Shrimpton et al. and as calculated using the dose matrix of the present study under either ICRP 60 or ICRP 103 tissue weighting factors.....	25
3.1 Specification of CT Toshiba Aquilion ONE 320 Detector.....	30
3.2 Specification of CT Siemens SOMATOM Sensation 64 Detector.....	31
3.3 Specification of DCT10-MM.....	35
3.4 Specifications of glass dosimeter element.....	37
3.5 Scanning parameters technique of Siemens Somatom Sensation.....	42
3.6 Scanning parameters technique of Toshiba Aquilion ONE.....	42
3.7 Patient-phantom age and gender mapping.....	42
3.8 Weight grouping for paediatric diagnostic reference levels (DRLs) recommended by the European Guidelines on DRLs for Paediatric Imaging and approximate equivalent ages (EC, 2016).....	44
4.1 Summary reports of CT system performance and physics testing at Radiology Department, Praram9 Hospital.....	46
4.2 Comparison of organ doses between glass dosimeter and Radimetrics (Siemens).	47
4.3 Comparison of organ doses between Glass dosimeter and Radimetrics (Toshiba).....	47
4.4 Patient characteristics of abdominal CT examination.....	49
4.5 Patient characteristics of 112 male patients.....	49
4.6 Patient characteristics of 52 female patients.....	49

Table	Page
4.7 No. of CT Examinations collected in pediatric patients 5 groups.	50
4.8 Summary of CT scanning technique and patient effective dose.	51
4.9 Effective doses to pediatric abdominal CT from two CT scanners.	51
4.10 Organ doses to pediatric abdominal CT from two CT scanners.	52
4.11 Effective doses to pediatric for lower abdominal CT, Siemens.	53
4.12 Organ doses to pediatric for lower abdominal CT, Siemens.	54
4.13 Effective doses to pediatric lower abdominal CT TOSHIBA.	55
4.14 Organ doses to pediatric lower abdominal CT TOSHIBA.	55
4.15 Effective doses to pediatric whole abdominal CT TOSHIBA.	56
4.16 Organ doses to pediatric whole abdominal CT TOSHIBA.	56
4.17 Effective doses to pediatric whole abdominal CT Siemens.	57
4.18 Organ doses to pediatric whole abdominal CT Siemens.	57
4.19 Median and 75 th percentile of CTDI _{vol} and DLP of various age groups.	67
5.1 Mean and 75 th percentile of CTDI _{vol} compared with national data by age group for abdominal CT scans.	70
5.2 Mean and 75 th percentile of DLP compared with national data by age group for abdominal CT scans.	71
A 1 Data collection sheet for patient information.	82
A 2 Data collection volume pediatric CT Examinations by age.	82
A 3 Data collection sheet for abdomen CT scan.	83
A 4 Data collection for patient specific organ dose of pediatric abdominal CT data form.	84
A 5 Effective dose (mSv) of pediatric CT examinations by age and gender.	85
A 6 Data collection dose indexes by age group for abdominal CT scans data form.	85
A 7 Median and 75th percentile of CTDI _{vol} and DLP of various age groups at Praram 9 Hospital data form.	85
B 1 Alignment of table to gantry.	87
B 2 Table increment Accuracy.	88
B 3 Position dependence and S/N ratio of C.T. numbers.	89
B 4 Reproducibility of C.T. numbers.	89
B 5 mAs linearity.	90

Table	Page
B 6 Linearity of CT Number.....	91
B 7 Slice thickness accuracy.....	92
B 8 High contrast resolution.....	93
B 9 Low contrast resolution.....	93
B 10 Image uniformity.....	94
B 11 The measured CTDI ₁₀₀ in air head protocols.....	95
B 12 The measured CTDI ₁₀₀ in air for body protocol.....	96
B 13 The measured CTDI ₁₀₀ at each position of head phantom.....	97
B 14 The measured CTDI ₁₀₀ at each position of body phantom.....	97
B 15 CTDI _{vol} displayed on monitor and calculated CTDI _w using head techniques.....	98
B 16 CTDI _{vol} displayed on monitor and calculated CTDI _w using body techniques.....	98
C 1 Alignment of table to gantry.....	100
C 2 Table increment Accuracy.....	101
C 3 Position dependence and S/N ratio of C.T. numbers.....	102
C 4 Reproducibility of C.T. numbers.....	103
C 5 mAs linearity.....	103
C 6 Linearity of CT Number.....	104
C 7 Slice thickness accuracy.....	105
C 8 High contrast resolution.....	106
C 9 Low contrast resolution.....	107
C 10 Image uniformity.....	108
C 11 The measured CTDI ₁₀₀ in air for head protocols.....	109
C 12 The measured CTDI ₁₀₀ in air for body protocol.....	109
C 13 The measured CTDI ₁₀₀ at each position of head phantom.....	111
C 14 The measured CTDI ₁₀₀ at each position of body phantom.....	111
C 15 CTDI _{vol} displayed on monitor and calculated CTDI _w using head techniques.....	112
C 16 CTDI _{vol} displayed on monitor and calculated CTDI _w using body techniques.....	112

LIST OF FIGURES

Figure	Page
2.1 CT image acquisition.....	5
2.2 X-ray beam is transmitted through the patient; different tissues are encountered with different linear attenuation coefficients.....	6
2.3 Volume elements (voxels) of CT.....	6
2.4 The display is defined using window level (WL) as CT number of mid-grey and window width (WW).....	7
2.5 A. Basic system components of CT system B. Electrical power supply.....	8
2.6 The X-ray tube and generator.....	8
2.7 Narrow fan beam and multi-slice scanners.....	9
2.8 Schematic diagram of a bowtie filter and a flat filter.....	9
2.9 CT detectors are curved in the axial plane (x-y plane), and rectangular along the longitudinal axis (z-axis).....	10
2.10 A. The detector arrays are mounted on electronics module B. A photograph of a detector module with electronics from a commercial	10
2.11 Multi-detector arrangements.....	11
2.12 Simple backprojection.....	12
2.13 Filtered backprojection and Simple backprojection.....	13
2.14 Iterative (statistical) reconstructions	14
2.15 Radiation dose profile.....	15
2.16 The MIRD phantom.....	19
2.17 Abdominal computed tomography with contrast enhancement.....	20
2.18 Radio-photoluminescence Glass Dosimeter (RPLGD).....	21
2.19 Exposure dose data using the SSDE in children. Effective dose calculated by simulation is indicated by box plot.....	22
2.20 Comparison of chest absolute organ dosimetry	23
2.23 Graph shows comparison of dose to 8 organs by chest CT scans with method of this study and methods from literature.....	27
2.24 Graph shows comparison of dose to 17 organs by abdomen and pelvis CT scans with method of this study and methods from literature.	27
3.1 Research design model.....	28
3.2 Conceptual framework.....	29

Figure	Page
3.3 CT Toshiba Aquilion ONE, 320-row detector.....	29
3.4 CT Siemens SOMATOM Sensation 64 Detector.....	31
3.5 SYNAPSE, PACS workstation.....	32
3.6 The stylized phantom and the scan region (highlighted in blue). The over-ranging for helical scan is indicated as the yellow stripes on the edges of the scan region.....	33
3.7 Monte Carlo-based patient dose tracking program (Radimetrics).....	33
3.8 Polymethyl methacrylate (PMMA) CTDI phantoms.....	34
3.9 Ionization chamber DCT10-MM.....	34
3.10 Anthropomorphic Rando phantoms.....	36
3.11 Radiophotoluminescent glass dosimeter (RPLGD).....	36
3.12 Laboratory oven (Carbolite Gero).....	37
3.13 Glass dosimeter reader (FGD-1000).....	38
3.14 Position chamber in stand so beyond couch.....	39
3.15 Positioning of the cylindrical PMMA phantoms for CTDI measurement.....	40
3.16 Catphan® 700 phantom.....	40
3.17 The anthropomorphic Rando phantom inserted with radiophoto luminescent glass dosimeters (RPLGDs).....	41
4.1 Comparison of organ doses between glass dosimeter and Radimetrics (Siemens)....	48
4.2 Comparison of organ doses between glass dosimeter and Radimetrics (Toshiba)....	48
4.3 No. of CT Examinations collected in pediatric patients.....	50
4.4 Nine highest organ doses found for pediatric abdominal CT at Praram9 Hospital....	53
4.5 The highest organ doses for pediatric abdominal CT.....	59
4.6 Correlation between CTDIvol and body weight for CT whole abdomen.....	60
4.7 Correlation between CTDIvol and patient age for CT whole abdomen.....	60
4.8 Correlation between CTDIvol and body weight for CT lower abdomen.....	61
4.9 Correlation between CTDIvol and patient age for CT lower abdomen.....	61
4.10 Correlation between SSDE and body weight for CT whole abdomen.....	62
4.11 Correlation between SSDE and patient age for CT whole abdomen.....	62
4.12 Correlation between SSDE and body weight for CT lower abdomen.....	63
4.13 Correlation between SSDE and patient age for CT lower abdomen.....	63
4.14 Nine organ doses for 0-1 yrs pediatric abdominal CT.....	64
4.15 Nine organ doses for 5 yrs pediatric abdominal CT.....	64
4.16 Nine organ doses for 10 yrs pediatric abdominal CT.....	65

Figure	Page
4.17 Nine organ doses for 15 yrs pediatric abdominal CT.	65
4.18 Comparisons of median and 75th percentile of CTDI _{vol} for various pediatric age groups.....	66
4.19 Comparisons of median and 75th percentile of DLP for various pediatric age groups.....	66
5.1 Organ dose (mGy) compared with previous published data in male pediatric patients 15y.....	72
5.2 Organ dose (mGy) compared with previous published data in female pediatric patients 15y.....	72
5.3 Organ dose (mGy) compared with previous published data in male pediatric patients.....	73
5.4 Organ dose (mGy) compared with previous published data in female pediatric patients.....	74
B 1 Localization light accuracy setting on the tape measurement.....	87
B 2 Draw region of interest for each of the positions 1 through 5.....	88
B 3 Draw region of interest of the positions 5.....	89
B 4 The relationship of mGy and mAs.....	90
B 5 Low contrast detectability.....	93
B 6 Image Uniformity	94
B 7 CTDI ₁₀₀ in air, head protocol.....	95
B 8 CTDI ₁₀₀ in air, body protocol.....	96
B 9 CTDI ₁₀₀ measurement PMMA phantoms	97
C 1 Localization light accuracy setting on the tape measurement.....	100
C 2 Draw region of interest for each of the positions 1 through 5.....	101
C 3 Draw region of interest of the positions 5.....	102
C 4 The relationship of mGy and mAs.....	104
C 5 Low contrast detectability.....	107
C 6 Image Uniformity.....	108
C 7 CTDI ₁₀₀ in air, head protocol.....	109
C 8 CTDI ₁₀₀ in air, body protocol.....	110
C 9 CTDI ₁₀₀ measurement in PMMA phantoms.....	111

LIST OF ABBREVIATIONS

Abbreviation	Terms
AAPM	American Association of Physicist in Medicine
AEC	Automatic exposure control
AP	Anterior posterior
CT	Computed tomography
cm	centimeter
cm ³	Cubic centimeter
CTDI ₁₀₀	CT air kerma index measure free in air integrated over 100 mm
CTDI	Computed tomography dose index
CTDI _{vol}	Volume computed tomography dose index
CTDI _w	Weighted computed tomography dose index
DLP	Dose-Length Product
ED	Effective dose
FOV	Field of view
HU	Hounsfield unit
IAEA	International Atomic Energy Agency
IC	Ionization chamber
ICRP	International Commission of Radiological Protection
Kg	Kilo gram
kVp	Kilo voltage peak
kW	Kilo watt
LAT	lateral
Lp/cm	Line pairs per centimeter
mA	Milliampere
mAs	Milliampere-second
MDCT	Multi-detector computed tomography.
MC	Monte Carlo simulation
μGy	MicroGray

mGy	MilliGray
mGy.cm	Milligray-centimeter
mm	Millimeter
mSv	MilliSievert
NRPB	National Radiological Protection Board
PMMA	Polymethylmethacrylate
PACS	Picture archiving and communications system
QA	Quality assurance
REP	Radimetrics™ Enterprise Platform
ROI	Region of interest
RIS	Radiology information system
ROI	Region of interest
RPLGD	Radiophotoluminescent glass dosimeter
S	Second
SD	Standard deviation
SSDE	size-specific dose estimate
WED	water equivalent diameter
WW	Window width
WL	Window level
TLD	Thermoluminescent dosimeter

CHAPTER I

INTRODUCTION

1.1 Background and Rationale

Computed tomography (CT) is mainly used in advanced imaging for diagnosis as the CT scan can be performed rapidly. CT scans in pediatrics have increased considerably in clinical, resulting increased the probability of stochastic effect of cancer induction in the future for pediatric patients (1). The assessment approach of radiation risk in CT led to the development of strategies to prevent and evaluate the excessive radiation exposure in children. The patient dose in CT examination depends on the amount of radiation output by the scanner and patient size. Presently, all CT scanners are required to report radiation dose at least by two values: volumetric CT dose index ($CTDI_{vol}$), and dose-length product (DLP). $CTDI_{vol}$ is a radiation dose measurement in a standardized polymethyl methacrylate (PMMA) phantom with a diameter of either 16 or 32 cm. $CTDI_{vol}$ does not represent real patients' dose or organ dose, and can be underestimated especially in small size patients, such as pediatric patients. In case of pediatric patients, they have radiosensitivity higher than the adult's due to smaller body size, more rapidly growing tissue, and longer potential lifespan to express any radiation-related detriment.

In 2011, the American Association of Physicist in Medicine (AAPM) task group 204 (2) has introduced the concept of size-specific dose estimate (SSDE) which derived from $CTDI_{vol}$ and take into account patient size for obtaining the conversion factors (f_{size}). SSDE is considered the scanning protocol and the effects of the geometric shape of the patient and tissue attenuation on the radiation dose. This provides higher accuracy on radiation dose to the patient. The SSDE can be defined using the equation as follows:

$$SSDE = f_{size} \times CTDI_{vol}, \quad \text{equation 1.1}$$

where f_{size} is a conversion factors (f_{size}) based on the patients' anterior posterior (AP) and lateral (LAT) dimensions, measured from a CT radiograph, to convert the dose applied to the theoretical 16 and 32 cm phantoms to the true size of the patient.

To be practically implemented, ideal patient-specific dosimetry for CT must be accurately and timely for implementation in clinical practice. However, organ dose cannot be measured directly, and the calculation depends on many factors, including the composition and density of the body, the morphology of the patient and the body parts that are exposed to radiation during CT examination (3). The development of a simple approach toward patient-specific CT dosimetry using SSDE to calculate the organ dose was published by Moore et al. (4).

Assessing the amount of radiation in children is therefore important. Currently, there are two mainly approaches for estimating patient's organ dose in CT: Firstly, the empirical dose measurement using the anthropomorphic physical phantoms, and secondly, software dose calculations using the computational phantoms in Monte Carlo simulation.

The use of physical anthropomorphic phantoms inserted with the dosimeter such as TLD (Thermoluminescent dosimeter), MOSFET (Metal Oxide Semiconductor Field Effect Transistor (MOSFET) detectors), or glass dosimeter is a gold standard for the organ dosimetry measurement. However, the radiation dose measurement using anthropomorphic phantoms can be very expensive and limited due to their discrete size including the uncertainty caused by the measurement set up. The use of Monte Carlo (MC) simulation can provide the approximation for individual patient dose measurements similar to the anthropomorphic phantom and has become the gold standard in different dosing techniques. However, patient-specific dosimetry calculated by Monte Carlo technique usually requires high computational efficiency, highly specialized programming skills and time-consuming (4).

Since the increasing concern of radiation dose from CT scans, it is crucial to have a dosimetry tool that offers accurate evaluation of patient-specific organ doses in an automatic manner to efficiently perform the calculation and to accurately analyze the associated effects. Recent efforts have focused on developing Monte Carlo simulation coupled with patient dose tracking software to routinely evaluate patient doses in diagnostic radiology including the CT examination. The patient dose tracking software to calculate the radiation dose for monitoring and reporting of cumulative radiation dose, and to analyze big data for patient safety inspections has also been developed for these purposes. By these software packages, the patient dose can be calculated based on the Monte Carlo simulation that uses the library of computational phantoms and matches patients to a particular phantom based on patient age, weight, or diameter. The software system will automatically extract the scanning data by connecting it to PACS and RIS systems (5). Currently, the patient dose tracking software namely Radimetrics, is one of the commercial dosimetry software packages that widely used worldwide as a gold standard software for monitoring and reporting radiation dose by device or by patient. Therefore, it is of great interest to calculate the patient-specific organ doses from abdominal CT examination in different ages of pediatric patients based on the Monte Carlo method using this dose tracking software as preliminary data to support the CT clinical dosimetry in Thailand and this region.

1.2 Research objective

To determine the patient-specific organ doses using dose tracking software in pediatric abdominal CT at Praram9 Hospital.

1.3 Definitions

Volume CT dose index (CTDI_{vol})	The multiplication of weighted CT Dose Index (CTDI_w) by pitch factor, the unit is mGy and it is used to compare radiation output level between different CT scanners.
Dose Length Product (DLP)	The product of CTDI_{vol} and scan length, the unit mGy.cm, is related to the total ionizing energy imparted to the referenced phantom.
Size-specific dose estimates (SSDEs)	A patient dose estimated from the factors that consider to the patient size and the body composition of different attenuation during CT scan.
Absorbed dose	The energy imparted to matter per unit mass of the irradiated matter (J/kg). The unit of absorbed dose is gray (Gy).
Effective dose	The mean absorbed dose from a uniform whole-body irradiation that results in the same total radiation detriment from the nonuniform partial-body irradiation. The effective dose is calculated as the weighted average of the mean absorbed dose to the various body organs and tissues, where the weighting factor is the radiation detriment for a given organ from a whole-body irradiation as a fraction of the total radiation detriment (Sv).
Dose tracking software:	The software packages in helping to calculate, manage and monitor medical imaging radiation doses for the patient and staff in Radiology Department.

CHAPTER II

REVIEW OF RELATED LITERATURE

2.1 Theory

2.1.1 Overview of Computed Tomography

The computed tomography or CT, refers to a computerized x-ray imaging procedure in which a narrow beam of x-rays is aimed at a patient and quickly rotated around the body, producing signals that are processed by the machine's computer to generate cross-sectional images or "slices" of the body. These slices are called tomographic images and contain more detailed information than conventional x-rays. Once several successive slices are collected by the machine's computer, they can be digitally "stacked" together to form a three-dimensional image of the patient that allows for easier identification and location of basic structures as well as possible tumors or abnormalities (6).

In general terms, the principle of computed tomography consists of measuring the spatial distribution of a physical quantity to be examined from different directions and to compute superposition free images from these data. Every time the x-ray source performs one full rotation, CT computers use complex mathematical techniques to create a 2-D image fragment of the patient. The thickness of the tissue shown in the individual images may vary depending on the CT machine used, but usually in the range of 1-10 mm. When all parts are complete, the images are stored, and the motorized bed will be moving forward little by little in the gantry. The x-ray scanning process is then repeated to create other image parts. This process will continue until the required number of pieces is obtained (7).

2.1.2 Principle of CT

2.1.2.1 X ray projection, attenuation, and acquisition of transmission profiles

The purpose of a computed tomography acquisition is to measure x ray transmission through a patient for many views. Different views are achieved in computed tomography. Primarily by using detectors with hundreds of detector elements along the detector arc (generally 800-900 detector elements), by rotation of the x ray tube around the patient, taking about 1000 angular measurements and by tens or even hundreds of detector rows aligned next to each other along the axis of rotation.

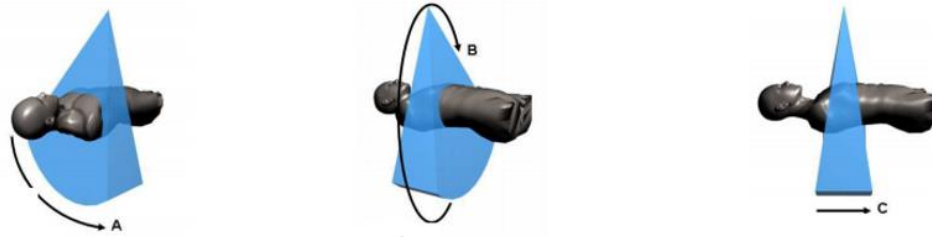


Figure 2.1 CT image acquisition showing the transmission of X-rays through the patient by using a detector row (a), with rotation of the x-ray tube and detector (b) and by multiple detectors (c) (8).

2.1.2.2. Displayed in CT images

The values that are assigned to the pixels in a CT image are associated with the average linear attenuation coefficient μ (m^{-1}) of the tissue represented within that pixel. The linear attenuation coefficient (μ) depends on the composition of the material, the density of the material, and the photon energy as seen in Beer's law:

$$I(x) = I_0 e^{-\mu x} \quad \text{equation 2.1}$$

where $I(x)$ is the intensity of the attenuated X ray beam, I_0 the unattenuated X ray beam, and x the thickness of the material.

Beer's law only describes the attenuation of the primary beam and does not consider the intensity of scattered radiation that is generated. For poly-energetic X ray beams Beer's law should strictly be integrated over all photon energies in the X ray spectrum. In the back projection methodologies developed for CT reconstruction algorithms, this is generally not implemented. Instead, typically a pragmatic solution is to assume where Beer's law can be applied using one value representing the average photon energy of the X ray spectrum. This assumption causes inaccuracies in the reconstruction and leads to the beam hardening artefact. As an X ray beam is transmitted through the patient, different tissues are encountered with different linear attenuation coefficients (Figure 2.2). The intensity of the attenuated X ray beam, transmitted a distance d , can be expressed as:

$$I(d) = I_0 e^{-\int_0^d \mu(x) dx} \quad \text{equation 2.2}$$

Where N is the number of acquire slices per rotation and T is nominal thickness of acquire slice (mm).

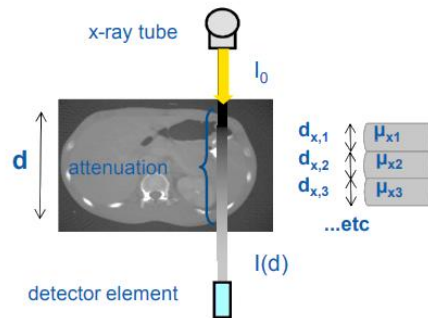


Figure 2.2 X-ray beam is transmitted through the patient; different tissues are encountered with different linear attenuation coefficients (8).

A CT image is composed of a matrix of pixels representing the average linear attenuation co-efficient in the associated volume elements (voxels).

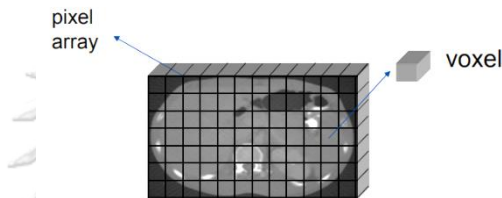


Figure 2.3 volume elements (voxels) of CT

The basic data needed for CT is the intensity of the attenuated and unattenuated X ray beam, respectively $I(d)$ and I_0 , and that this can be measured. Image reconstruction techniques can then be applied to derive the matrix of linear attenuation coefficients, which is the basis of the CT image (8).

In CT, the matrix of reconstructed linear attenuation coefficients (μ_{material}) is transformed into a corresponding matrix of Hounsfield units (HU_{material}), where the HU scale is expressed relative to the linear attenuation coefficient of water at room temperature (μ_{water}):

$$HU_{\text{material}} = \frac{\mu_{\text{material}} - \mu_{\text{water}}}{\mu_{\text{water}}} \times 100 \quad \text{equation 2.3}$$

It can be seen that.

$$HU_{\text{water}} = 0 \text{ as } (\mu_{\text{material}} = \mu_{\text{water}}),$$

$$HU_{\text{air}} = -1000 \text{ as } (\mu_{\text{material}} = 0)$$

$HU = 1$ is associated with 0.1% of the linear attenuation coefficient of water.

Hounsfield units are usually visualized in an eight-bit grey scale offering only 128 grey values. The display is defined using window level (WL) as CT number of mid-grey and window width (WW) as the number of HU from black to white (Figure 2.4).

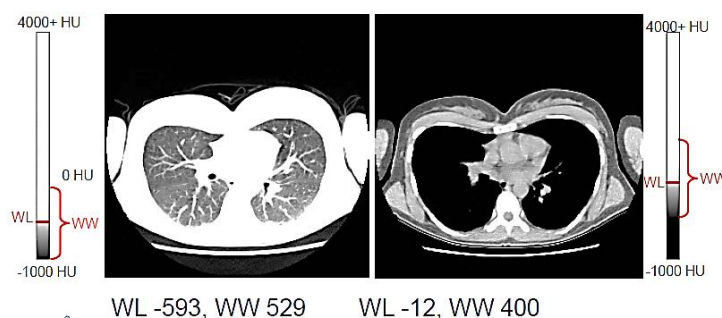


Figure 2.4 The display is defined using window level (WL) as CT number of mid-grey and window width (WW) (8).

The choice of WW and WL is dictated by clinical need optimal visualization of the tissues of interest in the CT image can only be achieved by selecting the most appropriate window width and window level (8).

2.1.3 Components of Computed Tomography Scanner

2.1.3.1 Gantry and table

The CT gantry contains all devices that are required to record transmission profiles of a patient, since transmission profiles must be recorded under different angles these devices are mounted on a support that can be rotated (Figure 2.5A). On the rotating part of the gantry are mounted for example the X-ray tube, the detector, the high voltage generator for the X-ray tube, the (water or air) cooling of the X-ray tube, the data acquisition system, the collimator, and the beam shaping filters.

Electrical power is generally supplied to the rotating gantry through contacts (brushes) from stationary slip rings. Projection profiles are transmitted from the gantry to a computer usually by wireless communication (or slip ring contacts) (Figure 2.5B).

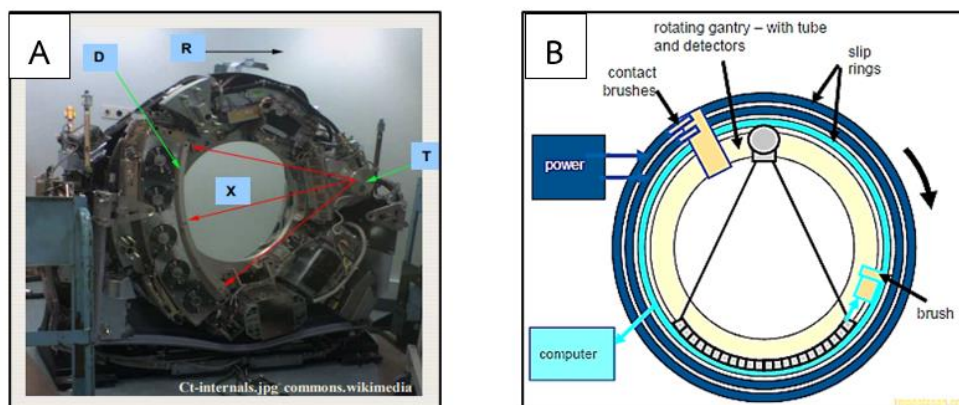


Figure 2.5 A. Basic system components of CT system T =X-ray tube D =X-ray detectors X =X-ray beam R =Gantry rotation B. Electrical power supply (8)

2.1.3.2 The X-ray tube and generator

An x ray tube (with a rotating tungsten anode) and high voltage generator are used for generating the x ray beam. The beam is collimated to create the ‘dose slice’ (or ‘cone’)

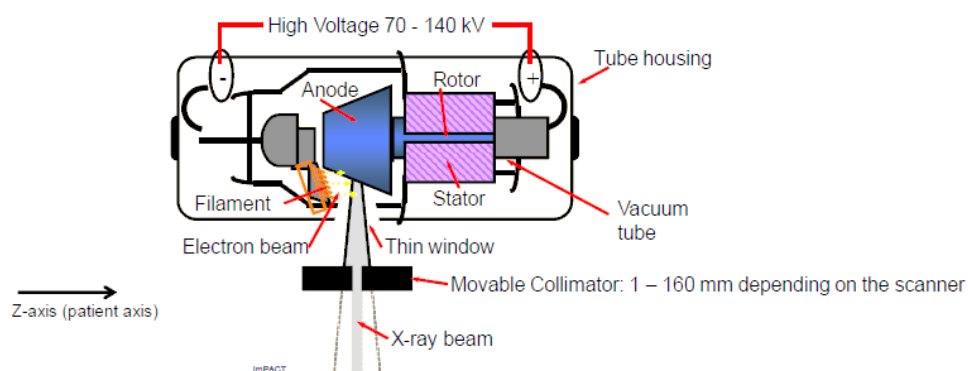


Figure 2.6 The X-ray tube and generator (8)

Rotation time, and the associated temporal resolution of CT scan, is limited due to the strong increase of centrifugal forces at shorter rotation times. In fast CT scanners with rotation times in the order of magnitude of 0.35 seconds, rotating parts are exposed to several tenths of g forces.

High-frequency generators are currently used in CT. They are small enough so that they can be located within the gantry. Highly stable three-phase generators have also been used, but because these are stand-alone units located near the gantry and require cables, they have become obsolete. Generators produce high voltage and transmit it to the x-ray tube. The power capacity of the generator is listed in kilowatts (kW). The power capacity of the generator determines the range of exposure techniques (i.e., kV and mA settings) available on a particular system. CT generators produce high kV (generally 120–140 kV) to increase the intensity of the beam, which

will increase the penetrating ability of the x-ray beam and thereby reduce patient dose. The incoming power supply of 60 hertz (Hz) is transformed into a high-voltage, high-frequency current of 500 to 25,000 Hz. The power demands on a multislice CT unit are enormous, typically 20 to 100 kilowatts (kW). A 60-kW generator produces enough voltage to provide 80 to 120 kV and 20 to 500 mA (9).

2.1.3.3 Collimation and filtration

The X-ray beam is often referred to as a fan beam where the beam width along the longitudinal axis is small. For multi-slice scanners where the longitudinal beam width is no longer small the X-ray beam is often referred to as 'cone beam' (Figure 2.7)

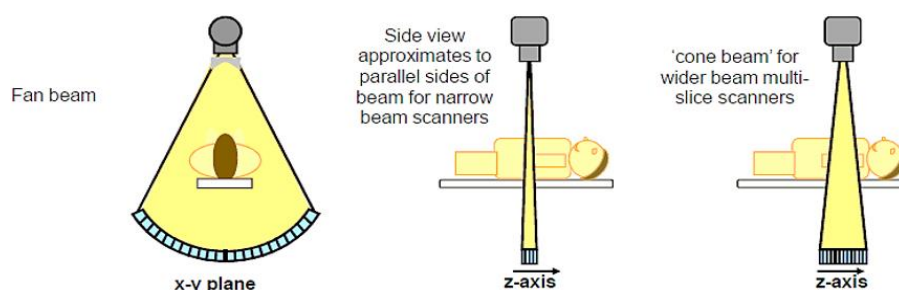


Figure 2.7 Narrow fan beam and multi-slice scanners (8)

Beam shaping filters are being used to create a gradient in the intensity of the X-ray beam. They are sometimes called “bow-tie” filters (Figure 2.8). They are mounted close to the X-ray tube. The purpose of the beam shaping filter is to reduce the dynamic range of the signal recorded by the CT detector and reduce the dose to the periphery of the patient. Attempt to normalize the beam hardening of the beam – to aid with calibration. Schematic figure showing the fan beam, flat and beam shaping ('bow-tie') filters.

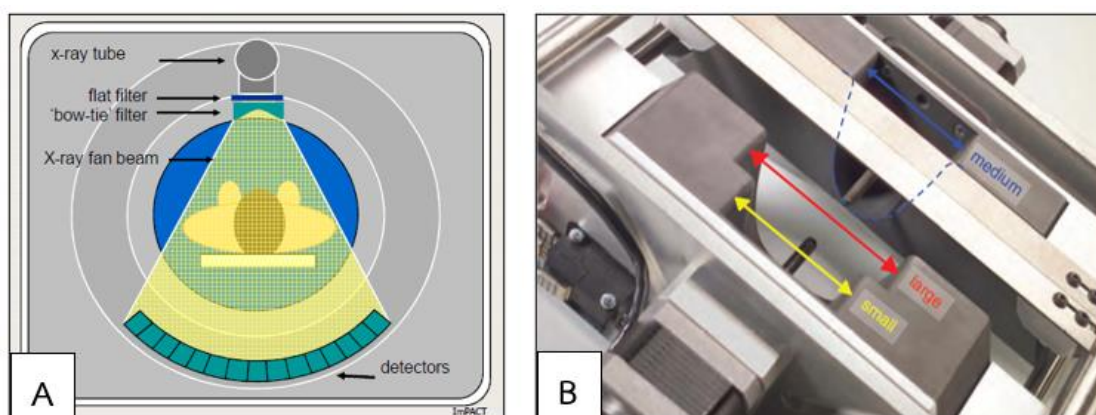


Figure 2.8 A. Schematic diagram of a bowtie filter and B. a flat filter (8) (9)

2.1.3.4 Detectors

The detectors, which measure the patients x-ray attenuation data, are located opposite the x-ray tube. CT scanner detectors have ~ 800-1000 detector elements along the detector arc and 1 – 320 detectors along z-axis. CT detectors are curved in the axial plane (x-y plane), and rectangular along the longitudinal axis (z-axis) (Figure 2.9).

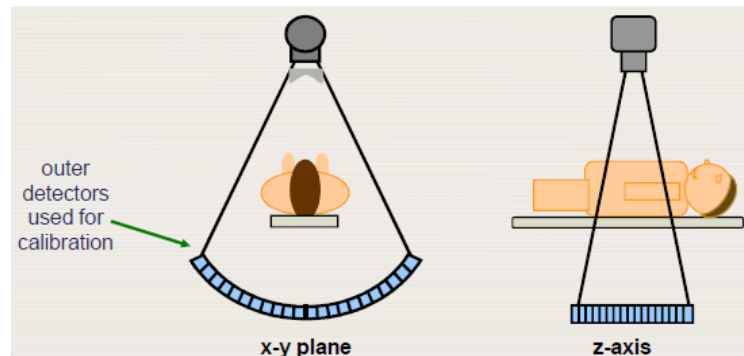


Figure 2.9 CT detectors are curved in the axial plane (x-y plane), and rectangular along the longitudinal axis (z-axis)

Xenon filled ionization chambers were used till ~ year 2000. They have few ring artefacts; Lower detection efficiency and currently solid-state detectors are used because better detection efficiency. Solid state detectors are generally scintillators. The photons interact with the detector and generate light. The light is converted into an electrical signal by photodiodes (Figure 2.10).

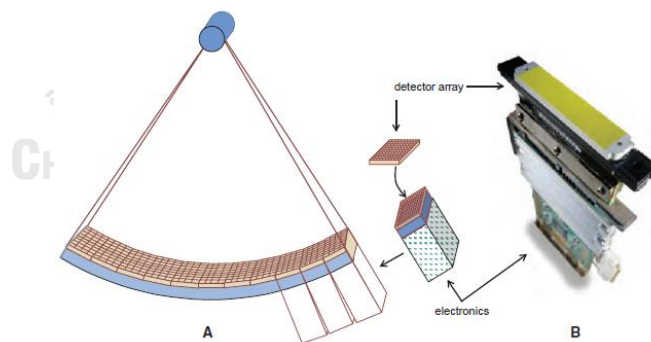


Figure 2.10 A. The detector arrays are mounted on electronics module B. A photograph of a detector module with electronics from a commercial CT(9).

2.1.3.5 Multidetector Computed Tomography

The principle of multi-slice CT is relatively straightforward. In a third generation single slice design, up to 900 detector elements were arranged in an arc that was concentric with the z-axis, but the detectors were only one element deep (typically 10 mm) in the z direction. To achieve slices less than 10 mm thick the beam width was restricted using physical collimators, often both between the X-ray tube

and the patient and between the patient and the detectors. In multi-slice systems the detectors are physically and electronically separated along the z-axis and thus form a matrix of elements (Figure 2.11).

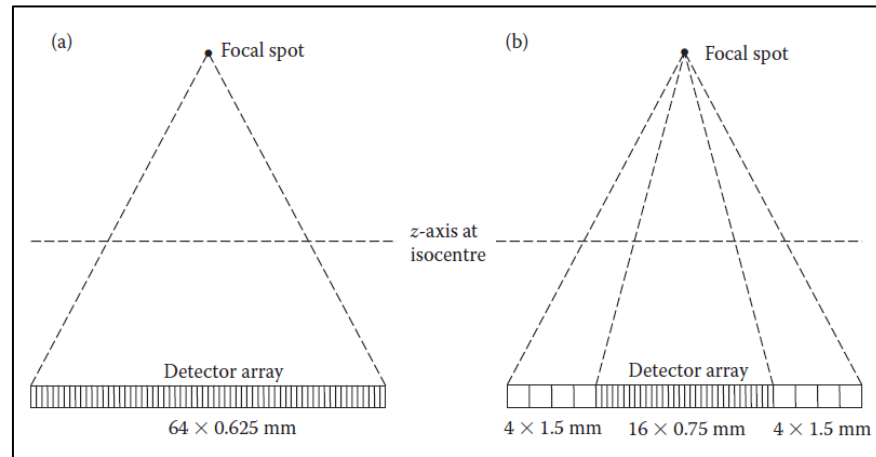


Figure 2.11 multi-detector arrangements; (a) A fixed array detector, (b) adaptive array detector

Several designs of detector array have been developed by different manufacturers. Two basic designs have been used—fixed array detectors, in which all elements have the same width, and adaptive array detectors, in which the outer detectors are wider than those nearer the center. An example of each is shown in Figure 2.11. Figure 2.11a shows a fixed array detector with 64 detector rows and a collimated detector of 0.625 mm giving a maximum coverage of 40 mm along the z-axis. Thicker z values may be obtained by combining the detectors in groups. Figure 2.11b shows an adaptive array detector with 24 detector rows. In the middle there are 16 detectors with a width of 0.75 at the center of rotation. These are flanked by eight outer detector rows 1.5 mm wide. This array may operate as a 16×0.75 mm array covering 12 mm or as a 16×1.5 mm array covering 24 mm (10).

2.1.3.6 Image reconstruction of CT

The rapid evolution of mathematical methods for generating new images in computed tomography (CT) reflects the competition in creating efficient and accurate new imaging methods while keeping the radiation dose to a minimum and has scheduled improvements in CT in the past. The mathematical problem that new CT imaging is trying to solve is the computation of the attenuation coefficients of the different X-ray absorption paths (radiation sum) obtained as a data set (projection). Techniques for reconstruction include Simple backprojection, Algebraic reconstruction, Iterative reconstruction and Filtered back projection (8).

During a CT scan, numerous measurements of the transmission of X-rays through a patient are acquired at many angles. This is the basis for reconstruction of the CT image,

The figure 2.12 below shows (a) the X-ray projection under a certain angle. (b) leading to one transmission profile. The backprojection distributes the measured signal evenly over the area (c) under the same angle as the projection (d) transmission profiles are taken from many angles and back projected yielding a strongly blurred image.

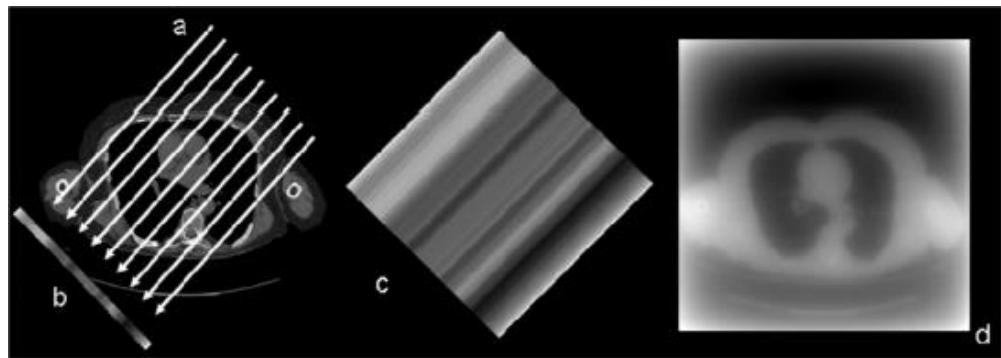


Figure 2.12 Simple backprojection (8)

The backprojection distributes the measured signal evenly over the area. Transmission profiles are taken from many angles and backprojected yield a strongly blurred image. Which are not used in clinical environments as it is unable to produce sharp images known to striking artifacts that resemble stars. Mathematics shows that simple backprojection is not sufficient for accurate image reconstruction in CT. Instead, a filtered backprojection must be used. It is the standard for image reconstruction in CT. Which still widely used in CT today (Figure 2.13).

Filtered backprojection utilizes a convolution filter to alleviate the blurring associated with back projection. it is fast, but it has several limitations, including noise and artifact. Other reconstruction techniques are algebraic or iterative reconstructions. Algebraic reconstruction solves several simultaneous equations. Algebraic reconstruction in clinical practice is not feasible, due to the large (512 x 512) matrices that are used in medical imaging and due to inconsistencies in the equations due to measurement errors and noise.

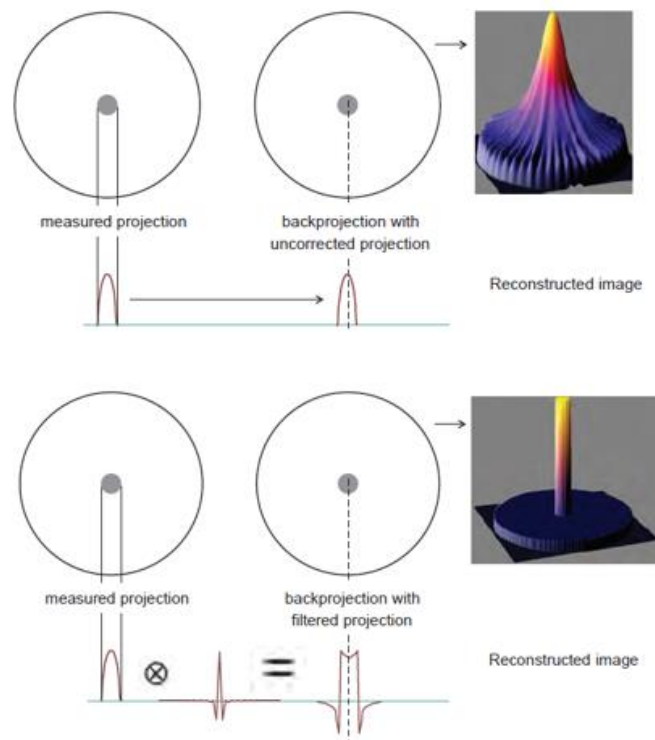


Figure 2.13 Filtered backprojection and Simple backprojection (9)

Iterative (statistical) reconstructions are sometimes used. These are routinely used in nuclear medicine. They are becoming available for commercial CT scanners. Potential benefits of iterative reconstructions are the removal of streak artefacts (particularly when fewer projection angles are used) and better performance in low-dose CT acquisitions (Figure 2.14). However, images may be affected by other artefacts, aliasing patterns and overshoot in the areas of sharp intensity transitions.

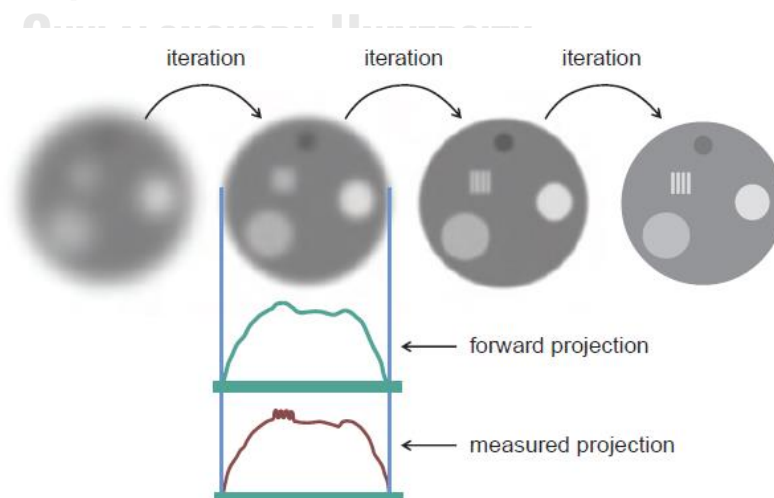


Figure 2.14 Iterative (statistical) reconstructions (9)

2.1.4 The dosimetry in computed tomography

Since CT examinations involve the irradiation of thin transverse slices of the body by a rotating beam of X-rays, conditions of exposure are very different from those used in conventional radiology and different methods are required to measure radiation doses and calculate effective doses. Weighted CT dose index ($CTDI_w$), volume weighted dose index ($CTDI_{vol}$), and dose length product DLP are all practical dose quantities that can be used. Some or all these quantities are displayed on the scanner console (10).

Early estimates of dose from a CT examination did not use the CTDI methodology and measured only the dose from a single scan acquisition. Specifically, only the peak radiation dose emitted by the scanner from a single tube rotation and at a single table position was measured, and this underestimated the dose delivered to a typical adult patient by a factor of two to three. The reason for this underestimation was that the measurement neglected the “tails” of the dose distribution caused by scattered radiation produced from scans at adjacent table positions (Figure 2.15a). Because most clinical examinations involve multiple scans (i.e., gantry rotations) as the patient is translated through the gantry, the dose distribution to the patient is the sum of the overlapped “single-scan” dose distributions (Figure 2.15b). For examinations with enough scans, the average dose over the central scan width of the imaged anatomy will reach an equilibrium value, which is referred to as the multiple scan average dose (MSAD) (Figure 2.15b) (11).

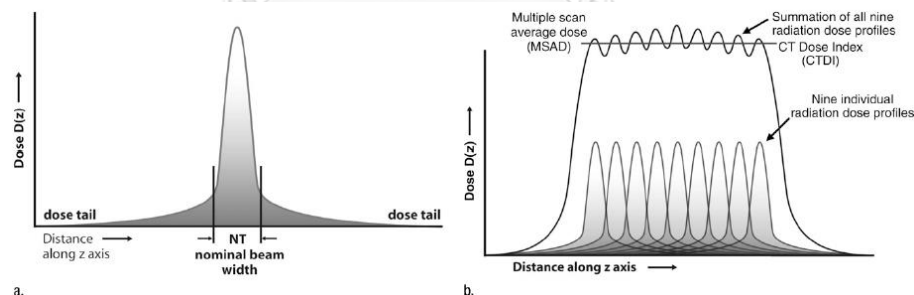


Figure 2.15 (a) Radiation dose profile along a line perpendicular to the scan plane (b) The radiation dose profile from nine adjacent transverse CT scans along a line perpendicular to the transverse scans (11).

2.1.4.1 $CTDI_{100}$

The dose integral in the CTDI equation is usually acquired from a measurement of a single axial rotation with the standard 100 mm pencil ion chamber, directed along the z-axis. When the pencil ion chamber is used the measurement integration limits are defined by the length of the chamber, usually 100 mm.

The $CTDI_{100}$ is integration of the radiation dose profile from a single axial scan over specific integration limits and the integration limits are ± 50 mm as shown in

Figure 2.15, which corresponds to the 100-mm length of the “pencil” ionization chamber. The $CTDI_{100}$ is calculated as the integral of air kerma along chamber divided by nominal slice thickness as in equation.

$$CTDI_{100} = \int_{-50mm}^{+50mm} D(z) dz \quad \text{equation 2.4}$$

where n is the number of acquire slices per rotation and T is nominal thickness of acquire slice (mm).

2.1.4.2 Weighted CT Dose Index ($CTDI_w$)

CT dose index is obtained from a measurement made in a 16 cm or 32 cm diameter polymethyl-methacrylate (PMMA) cylinder to represent a head and body, respectively. The measurement is made using a 100 mm active length pencil ionisation chamber. This measured quantity is denoted $CTDI_{100}$ and is the integration of the dose from a single rotation, so it includes the spread of the radiation dose profile. Note that the X-ray beam will not have a dose profile that is an ideal rectangular shape but will have a more spread distribution (Figure 13.6). The $CTDI_{100}$ will vary across the field of view tending to be greater near the periphery of the phantom than at the center. To account for this variation $CTDI_w$ is defined as one-third the $CTDI_{100}$ at the center plus two-thirds the $CTDI_{100}$ at the periphery (10).

$$CTDI_w = 1/3CTDI_{100, \text{center}} + 2/3CTDI_{100, \text{periphery}} \quad \text{equation 2.5}$$

In helical (also called spiral) CT scanning, the CT dose is inversely related to the helical pitch used, that is,

$$\text{dose} \propto \frac{1}{\text{pitch}} \quad \text{equation 2.6}$$

where the pitch is defined as the table translation distance (mm) during a full rotation (360 degrees) of the gantry, divided by the nominal beam width nT (in mm) (9).

2.1.4.3 Volume CT Dose Index ($CTDI_{vol}$)

CT dose index is a useful quantity when comparing two scanners, most scanners have the ability to display the $CTDI_{vol}$ on the CT scanner console prior to the actual scan. The value can be displayed because the CT manufacturer has measured $CTDI_{vol}$ in the factory over the range of kV values for that model of scanner, and then that stored value, scaled appropriately by the mAs and pitch, is displayed on the console (9).

$CTDI_{vol}$ is therefore defined as

$$CTDI_{vol} = \frac{CTDI_w}{\text{pitch}} \quad \text{equation 2.7}$$

2.1.4.4 Dose-Length Product (DLP)

The product of the $CTDI_{vol}$ and the length of the CT scan along the z-axis of the patient, L, is the dose length product (DLP):

$$DLP = CTDI_{vol} \times L \quad \text{equation 2.8}$$

It is usually measured in mGy.cm and is displayed on the scanner console.

2.1.4.4 Effective dose

To assess the effective dose and thus be able to estimate risk, it is necessary to know the dose to all the radiosensitive organs of the patient arising from the various highly localized patterns of exposure. Organ doses may be estimated from axial air doses using Monte Carlo techniques which have been developed into a computer program by ImPACT 2004. However, a simpler method has been developed whereby coefficients, depending on the region of the body irradiated and the age of the subject, have been derived using Monte Carlo techniques to convert DLP into effective doses. This method has been used in the 2003 review of doses from CT examinations in the UK (Shrimpton et al. 2006). Table 2.1 shows the coefficients used for adults (10).

Table 2.1 Normalised Values of Effective Dose per Dose Length Product for Adults Over Various Regions

Normalised Values of Effective Dose per Dose Length Product for Adults Over Various Regions

Region of Body	Effective Dose per DLP (mSv [mGy.cm] ⁻¹)
Head and neck	0.0031
Head	0.0021
Neck	0.0059
Chest	0.014
Abdomen and pelvis	0.015
Trunk	0.015

Source: Shrimpton PC, Hillier MC, Lewis MA and Dunn M, National survey of doses from CT in the UK: 2003. *Br. J. Radiol.* 79, 968–980, 2006.

2.1.4.5 size specific dose estimates (SSDEs)

In 2011, the AAPM task group 204 has introduced the concept of size-specific dose estimate (SSDE) derived from $CTDI_{vol}$ and measured patient diameters for conversion factors (f_{size}). SSDE considers the scanning protocol and the effects of the geometric shape of the patient and tissue attenuation on the radiation dose. This provides higher accuracy on radiation dose to the patient. The SSDE can be defined using the equation as follows:

$$SSDE = f_{\text{size}} \times \text{CTDI}_{\text{vol}} \quad \text{equation 2.9}$$

2.1.4.6 Absorbed dose

Absorbed dose is the amount of energy deposited by radiation in a mass. The mass can be anything: water, rock, air, people, etc. Absorbed dose is expressed in milligrays (mGy).

In radiation biology, clinical radiology, and radiological protection the absorbed dose, D , is the basic physical dose quantity, and it is used for all types of ionizing radiation and any irradiation geometry. It is defined as the quotient of $d\bar{\epsilon}$ by dm , where $d\bar{\epsilon}$ is the mean energy imparted to matter of mass dm by ionising radiation, that is

$$D = \frac{d\bar{\epsilon}}{dm} \quad \text{equation 2.10}$$

Absorbed dose is a measurable, physical quantity. It is expressed in grays (Gy), or, more frequently milligrays (mGy), which are 1/1000th of a gray. 1 gray = 1 joule of energy deposited in 1 kilogram of material i.e., 1 Gy = 1 J/kg. (12)

Due to the rotational irradiation geometry used in CT, the radiation dose distribution in the patient is far more homogeneous than in radiography or fluoroscopy. The use of a beam-shaping filter further reduces heterogeneity in the dose distribution. Thus, in CT, the dose gradients are very slight, and the distribution depends on the diameter and shape of the patient and on the beam quality (kV).

In helical (spiral) acquisition, most modern CT scanners have dose modulation modes that adjust the x-ray tube output (by varying the mA) as the gantry rotates around the patient and as the table translates the patient through the rotating x-ray beam. Dose modulation modes generally increase the mA (and hence dose rate) as the x-ray beam is aligned along thicker x-ray paths through the patient, and the mA is reduced for thinner x-ray path lengths through the patient. The changing mA in dose modulation mode slightly reduces the accuracy of table lookup CT.

The estimation of radiation risk from a medical imaging procedure is typically computed by first computing the organ doses from the procedure. Organ dose assessment is usually performed using a generic-sized patient, and the dose deposition is computed using Monte Carlo procedures based on the medical imaging procedure being performed. Typically, a mathematical phantom such as the MIRD phantom is used, and this phantom simulates each organ as a mathematical shape in a standard-size “body” (Figure 2.16). So-called voxelized phantoms have also been used, and these are full CT scans of humans, where each organ has been outlined so that organ dose can be estimated after the Monte Carlo procedure.

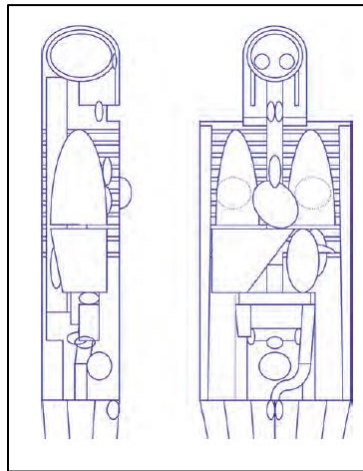


Figure 2.16 The MIRD phantom

In these Monte Carlo exercises, the dose for each organ is computed, for various entrance x-ray beam geometries. Organ doses are computed in the units of absorbed dose (mGy), usually normalized to entrance skin air kerma (ESK) in radiography or to air kerma at isocenter in computed tomography. Such tables allow the estimation of organ doses for given radiological imaging procedures that use different technique factors. For example, in Table 2.2 for abdominal radiography, the organ dose coefficients for different beam qualities (half-value layers) are provided (9).

Table 2.2 Organ conversion factors for selected radiography procedures.

	μ Gy PER mGy ENTRANCE KERMA				
	HVL FOR ENTRANT X-RAY BEAM (mm Al)				
	1.0	2.0	3.0	4.0	5.0
Lungs	2.4	9.6	17.2	24.0	28.6
Active bone marrow	7.4	30.9	59.5	85.9	109.9
Thyroid	0.0	0.1	0.2	0.3	0.3
Trunk tissue	68.7	137.4	187.8	224.4	253.0
Ovaries	59.5	183.2	296.6	385.9	453.4
Uterus	83.6	249.6	395.0	506.1	586.2

Adapted from Table 41 (AP Abdominal Radiography) 100 cm SID, 35 × 43 cm field of view, in *Handbook of Selected Tissue Doses for Projections Common in Diagnostic Radiology*, HEW publication (FDA) 89-8031 (1989).

2.1.5 Abdominal computed tomography

The abdomen contains organs of the gastrointestinal, urinary, endocrine, and reproductive systems. A CT scan of the abdomen may be performed to assess the abdomen and its organs for tumors and other lesions, injuries, intra-abdominal bleeding, infections, unexplained abdominal pain, obstructions, or other conditions, particularly when another type of examination, such as X-rays or physical examination, is not conclusive.

In general, a CT examination of the abdomen includes transaxial images from just above the dome of the diaphragm to the upper margin of the sacroiliac joints with a 5-mm or less slice thickness. A CT of the pelvis extends from the iliac crest through just below the ischial tuberosities with a 5-mm or less slice thickness. Occasionally, more inferior extension of imaging may be required to fully image pelvic structures of concern. Often, depending on the clinical indication for the study, both the abdomen and pelvis may be examined concurrently. Scans should be obtained through the entire area of interest. The scan field of view should be optimized for each patient. Scans should generally be obtained during suspended respiration but may be obtained during free breathing for certain indications, such as radiation therapy planning (13) (14).

Abdominal and pelvic CT examinations may be performed during after administering intravenous (IV) contrast medium using appropriate injection techniques. The majority of clinical questions for abdominal and pelvic CT can be appropriately answered with a single-phase study. Multiple-phase studies such as unenhanced, arterial, portal venous, or delayed-phase scanning might be required in certain indications for improved detection and characterization of lesions such as for possible hepatocellular carcinoma, hypervascular metastases, etc. For specific indications, it may be necessary to perform a non-IV contrast-enhanced study first.

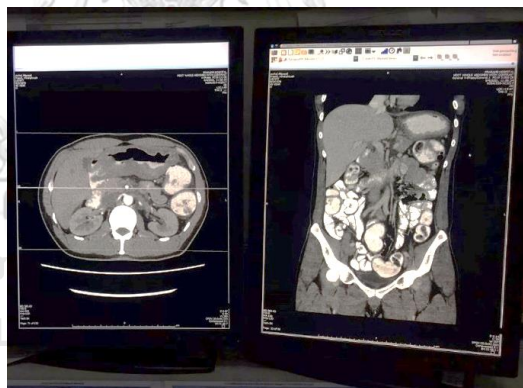


Figure 2.17 Abdominal computed tomography with contrast enhancement.

Pediatric computed tomography (CT) is a fast, painless exam that uses special x-ray equipment to create detailed images of child's internal organs, bones, soft tissues, and blood vessels. It may be used to help diagnose abdominal pain or evaluate for injury after trauma.

Acute abdominal pain is one of the most common presenting complaints to the emergency department for the pediatric population. While the differential diagnosis for acute abdominal pain in children is broad and includes infectious, inflammatory, musculoskeletal, traumatic, gynecologic, and other etiologies, acute appendicitis is an important differential diagnostic consideration because of the potential need for surgical intervention. Acute appendicitis represents the most common abdominal surgical urgency/emergency in children (14).

2.1.6 Radio-photoluminescence Glass Dosimeter (RPLGD)

The basic principle of RPLGD is that the color centers are formed when the luminescent material inside the glass compound exposed to radiation and fluorescence are emitted from the color centers after irradiated with ultra-violet light with 337.1 nm length will stimulate the electrons in the color center to emit the fluorescence light (600–700 nm). This process is called radio-photoluminescence phenomena. Because the electrons in the color centers return to the electron traps after emitting the fluorescence, it can be re-readout for a single irradiation.

The RPLGD comes in a cylindrical shape with three different models: GD-302M, GD-352M, and GD-301. The size of both GD-302M and GD-352M is similar where the length is 12 mm, and the diameter is 1.5 mm. For GD-301, the diameter remains similar with other models, except its length. GD-301 possesses a smaller length of 8.5 mm (Figure 2.18) (15) (16).



Figure 2.18 Radio-photoluminescence Glass Dosimeter (RPLGD)

2.1.6.1 Characteristics of RPLGD for clinical applications

1. Repeatable readout: the luminescence signal does not disappear after readout; therefore, repeated readout for a single exposure is possible for RPLGD.
2. Small difference in individual sensitivity: the readout variation between different RPLGDs with the same exposure is small. RPLGD is manufactured with melted glass; therefore, its individual sensitivity is small as compared to that of either TLD or OSLD.
3. No correction factor needed: the luminescence signal can be converted to the exposure dose directly without the need of correction factors. The exposure dose can be determined with the help of readout from reference RPLGD built-in to the readout system.
4. Small energy dependence: the energy dependence existed in glass, if there is no energy compensator filter with it. However, energy dependence can be reduced with energy compensator filter (15) (16).

2.2 Review of related literature

Babak A, et al. (17) (2018) collected the data from 13,544 patients who underwent CT examinations of the torso, head and knee and then calculated f_{size} of BMI. Then compared f_{size} as calculated from the AP and LAT dimensions to f_{size} calculated as a function of BMI. The results showed there was no significant difference between f_{size} calculated from AP-LAT dimensions, effective diameter, and BMI, as shown in Table 2.3. Their study demonstrated that it is possible to estimate f_{size} using the patients' BMI for the torso as well as the head and knee CT, thereby enabling calculation of the probable SSDE prior to image acquisition on the basis of the presumed $CTDI_{vol}$ provided by the scanner. By providing information on the expected patient dose prior to image acquisition, this method is advantageous over the traditional calculation of f_{size} via the AP and LAT dimensions and effective diameter.

Table 2.3 f_{size} determination for patients with different BMI, LAT and AP dimensions and effective diameter.

BMI	LAT	AP	d_{eff}	f_{size}	f_{size}	f_{size}
(kg/m ²)	(cm)	(cm)	(cm)	via Eq. (2)	via Eq. (5)	via Eq. (6)
17.71	27.98	20.73	24.08	1.52	1.50	1.50
24.62	31.15	27.00	29.00	1.27	1.30	1.28
30.02	32.73	29.73	31.19	1.17	1.16	1.14

Tsujiguchi T, et al (18) (2018) investigated the effective dose for CT examinations with consideration of patients' body type using SSDE in pediatric CT. They collected data from 753 patients who underwent CT examination of trunk region. Impact Dose software was used to calculate based on the Monte Carlo method. Six types of phantoms were assessed: newborn; 1, 5, 10, 15 years; and adult (≥ 16 years). The effective dose was calculated by Impact Dose Program based on the CT data of patient's trunk region. The AP and LAT diameter (of phantom) was measured and performed SSDE calculation. The SSDE and the SSDE-corrected value were used to calculate the effective dose. Results show the effective dose calculated using SSDE was higher than the conventional method in all cases, as shown in Figure 2.19, and the SSDE-corrected value is less likely to underestimate the exposure dose than the conventional method, making SSDE a very effective method for pediatric patient.

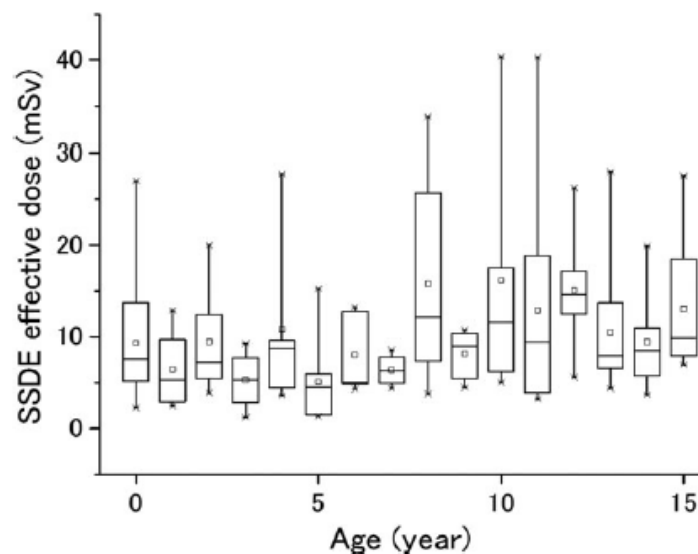


Figure 2.19 Exposure dose data using the SSDE in children. Effective dose calculated by simulation is indicated by box plot.

Moore BM and Brady SL (19) (2014) investigated the correlation of size-specific dose estimate (SSDE) with absorbed organ dose and to develop a simple methodology for estimating patient organ dose in a pediatric population (5–55 kg). The absolute organ dose at 23 locations were measured in 4 physical anthropomorphic phantoms using metal oxide semiconductor field effect transistor (MOSFET) dosimeters. The correlation between organ dose and SSDE the following scaling dose correlation factors (CF_{SSDE}) were established each organ and phantom size. Organ dose correlation factors (CF_{SSDE}) were multiplied by patient specific SSDE to estimate patient organ dose. The comparison of absolute organ dosimetry to previously published pediatric patient doses and was found to agree better than $\pm 10\%$ in the chest and in the abdominopelvic region. This study provides a complete list of organ dose correlation factors (CF) for the chest and abdominopelvic regions, which provide a simple methodology to estimate pediatric patient organ dose based on SSDE. The use of SSDE is a new CT dose index that consider the patient's size to further estimate the organ doses would provide more accurately for patient dosimetry and radiation risk estimation in pediatric patients.

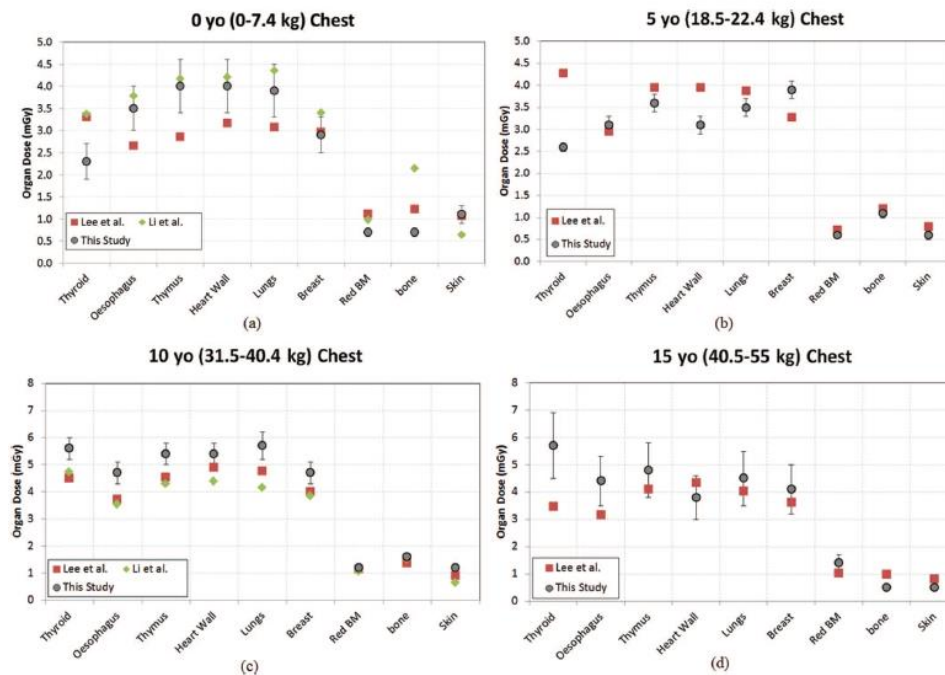


Figure 2.20 Comparison of chest absolute organ dosimetry. Monte Carlo computerized phantom based pediatric dosimetry studies were compared with this study.

Guberina N, et al (20) (2017) verified the results of a dose-monitoring software tool based on MCS in assessment of effective and organ doses in thoracic CT protocols. Phantom measurements were performed with thermoluminescent dosimeters (TLD LiF: Mg,Ti) using two different thoracic CT protocols of the clinical routine: (I) standard CT thorax (CTT); and (II) CTT with high-pitch mode. Radiation doses estimated with MCS and measured with TLDs were compared. Results showed inter-modality comparison showed an excellent correlation between MCS-simulated and TLD-measured doses ((I) after localizer correction $r = 0.81$; (II) $r = 0.87$). The following effective and organ doses were determined: (I) (a) effective dose $\frac{1}{4}$ MCS 1.2 mSv, TLD 1.3 mSv; (b) thyroid gland $\frac{1}{4}$ MCS 2.8 mGy, TLD 2.5 mGy; (c) thymus $\frac{1}{4}$ MCS 3.1 mGy, TLD 2.5 mGy; (d) bone marrow $\frac{1}{4}$ MCS 0.8 mGy, TLD 0.9 mGy; (e) breast $\frac{1}{4}$ MCS 2.5 mGy, TLD 2.2 mGy; (f) lung $\frac{1}{4}$ MCS 2.8 mGy, TLD 2.7 mGy; (II) (a) effective dose $\frac{1}{4}$ MCS 0.6 mSv, TLD 0.7 mSv; (b) thyroid gland $\frac{1}{4}$ MCS 1.4 mGy, TLD 1.8 mGy; (c) thymus $\frac{1}{4}$ MCS 1.4 mGy, TLD 1.8 mGy; (d) bone marrow $\frac{1}{4}$ MCS 0.4 mGy, TLD 0.5 mGy; (e) breast $\frac{1}{4}$ MCS 1.1 mGy, TLD 1.1 mGy; (f) lung $\frac{1}{4}$ MCS 1.2 mGy, TLD 1.3 mGy. Overall, in thoracic CT protocols, organ doses simulated by the dose-monitoring software tool were coherent to those measured by TLDs. Despite some challenges, the dose-monitoring software was capable of an accurate dose calculation.

Lee C, et al (21) (2012) established an organ dose database for pediatric and adolescent reference individuals undergoing computed tomography (CT) examinations by using Monte Carlo simulation. The data will permit rapid estimates of organ and effective doses for patients of different age, gender, examination type, and CT scanner model. The Monte Carlo simulation model of a Siemens Sensation 16 CT scanner was employed as a base CT scanner model. A set of absorbed doses for 33 organs/tissues normalized to the product of 100 mAs and CTDI_{vol} (mGy=100 mAs mGy) was established by coupling the CT scanner model with age-dependent reference pediatric hybrid phantoms. A series of single axial scans from the top of head to the feet of the phantoms was performed at a slice thickness of 10 mm, and at tube potentials of 80, 100, and 120 kVp. Using the established CTDI_{vol} and 100 mAs normalized dose matrix, organ doses for different pediatric phantoms undergoing head, chest, abdomen-pelvis, and chest-abdomen-pelvis (CAP) scans. In this study, organ doses from axial and helical scans with a given scan range were approximated as the sum of doses from multiple axial slices included in the scan range of interest; this is the same approach adopted within existing CT organ dose estimation programs. The following equation explains one calculates scanner-specific organ doses (mGy) using the organ dose matrix and user input (SS, SE, v, CTDI_{vol}(v), t, and I).

$$D(\text{mGy}) = \frac{\sum_{z=SS}^{z=SE} D(\text{organ}, \text{age}, \text{sex}, v, z)}{CTDI_{vol, Siemens}(v)} \times CTDI_{vol}(v) \cdot \left(\frac{t \cdot I}{100} \right), \quad \text{equation 2.11}$$

where D (organ, age, sex, v, z) is the organ dose per 10 mm axial slice at longitudinal position z on the phantom and normalized to a fixed integrated tube current of 100 mAs; v is the tube potential (kVp) of the particular CT scan; z is the slice number ranging from the top of the head to the bottom of the patient's feet; SS designates the slice number where scan starts; SE designates the slice number where scan ends; CTDI_{vol, Siemens} (v) is the CTDI_{vol} (mGy) measured on our reference Siemens Sensation 16 scanner at a pitch of 1 and 100 mAs/rotation; CTDI_{vol}(v) is for the particular scanner for which organ doses are sought is defined as CTDI_w divided by pitch at 100 mAs/rotation; and t is the single rotation time (s); and I is the tube current (mA) for that particular CT scan. The results from this study were compared with three different published studies and/or techniques. First, organ doses were compared to those given by CT-Expo which revealed dose differences up to several-fold when organs were partially included in the scan coverage. Second, selected organ doses from our calculations agreed to within 20% of values derived from empirical formulae based upon measured patient abdominal circumference (Table 2.4). Third, the existing DLP-to-effective dose conversion coefficients tended to be smaller than values given in the present study for all examinations except head scans (Table 2.5).

Table 2.4 Comparison of major organ doses (mGy/100 mAs mGy) for the organs completely included in the abdomen/pelvis scan as derived by empirical correlation with patient abdominal circumference (Turner et al.) and as calculated from the organ dose matrix of the present study.

	Organs	Regression coefficients		Age (year)					
		A ₀	B ₀	0	1	5	10	15F	15M
<i>Turner et al.</i>	Liver	3.8240	−0.0120	2.45	2.02	1.91	1.63	1.41	1.33
	Stomach	3.7800	−0.0113	2.49	2.08	1.96	1.69	1.48	1.40
	Adrenals	4.0290	−0.0128	2.51	2.04	1.92	1.62	1.39	1.31
	Kidney	3.9690	−0.0124	2.51	2.06	1.93	1.65	1.42	1.33
	Pancreas	3.7150	−0.0122	2.37	1.95	1.83	1.56	1.35	1.27
	Spleen	3.5140	−0.0111	2.33	1.95	1.85	1.60	1.40	1.32
	Gall bladder	3.9940	−0.0115	2.61	2.17	2.05	1.77	1.54	1.45
<i>Our study</i>	Liver			2.30	2.03	1.85	1.62	1.53	1.38
	Stomach			2.28	1.95	1.85	1.66	1.56	1.33
	Adrenals			2.07	1.75	1.64	1.41	1.27	1.16
	Kidney			2.34	2.26	2.12	1.86	1.70	1.42
	Pancreas			2.28	2.01	1.87	1.57	1.43	1.16
	Spleen			2.28	2.06	1.85	1.70	1.54	1.37
	Gall bladder			2.15	1.97	1.84	1.64	1.41	1.25

Table 2.5 Comparison of effective doses normalized to dose length product (DLP) (mSv/mGy cm) as given by Shrimpton et al. and as calculated using the dose matrix of the present study under either ICRP 60 or ICRP 103 tissue weighting factors.

	Scan type	kVp	Age (year)					
			0	1	5	10	15	30
<i>Shrimpton et al.^a</i>	Head	120	0.0110	0.0067	0.0040	0.0032		0.0021
	Chest		0.0390	0.0260	0.0180	0.0130		0.0140
	Abdomen/pelvis		0.0490	0.0300	0.0200	0.0150		0.0150
	Trunk		0.0440	0.0280	0.0190	0.0140		0.0150
NCI ED60	Head	80	0.0084	0.0049	0.0033	0.0023	0.0016	0.0013
		100	0.0085	0.0054	0.0037	0.0026	0.0018	0.0015
		120	0.0092	0.0060	0.0043	0.0029	0.0021	0.0017
	Chest	80	0.0428	0.0268	0.0190	0.0126	0.0087	0.0168
		100	0.0432	0.0277	0.0198	0.0134	0.0096	0.0180
		120	0.0446	0.0291	0.0210	0.0146	0.0106	0.0186
	Abdomen/Pelvis	80	0.0447	0.0283	0.0193	0.0122	0.0093	0.0195
		100	0.0451	0.0294	0.0203	0.0132	0.0102	0.0210
		120	0.0465	0.0313	0.0222	0.0149	0.0114	0.0219
	CAP	80	0.0413	0.0261	0.0184	0.0120	0.0087	0.0155
		100	0.0417	0.0274	0.0193	0.0129	0.0095	0.0168
		120	0.0430	0.0290	0.0208	0.0144	0.0106	0.0175
NCI ED103	Head	80	0.0075	0.0048	0.0034	0.0023	0.0017	0.0013
		100	0.0079	0.0052	0.0038	0.0026	0.0019	0.0015
		120	0.0086	0.0058	0.0043	0.0029	0.0022	0.0017
	Chest	80	0.0492	0.0306	0.0219	0.0146	0.0103	0.0191
		100	0.0494	0.0315	0.0227	0.0155	0.0110	0.0203
		120	0.0508	0.0330	0.0240	0.0168	0.0121	0.0210
	Abdomen/pelvis	80	0.0460	0.0281	0.0198	0.0120	0.0094	0.0159
		100	0.0463	0.0292	0.0207	0.0129	0.0103	0.0172
		120	0.0475	0.0309	0.0221	0.0142	0.0114	0.0179
	CAP	80	0.0425	0.0263	0.0186	0.0123	0.0089	0.0162
		100	0.0428	0.0273	0.0194	0.0132	0.0097	0.0173
		120	0.0440	0.0288	0.0207	0.0144	0.0108	0.0180

^aTissue weighting factors in ICRP60 were adopted to calculate effective doses in Shrimpton et al.

Gao Y, et al (22) (2020) estimated organ and effective doses from CT scans of pediatric oncologic patients using patient-specific information. The patient size

obtained from the DICOM images and the vendor-supplied dose monitoring application for a cross-sectional study of 1,250 pediatric patients from subjects 0 to 20 years of age treated. CT scan of the head, chest, pelvis, abdomen, or abdomen-pelvis. Patients are divided by age. Organ doses and effective doses were estimated using VirtualDose™ CT based on patient-specific information, tube current modulation (TCM), and age-specific realistic phantoms. CTDI_{vol}, DLP, and dose results were compared with those reported in the literature. Results show CTDI_{vol} and DLP varied widely as patient size varied. The 75th percentiles of CTDI_{vol} and DLP were no greater than in the literature except for head scans of 16–20 years old and of abdomen-pelvis scans of larger patients. Eye lens dose from a head scan was up to 69 mGy. Mean organ doses agreed with other studies at maximal difference of 38% for chest and 41% for abdomen-pelvis scans (as shown in Figure 2.21-2.22). Mean effective dose was generally higher for older patients. The highest effective doses were estimated for the 16–20 years old as: head 3.3 mSv, chest 4.1 mSv, abdomen-pelvis 10.0 mSv, chest-abdomen-pelvis 14.0 mSv. Conclusion: Patient-specific organ and effective doses have been estimated for pediatric oncologic patients from <1 through 20 years old. The effect of TCM was successfully accounted for in the estimates. Output parameters varied with patient size. CTDI_{vol} and DLP results are useful for future protocol optimization.

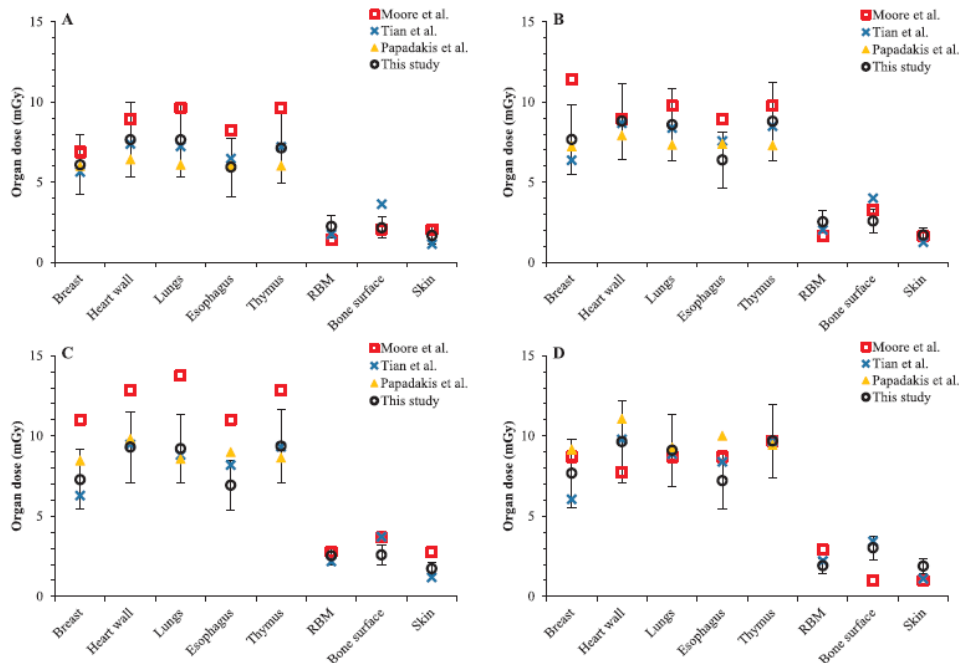


Figure 2.21 Graph shows comparison of dose to 8 organs by chest CT scans with method of this study and methods from literature (references).

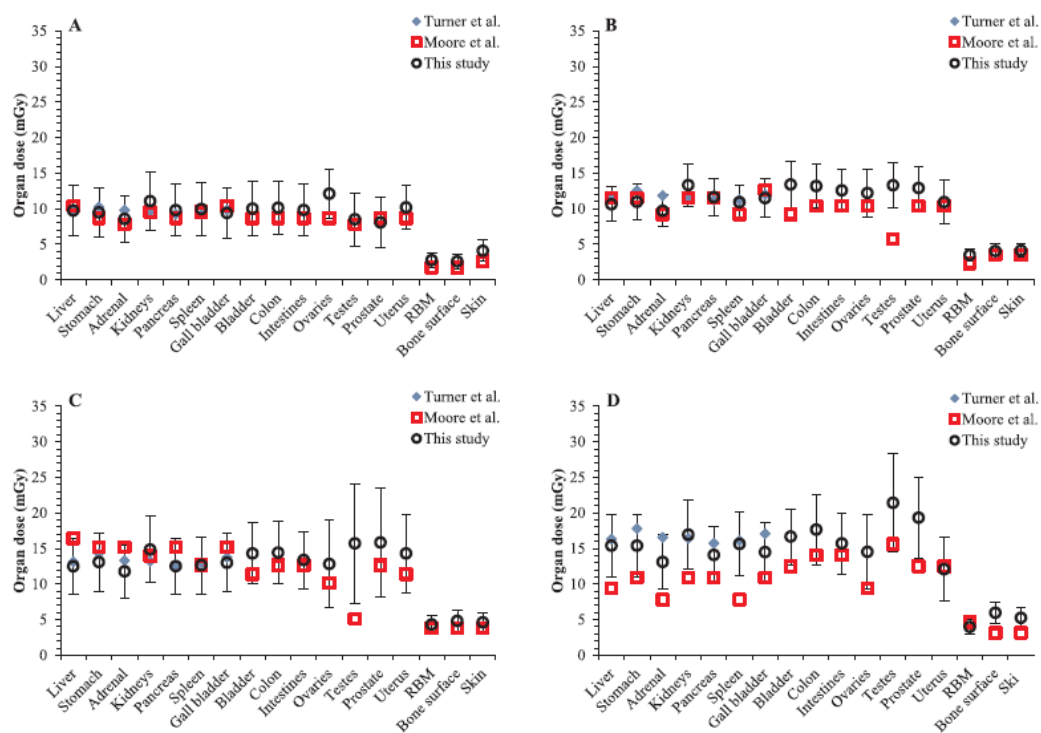
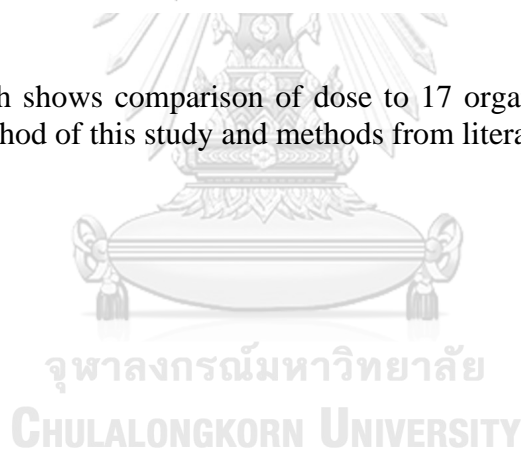


Figure 2.22 Graph shows comparison of dose to 17 organs by abdomen and pelvis CT scans with method of this study and methods from literature (references).



CHAPTER III

RESEARCH METHODOLOGY

3.1 Research design

This study is an observational descriptive design in the type of retrospective.

3.2 Research design model

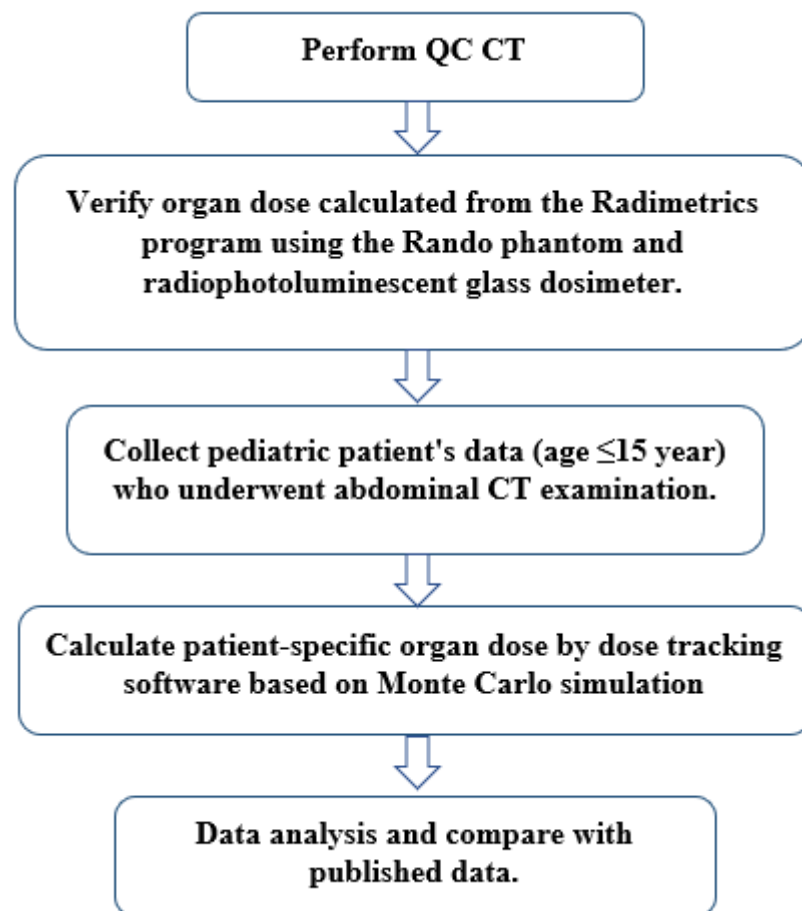


Figure 3.1 Research design model

3.3 Conceptual framework

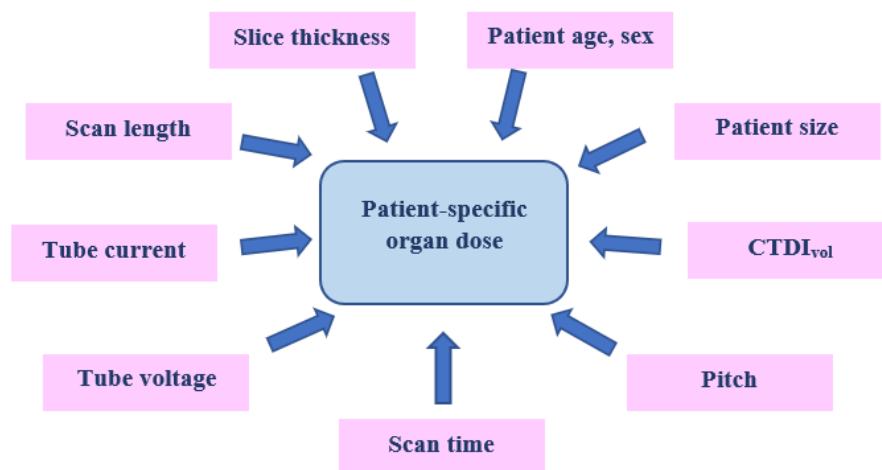


Figure 3.2 Conceptual framework

3.4 Research question

What are the organ doses calculated by the patient dose tracking software based on Monte Carlo (MC) simulation in pediatric abdominal CT?

3.5 Key words

Computed tomography, Size-specific dose estimates, Patient-specific organ dose, Abdominal CT examination, Patient size, Dose tracking program

3.6 Materials

3.6.1 Materials

- 1) CT Toshiba Aquilion ONE 320-Row Detector at Praram9 Hospital (installed in 2017). The characteristic performance of CT Toshiba Aquilion ONE is shown in table 3.1.



Figure 3.3 CT Toshiba Aquilion ONE, 320-row detector.

Table 3.1 Specification of CT Toshiba Aquilion ONE 320 Detector

Toshiba Aquilion ONE	Specifications
X-ray tube voltage	80, 100, 120, and 135 kV
X-ray tube current	10 mA to 600 mA
High-voltage generator	The high-frequency inverter method Max. power: 100 kW 144 (180*1) kW equivalent with AIDR 3D*
Collimator	Active Collimator: To reduce the exposure dose, the collimator operates asymmetrically at the start/end of scanning (except in the case of 4-row scanning).
Detector	Solid-state detectors <ul style="list-style-type: none"> • Main detector: 896×320 elements • Data acquisition: $896 \text{ channels} \times 320$ rows
Power supply conditions	Phase: Three-phase <ul style="list-style-type: none"> • Line voltage: 380, 400, 415, 440, 460, or 480 VAC • Frequency: 50 Hz or 60 Hz • Power capacity: 125 kVA (150 kVA*) • Voltage fluctuation due to load variation: Less than 5% • Power voltage fluctuation: Less than 10%**
Focal spot size	– IEC 60336: 2005, nominal: $0.9 \text{ mm} \times 0.8 \text{ mm}$ (small) $1.6 \text{ mm} \times 1.5 \text{ mm}$ (large)
Gantry opening	78 cm

- 2) CT Siemens SOMATOM Sensation 64-Row Detector at Praram9 Hospital (installed in 1992). The characteristic performance of CT Siemens SOMATOM Sensation is shown in table 3.2.

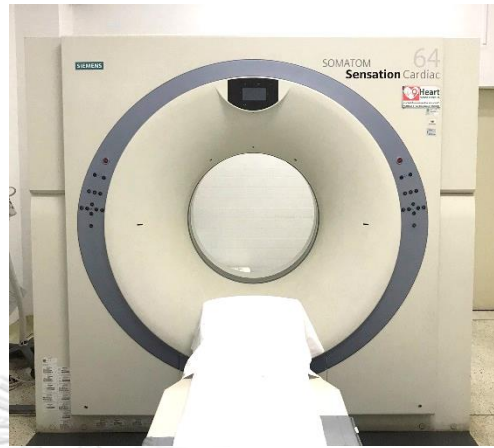


Figure 3.4 CT Siemens SOMATOM Sensation 64 Detector.

Table 3.2 Specification of CT Siemens SOMATOM Sensation 64 Detector

Siemens SOMATOM Sensation 64	Specifications
X-ray tube voltage	80, 100, 120, and 140 kV
X-ray tube current	28 mA to 666 mA
High-voltage generator	The high-frequency inverter method Min. power: 4 kW Max. power: 80 kW
Collimator	0.5 mm Al, 0.6 mm Ti (Equivalent to 5.5 Al)
Detector	UltraFast Ceramic with adaptive array detector Rows: 64 • Elements/row: 672 • # detection channels: 64 x 1,344
Power supply conditions	Phase: Three-phase • 380-480 VAC, 63-111 kVA
Focal spot size	– IEC 60336 0.7 mm × 0.7 mm (small UHR) 0.8 mm × 1.1 mm (large)
Gantry opening	70 cm

- 3) Medical records of pediatric abdomen CT examination: Medical records used to collect the patient data in this study contain the patient information such as patient age, sex, date of radiological examination including the specialist imaging protocol during an exam.

- 4) PACS workstation: Fujifilm's medical imaging and information management system, SYNAPSE. PACS is a system for digital storage, transmission, and retrieval of radiology images. PACS systems have both software and hardware components, which directly interface with imaging modalities and acquire the digital images from the modalities. The images are transferred to a workstation for viewing and reporting. The PACS viewer is a software that is installed on the workstation to receive and display the radiology images. The images are then archived into storage for retrieval later. The PACS system manages the storage of these radiology images.



Figure 3.5 SYNAPSE, PACS workstation.

- 5) Monte Carlo-based patient dose tracking program (Radimetrics)

Radimetrics™ Enterprise Platform (REP) used in this analysis provides several measures of radiation dose from computed tomography, including organ dose and effective dose calculated from Monte Carlo simulations. In addition, a size-specific dose estimate (SSDE) based on the water equivalent diameter (WED or D_w) or effective diameter was also calculated (23).

The components of the REP Monte Carlo simulator include the modeling of the x-ray source, the patient phantoms, and the interaction between x-ray photons with the patient. The x-ray source spectrum is based on the model described in the National Radiological Protection Board (NRPB) R204. Patients are currently modeled as Christy-Eckerman computational stylized phantoms where organs are represented by simple geometric shapes described by mathematical equations. The current Radimetrics™ Enterprise Platform phantom library contains a set of 9 reference phantoms that represent the average of the population, as well as a set of bariatric phantoms. The reference phantom (Figure 3.6.) set includes the original 6 Cristy-Eckerman phantoms (newborn, 1, 5, 10, 15-yr-old, and adult) and 3 pregnancy phantoms (1 for each trimester) The example of Radimetrics software is shown in Figure 3.7.

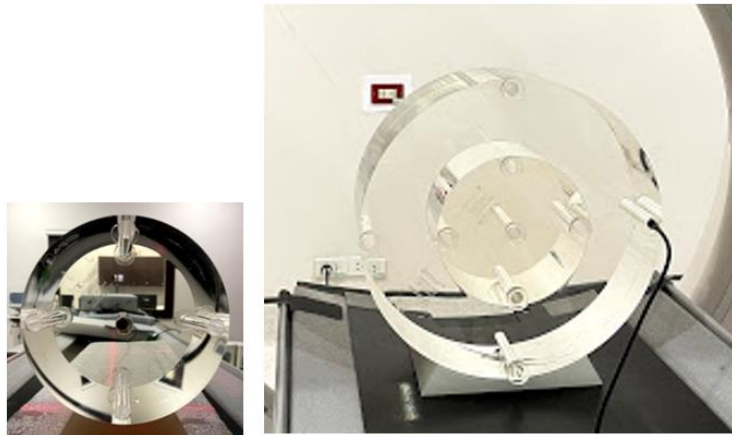


Figure 3.8 Polymethyl methacrylate (PMMA) CTDI phantoms.

2) Pencil ionization chamber, 10 cm active length

The ionization pencil chamber utilized for CT dosimetry as illustrated in figure 3.9 is a non-sealed cylindrical chamber with sensitive length 10 cm. One typical characteristic of this chamber is uniform response to incident radiations in every angle around its axis. In this study, the pencil ionization chamber model IBA Dosimetry – Multimeter MagicMaX Universal was used for CTDI measurement. The specification of IC is illustrated in Table 3.3.



Figure 3.9 Ionization chamber DCT10-MM

Table 3.3 Specification of DCT10-MM

DCT10-MM	Specifications
Features	Air ionization chamber.
Material	<u>External electrode</u> carbon fiber reinforced epoxy (CFRP) <u>Inner electrode</u> carbon fiber reinforced epoxy (CFRP) <u>Connector</u> 7-pin multi plug connector. <u>Cable</u> 2 m flexible, low noise
Size	active volume 4.9 cm ³ Total active length 100 mm Inner diameter of the external electrode 8.0 mm Diameter of the inner electrode 1.0 mm
Calibration factor (typical)	ND, K = 72 mGy cm / nC (120 kV / 4.5 mm Al HVL)
Dose measuring range	0.01 mGy – 15 Gy
Uncertainty	< 5 %
Calibration reference	120 kV, 2.5 mm Al; 1 m (RQR 9); in the chamber axis at the center of the cavity volume
Beam incidence direction	The central beam axis is perpendicular to the chamber axis.

3) Material for measurement Patient-specific organ dose

- Anthropomorphic Rando phantoms

Anthropomorphic Rando phantoms is a simulated object made of a tissue-like material of normal biological organisms as illustrated in Figure 3.10. Due to its availability and resemblance to a real patient, the human phantoms can be used for various tasks. Instead of images, many patients can use the human phantoms for trial and error to assess the optimal use of radiation, such as in new protocols or new imaging techniques. In the same hypothesis, human beings can be used to teach staff different photography techniques or exposure factors.



Figure 3.10 Anthropomorphic Rando phantoms.

- Radiophotoluminescent glass dosimeter (RPLGD)

Radiophotoluminescent (RPL) glass dosimeter as illustrated in Figure 3.11 is a true accumulation type solid state dosimeter, which is based on radiophotoluminescent phenomenon of silver activated phosphate glass exposed to ionizing radiation. RPLGD uses glass compound as the luminescent material and applies different excitation method along with different readout technique.

After exposed to radiation, stable color centers are formed in the glass and more color centers are formed with increasing radiation intensity. After irradiated by ultraviolet light, color centers are excited and emit 600 nm to 700 nm visible orange light. It is called radiophotoluminescence phenomenon. The amount of orange light emitted from RPLGD is linearly proportional to the radiation received; therefore, it is suitable for long term personal dose monitor or environmental radiation monitor (15) (16).



Figure 3.11 Radiophotoluminescent glass dosimeter (RPLGD).

Table 3.4 Specifications of glass dosimeter element.

Specifications of glass dosimeter element	
Mode	GD-352M (with ID and tin filter)
Glass element dimensions	Diameter 1.5×12 mm
Measuring	Photon (gamma ray & x-ray)
Dose range	10 μ Gy to 10 Gy [to 500 Gy by option]

- Laboratory oven

Laboratory ovens use convection to transmit heat to the glass refractometer element, which allows a consistent temperature to be maintained. The details of the melting, preheating, and shaping processes using a laboratory oven are described below.

**Figure 3.12** Laboratory oven (Carbolite Gero)

Before irradiation, the residual signal was removed by an annealing process at 400°C for 60 minutes, (program 3) and cools it down to room temperature. After the glass dose was irradiated, the luminescent signal was stabilized by the preheat process at 70°C for 30 min (program 1), and then used a suitable read out magazine (length, irradiated dose value). Mind the direction of glass with ID for setting into the magazine. The automatic reader FGD-1000 was used to read out the signal.

- Glass dosimeter reader (FGD-1000)

Instrument unit used to make an UV excitation to glass elements, read-out RPL quantity from glass elements and indicate the read-out dose value. The reader is automatically calibrated using the internal calibration glass which is traced with standard glass. Automatic calibration using the internal calibration by standard calibration, the dose value of the internal calibration glass is used to determine the reader correction factor (unit in nanocoulombs, nC) for daily use. When starting read-out, and when exchanging a read-out magazine, the internal calibration is executed automatically. At this

time, the type of the calibration mode and the read-out magazine is detected automatically, and the calibration is executed on suitable conditions.



Figure 3.13 Glass dosimeter reader (FGD-1000).

3.7 Methods

3.7.1 Perform quality control (QC) of CT scanner according to IAEA Human health series no. 19 (2012) (24).

3.7.2 Verification of $CTDI_{100}$

To verify the Computed Tomography Dose Index (CTDI) in air, the measurement was performed as following steps:

- Positioned chamber in stand so beyond couch as illustrated in Figure 3.14.
- Adjusted couch position so chamber along axis of scanner and beam centered at central point of chamber.
- Single axial was scanned using head and body protocols.
- For Toshiba CT scanner, the scanning parameters were set at 100 mA, 1 sec scan time and 1, 2, 4, 8, 12, 16, 20, 32 mm slice thickness. For Siemens CT scanner, the scanning parameters were set at 100 mA, 1 sec scan time and 10 mm slice thickness. The tube voltage at 80, 100, 120 and 135 were used for both CT scanners.
- Measured on axis of scanner using pencil ionization chamber.
- Calculated as integral of air kerma along chamber divided by nominal slice thickness.
- Record 3 dose measurements for single axial scan at selected parameters (no couch movement)
- Recorded all data for the CTDI in air measurement.

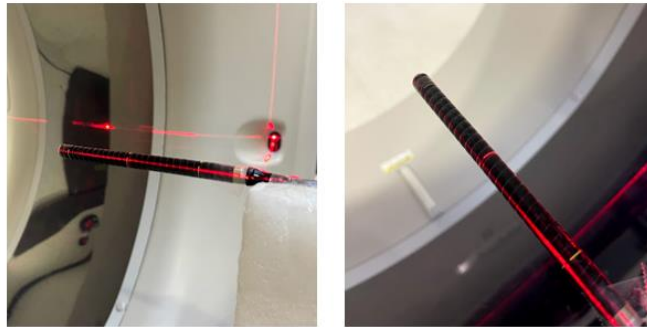


Figure 3.14 Position chamber in stand so beyond couch.

3.7.3 Verification of $CTDI_{vol}$

To verify the volumetric CT Dose Index (CTDI), the following steps were performed:

- The cylindrical PMMA phantoms with holes for insert the pencil ionization chamber in the 16 and 32 cm diameters was positioned on the couch. The IC chamber was first placed at the central position of the phantom as illustrated in Figure 3.15.
- Adjusted couch position so PMMA phantoms along axis of scanner and beam centered at central point of PMMA phantoms and IC chamber.
- The scan parameters were 100 mA, 1 sec scan time, 240 and 500 mm FOV for head and body protocol measurements at kVp setting of 80, 100, 120 and 135 in axial volume mode for Toshiba, and 120 kVp for Siemens.
- Computed Tomography Dose Index (CTDI) displayed on the CT monitor console and pencil ionization chamber were recorded and scanned three times for each kVp setting.
- Recorded all data for the CTDI in PMMA phantom measurement.
- Repeat for peripheral positions (north, south, east & west)
- The data shown on dosimeter will be calculated for $CTDI_{vol}$ and compared to the displayed values on CT monitor console. The agreement between displayed value and measured value must be within 20% (24) (25).

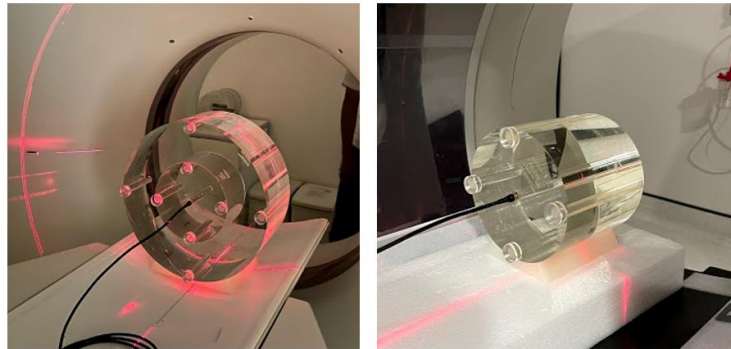


Figure 3.15 Positioning of the cylindrical PMMA phantoms for CTDI measurement.

3.7.4 Image quality evaluation

The Catphan® 700 phantom was used for evaluating the performance of CT scanner study in part of the image quality. The Catphan® 700 phantoms are designed so all test sections can be located by precisely indexing the table from the center of section 1 (CTP682) to the center of each subsequent test module as shown in figure 3.16.

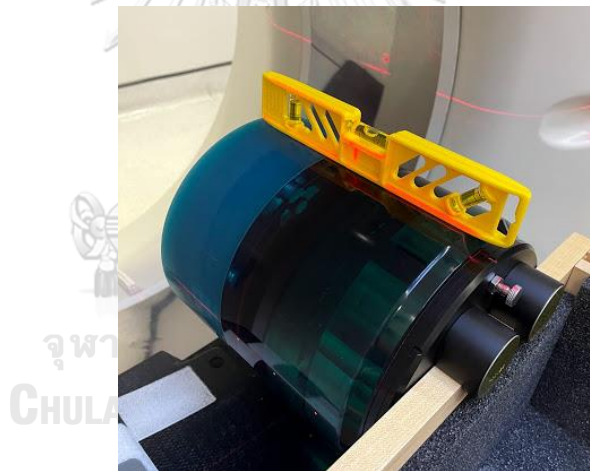


Figure 3.16 Catphan® 700 phantom.

3.7.5 Verify organ doses calculated from the Radimetrics program using the Rando phantom and radiophotoluminescent glass dosimeter.

3.7.5.1 The organ doses were measured using the anthropomorphic Rando phantom (female) inserted with radiophotoluminescent glass dosimeters (RPLGDs) following the scanning techniques that used in clinical protocol to verify the organ doses calculated by Radimetrics dose monitoring program. The scanning techniques for Toshiba machines were 120 kVp, 120 mAs, pitch 0.813, slice thickness 2 mm, and scan time 0.5 sec. For Siemens used 120 kVp, 220 mAs, pitch 1, slice thickness 2 mm, and scan time 0.5 sec.

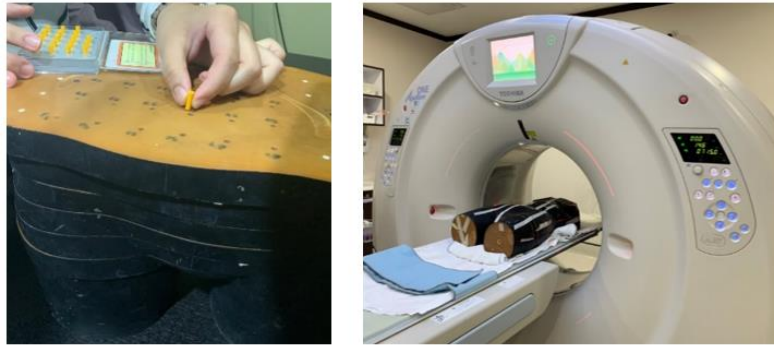


Figure 3.17 The anthropomorphic Rando phantom inserted with radiophoto luminescent glass dosimeters (RPLGDs).

3.7.5.2 Reading out of accumulated value and saving readout data file.

3.7.5.3 The tabulations of organ dose conversion coefficients for using in CT have been provided by the GSF and the NRPB in order to calculate the organ doses. Both sets of tabulations provide conversion coefficients for a series of CT slices that cover the length of the patient (25) (26). The features of these tabulations are described below. The conversion coefficients are normalized to the air kerma measured free in air on the axis of the scanner, K_i , thus:

$$D_T = c_{D_T, K_i} K_i \quad \text{equation 3.1}$$

c_{D_T, K_i} = The conversion coefficients (26)

3.7.5.4 The organ doses were compared between the Glass dosimeter and the Radimetrics program and the difference of the measurement should be within 20%. The organs doses were measured in the liver, pancreas, stomach, spleen, gallbladder, adrenal, kidney, colon, small intestine, bladder, ovary, and uterus.

3.7.6 Collect patient data who underwent abdomen CT examination from Radimetrics software as followings:

- Sub-divided patient age into 0, 1, 5, 10 and 15 years old following Radimetrics program.
- Patient information including gender, patient height, body weight.
- $CTDI_{vol}$ and DLP from CT monitor or PACS system
- Scanning parameters (CT scanner, kVp, mAs, scan length, beam collimation, pitch, rotation time, scan length, and scan field of view) as shown in Table 3.5 and 3.6.

Table 3.5 Scanning parameters technique of Siemens Somatom Sensation

Age	kVp	mAs	Rotation Time (s)	Slice Thickness (mm)	Pitch	Collimation	Scan Field of View
Child	80	AEC	0.5	2	1.4	28.78	500
Adult	120-135	AEC	0.5	2	1	28.78	500

Table 3.6 Scanning parameters technique of Toshiba Aquilion ONE

Age (year)	kVp	mAs	Rotation Time (s)	Slice Thickness (mm)	Pitch	Collimation	Scan Field of View
0	80	AEC	0.35	5	0.638	40	240
1	80	AEC	0.35	2	0.638	40	240
5	100	AEC	0.5	2	0.813	40	320
10	120	AEC	0.5	2	0.813	40	320
15	120	AEC	0.5	2	0.813	40	400

3.7.7 Calculate the organ dose based on patient age computational phantom model using the Radimetrics Monte Carlo-based program. The organs were defined as ellipsoids, cylinders, or spheres, as in the original description by Cristy and Eckerman (23). The patient to phantom mapping for patient dose calculation is based on age, gender, weight, and diameter. The criteria for age and gender mapping are listed in Table 3.7. The simulations are pre-run for various scan protocols with different parameters (such as kVp) for each phantom in library. In each run, the phantom is “scanned” from head to toe along the z-axis in a series of slices. At each slice position, the energy deposited in each organ is recorded and stored in a lookup table.

Table 3.7 Patient-phantom age and gender mapping.

Patient age range	Matched phantom
0 month < age ≤ 5 months	Newborn (F, M)
5 months < age ≤ 3 yrs.	Age 1 (F, M)
3 yrs. < age ≤ 7.5 yrs.	Age 5 (F, M)
7.5 yrs. < age ≤ 12.5 yrs.	Age 10 (F, M)
age > 12.5 yrs.	Age 15 (F); Adult (M)

When a CT exam is sent to the Radimetrics, the scan parameters and patient information are used to determine which simulation is run under the setup that is the closest to the actual exam, and the lookup table from that simulation is used. For a given procedure, the total energy deposited in each

organ is the sum of the deposited energy from all slices that fall in the scan region. The absorbed organ dose is then the total energy deposited in each organ divided by the total mass of the organ regardless of whether that organ is fully or partially irradiated (23). Total organ dose is calculated first for each slice using the $CTDI_{vol}$ at that slice and then summed over the slices that all into the scan region: The organ dose can be calculated using the equation as follows:

$$D_{organ} = \sum_i (coeff * CTDI_{vol_i}) \quad \text{equation 3.2}$$

where *coeff* is the ratio of the simulated organ to the simulated $CTDI_{vol}$, and *i* indicates slice specific values.

The absorbed dose is converted to an equivalent dose using the radiation-weighting factor that accounts for the different damaging effects of different types of radiation. The radiation-weighting factor for x-ray is 1; therefore, the equivalent dose is the same as absorbed dose in this case.

3.7.8 Calculate the effective dose based on patient age computational phantom model using the Radimetrics Monte Carlo-based program. The effective dose (mSv) is defined as the sum of equivalent doses from all organs, weighted by tissue weighting factors to reflect their different radiation sensitivities:

$$E = \sum_T W_T H_T \quad \text{equation 3.3}$$

where H_T is the equivalent organ dose, W_T is the tissue weighting factor.

For Radimetrics, the effective dose is directly calculated using Monte Carlo simulations and not from the measured dose-length product (DLP) using k-factors. The k-factor is a convenient way of estimating the effective dose and is estimated through Monte Carlo simulations as well, however there are significant limitations: a) the k-factors in the published studies are based on phantoms that represent the average of the population b) the k-factors are estimated for a few protocols with specific start and end scan positions [25].

3.7.9 Determine the local diagnostic reference level for pediatrics abdominal CT. To establish LDRL for Praram9 Hospital, $CTDI_{vol}$ and DLP for CT were calculated the median values and 75th percentile of dose quantities. The age groups classified following the criteria of European Commission (EC). European Guidelines on DRLs for Paediatric Imaging, 2016 (27) as shown in Table 3.8.

Table 3.8 Weight grouping for pediatric diagnostic reference levels (DRLs) recommended by the European Guidelines on DRLs for pediatric imaging and approximate equivalent ages (EC, 2016), and age groups used for earlier surveys.

Description	Weight group (kg)	Age group based on weight-for-age charts	Most common age groups used for the previous national DRLs (years)
Neonate	<5	<1 month	0
Infant, toddler, and early childhood	5–<15	1 month to <4 years	1
Middle childhood	15–<30	4–<10 years	5
Early adolescence	30–<50	10–<14 years	10
Late adolescence	50–<80	14–<18 years	15

3.7.10 Analyze the data and compare with the radiation doses in pediatrics abdominal CT from literatures.

3.8 Outcome measurements

- Patient-specific organ dose in pediatrics patient
- Effective dose
- Size specific dose estimate (SSDE)
- Correlation between age and patient-specific organ dose
- Correlation between body weight and patient-specific organ dose
- Local diagnostic reference level for pediatrics abdominal CT at Praram9 hospital

3.9 Statistical analysis

- Maximum, Minimum, Mean, Median, Standard deviation (SD)
- 75th Percentile
- The correlation between age, weight and patient-specific organ dose will be analyzed by Pearson correlation coefficients (r).

3.10 Sample size determination

The pediatric patient underwent abdominal CT examination during January 2017- Dec 2020 were collected.

Sample size determination

$$n = \frac{Z_{\alpha/2}^2 \sigma^2}{d^2} \quad \text{equation 3.4}$$

where

- $Z_{\alpha/2}$ = 95% confidence interval
- σ^2 = 0.9 (variance of data)

$$\begin{aligned}
 d &= 20 \% \text{ Acceptable error for Radiography} \\
 n &= \frac{1.96^2 \times 0.9^2}{0.2^2} \\
 n &= 77.79
 \end{aligned}$$

Alternatively, this prospective study will be conducted in pediatric abdominal CT from Jan 2017 -May 2020 consecutively.

3.11 Target population

The pediatric patients aged between 0-15 years underwent abdominal CT examination during January 2017- May 2020 at Praram9 hospital were collected as target population. The patient's body weight was classified in the range in accordance with Radimetrics Program.

3.11.1 Inclusion criteria

- Patient aged 0-15 years who underwent abdomen CT examination.
- Patient data analyzed from CT Toshiba's Aquilion ONE, 320-detector row and CT Siemens SOMATOM Sensation 64 Detector Praram9 Hospital
- CT scan protocol using automatic exposure control systems (AEC)
- Non-contrast CT of abdomen CT examination

3.11.2 Exclusion criteria

- Patient's images with patient motion and does not cover region of interest.
- Patient has a metallic foreign body in the CT image.

3.12 Ethic consideration

This research involves the determination of patient dose in Computed Tomographic. The patient data were collected during the period from January 2017- May 2020 at Praram9 hospital. The research proposal has been submitted and approved by Institutional Review Board (IRB) of the Faculty of Medicine, Chulalongkorn University and Praram9 Hospital, Bangkok, Thailand.

CHAPTER V

RESULTS

4.1 Quality control of the multidetector computed tomography canner: Toshiba Aquilion ONE and Siemens Somatom Sensation

The quality control of CT scanner was performed following IAEA Human Health Series N0.19 (24). The details of quality control results of CT scanners with the summarized reports of CT scanner performance testing are described in Appendix B.

Table 4.1 Summary reports of CT system performance and physics testing at Radiology Department, Praram9 Hospital.

Program	Manufacturer	
	TOSHIBA	SIEMENS
	Model: AQUILION ONE	Model:SOMATOM
	Install date:17 January 2013.	sensation
	Date: 4 April 2021	Install date: July 1992.
		Date: 4 April 2021
Scan localization light accuracy	Pass	Pass
Alignment of table to gantry	Pass	Pass
Table increment accuracy	Pass	Pass
Reproducibility of CT numbers	Pass	Pass
mAs linearity	Pass	Pass
Linearity of CT Numbers	Pass	Pass
Accuracy of distance measurement	Pass	Pass
High contrast resolution	Pass	Pass
Low contrast detectability	Pass	Pass
Slice thickness accuracy	Pass	Pass
Image uniformity	Pass	Pass
CTDI verification	Pass	Pass

4.2 Verification of organ doses: Radimetrics Program

The %difference of the organ doses between the glass dosimeter and the Radimetrics program can be defined as the following equation:

$$\% \text{Difference} = \frac{\text{organ doses from Radimetrics} - \text{organ doses from glass dosimeter}}{\text{organ doses from glass dosimeter}} \times 100$$

Table 4.3 Comparison of organ doses between Glass dosimeter and Radimetrics (Toshiba).

Organs	Glass dosimeter Air Kerma (mGy) at position				Organ doses (mGy)			
	1	2	3	Average	D_T $= c_{D_T, K_i} K_i$	Radimetrics	% Difference	
Liver	35.85	30.30	33.18	33.11	31.26	26.74	-14.47	
Pancreas	30.42	21.90	31.83	28.05	24.70	22.30	-9.70	
Stomach	38.88	31.84	31.68	34.13	32.06	27.54	-14.09	
Spleen	27.21	27.99	28.22	27.81	26.70	26.40	-1.12	
Adrenal	28.15	28.28	n/a	28.22	24.14	23.48	-2.74	
Kidney	34.04	35.64	n/a	34.84	32.39	28.66	-11.53	
Colon	33.76	32.45	36.17	29.28	26.48	24.68	-6.81	
Small intestine	30.44	29.24	33.02	30.90	27.92	24.15	-13.51	
Bladder	21.08	22.08	28.06	23.74	21.52	27.26	26.69	
Ovaries	21.96	24.84	22.40	23.07	20.95	23.86	13.87	
Uterus	20.60	22.28	20.63	21.31	18.09	23.83	31.76	
				Minimum				-14.47
				Maximum				31.76

By measuring the organ doses and compared them with the calculation by Radimetrics in Siemens CT scanner, it was found that the organs with the largest difference were the uterus, with the difference of 51.85% between glass dosimeter measurement and Radimetrics.

Table 4.3 Comparison of organ doses between Glass dosimeter and Radimetrics (Toshiba).

By measuring the doses and compared them with Radimetrics for Toshiba Aquilion ONE scanner, it was found that the organ with the largest difference was the uterus, which had a difference of 31.76% in between glass dosimeter and Radimetrics.

Figure 4.1-4.2 show the comparison of organ doses between glass dosimeter and Radimetrics on Siemens and Toshiba CT scanners. We observed that organ doses calculated by Radimetrics were greater than glass dosimeter in all organs except pancreas in Siemens CT scanner and small intestine, colon, kidney, adrenal, spleen, stomach, pancreas and liver in Toshiba CT scanner.

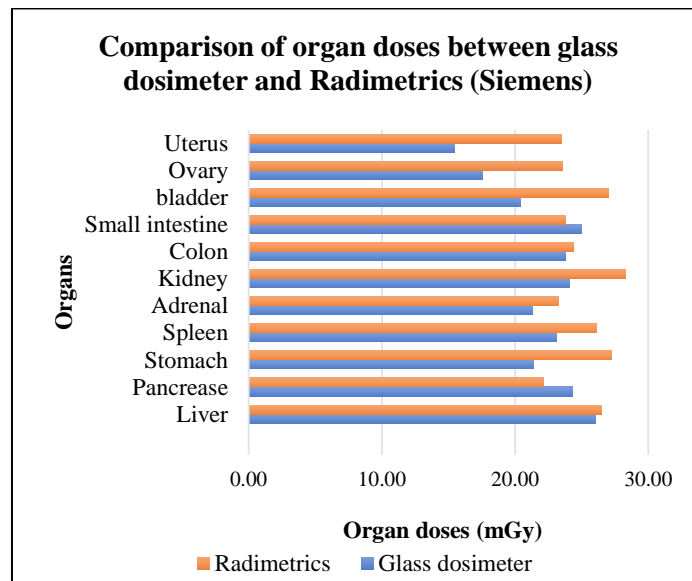


Figure 4.1 Comparison of organ doses between glass dosimeter and Radimetrics (Siemens).

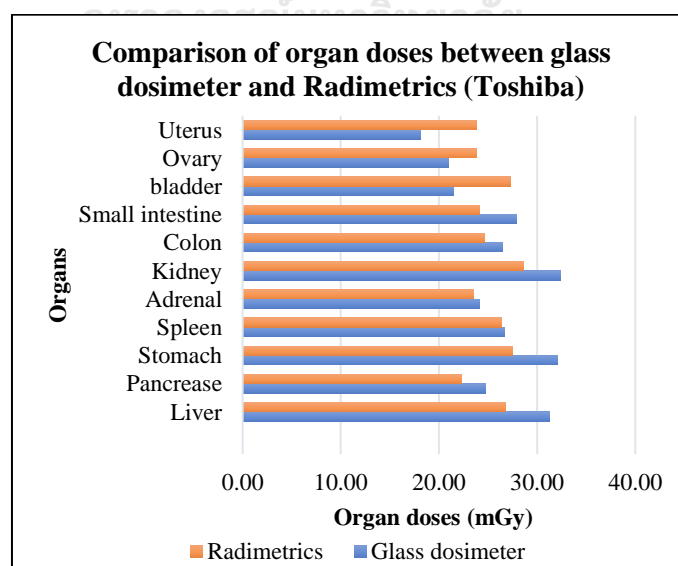


Figure 4.2 Comparison of organ doses between glass dosimeter and Radimetrics (Toshiba).

4.3 Patient data and radiation dose determined from abdominal CT examination.

For this work, the retrospective data were collected from 78 pediatric patients who underwent single phase with and without contrast abdominal CT, age ranged between 0-15 years old, scanned by CT Toshiba Aquilion ONE, 320-row detector and Siemens Somatom Sensation 64-detector-row from January 2017- May 2020 at Praram9 Hospital.

4.3.1 Patient characteristics of abdominal CT examination

The pediatric patients were collected from 164 studies, age range 0.15-15.8 years-old, who underwent single phase abdominal CT. The average patient body weights of 38.59 ± 18.5 kg was obtained in this study. The pediatric patients collected in this study were 112 males and 52 females. The patient demographic is shown in Table 4.4-4.6.

Table 4.4 Patient characteristics of abdominal CT examination.

Patient data	Mean \pm SD	Minimum	Maximum
Age (year)	10.59 ± 3.90	0.15	15.8
Body weight (kg)	38.59 ± 18.5	3.89	94
BMI (kg/m^2)	18.48 ± 4.63	12.14	33.28
Height (cm)	140.2 ± 25.6	48	175

Table 4.5 Patient characteristics of 112 male patients.

Patient data	Mean \pm SD	Minimum	Maximum
Age (year)	10.21 ± 3.99	0.15	15.8
Body weight (kg)	37.27 ± 19.98	3.89	94
BMI (kg/m^2)	18.18 ± 4.58	12.14	32.24
Height (cm)	138.5 ± 27.34	48	175

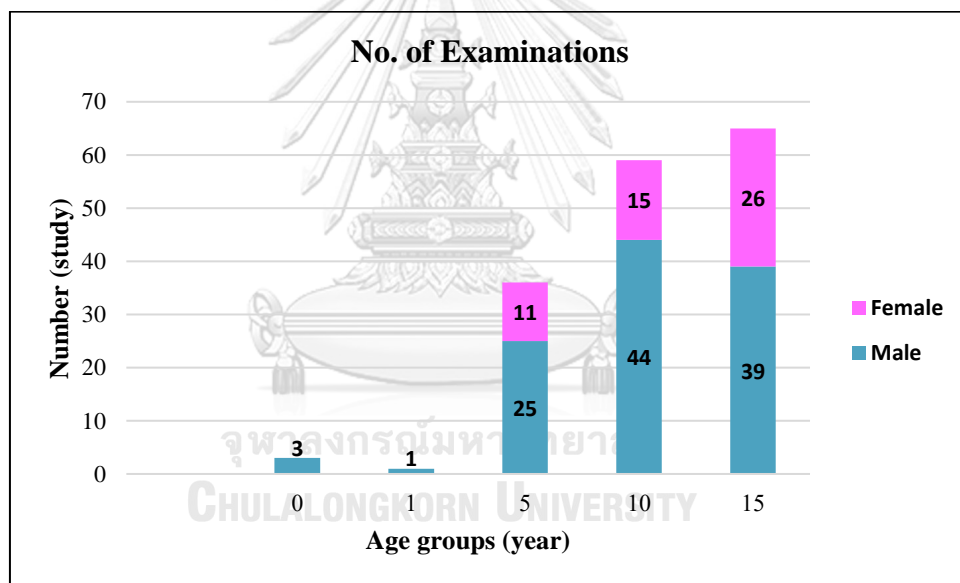
Table 4.6 Patient characteristics of 52 female patients.

Patient data	Mean \pm SD	Minimum	Maximum
Age (year)	11.4 ± 3.60	4.12	15.8
Body weight (kg)	41.43 ± 14.59	15	70.2
BMI (kg/m^2)	19.17 ± 4.7	13.17	33.28
Height (cm)	143.8 ± 21.16	80	172

Table 4.7 No. of CT Examinations collected in pediatric patients 5 groups.

Age Groups (year)	Mean(min-max)	Body weight (kg)	Examination type		
			MDCT whole abdomen	MDCT lower abdomen	Total
0	0.15 yrs.	3.89	3	0	3
1	1.64 yrs.	13	1	0	1
5	5.64 (3.49 yrs. - 7.42 yrs.)	19.5 (15.00-27.40)	20	16	36
10	10.12 (7.75 yrs. - 12.44 yrs.)	34.21 (21.60-57.40)	37	22	59
15	14.38 (12.62 yrs. - 15.8 yrs.)	55.10 (28.60-94.00)	17	48	65
Overall	0-15 yrs.	38.59 (3.89-94.00)	78	86	164

Table 4.7. illustrates the number of patients in each age group. The number of patients in the age groups 0 and 1 were relatively low, i.e., three examinations for the newborn and only one examination for 1-yr-old. Proportional of the number of patients in each age group is shown in figure 4.3.

**Figure 4.3** No. of CT examinations collected in pediatric patients.

4.3.2 Patient radiation dose

Most patient data were carried out by Toshiba CT machines in 133 examinations and otherwise from Siemens machines 31 examinations. The tube voltages ranged between 80 and 135 kVp were adjusted according to the size and age of patients. Table 4.8 depicts the average effective dose (ED) for pediatrics abdominal CT in this study. There were found that the ED of 2.24, 3.23, 4.05, 4.46 and 8.46 mSv and the average SSDE of 2.72, 4.52, 6.15, 7.28 and 14.21 mGy, were seen in newborn, 1, 5, 10 and 15 years-old, respectively.

Table 4.8 Summary of CT scanning technique and patient effective dose.

Age	kVp	mAs	CTDI _{vol} (mGy)	DLP* (mGy.cm)	SSDE* (mGy)	ED* (mSv)
0 (M=3, F=0)	80	22	1-1.1	25.33 (25-25.8)	2.72 (2.71-2.72)	2.24 (2.16-2.29)
1 (M=1, F=0)	80	43	2.1	60.3	4.52	3.23
5 (M=25, F=11)	80-120	28-94	1.7-5.1	97.83 (44.1-170)	6.15 (3.27-10.70)	4.05 (1.92-7.64)
10 (M=44, F=15)	80-120	26-176	1.6-15.3	162.40 (61-516)	7.28 (3.22-26.33)	4.46 (1.86-17.32)
15 (M=39, F=26)	120-135	30-247	3.1-25.9	400.91 (75.5-1142.7)	14.21 (5.68-30.87)	8.46 (1.60-20.64)

* Data presents in average (min-max)

Table 4.9 Effective doses to pediatric abdominal CT from two CT scanners.

Patient age	0y		1y		5y		10y		15y	
Gender	M=3	F=0	M=1	F=0	M=25	F=11	M=44	F=15	M=39	F=26
Effective dose (mSv) ICRP103										
Min	2.16	n/a	3.23	n/a	2.44	1.92	1.89	1.86	1.60	4.83
25 th percentile	2.21	n/a	3.23	n/a	2.93	4.16	2.85	2.94	4.60	7.64
Median	2.25	n/a	3.23	n/a	3.69	5.13	3.17	3.33	6.62	9.26
75 th percentile	2.27	n/a	3.23	n/a	4.11	5.81	6.20	3.75	9.84	10.70
Max	2.29	n/a	3.23	n/a	6.97	7.64	17.32	5.14	20.64	16.61
Mean	2.24	n/a	3.23	n/a	3.68	4.89	4.83	3.38	7.55	9.84
SD	0.07	n/a	n/a	n/a	0.90	1.61	3.13	0.91	4.35	3.03

When considering the effective dose (ED) based on the gender, the high ED were found in female pediatric patients with the average values of 9.26 mSv.

Table 4.10 Organ doses to pediatric abdominal CT from two CT scanners.

Patient age	0y		1y		5y		10y		15y	
Gender	M=3	F=0	M=1	F=0	M=25	F=11	M=44	F=15	M=39	F=26
body weight (kg)	3.89	n/a	13.00	n/a	18.64	21.62	33.64	35.87	56.49	53.02
Organ dose (mGy) (29)										
Adrenals	2.84	n/a	4.03	n/a	4.80	5.96	6.00	4.19	10.93	14.08
Brain	0.01	n/a	0.01	n/a	0.01	0.01	0.00	0.00	0.01	0.01
Breasts	-	n/a	-	n/a	n/a	2.53	n/a	0.25	n/a	1.17
Colon	2.95	n/a	4.52	n/a	5.81	7.24	7.88	5.89	12.90	15.57
Esophagus	2.30	n/a	2.36	n/a	2.29	3.13	2.12	1.42	0.01	4.84
Eye Lenses	0.03	n/a	0.01	n/a	0.01	0.01	0.01	0.00	0.01	0.01
Gall Bladder	3.20	n/a	4.46	n/a	5.58	7.14	7.85	5.60	13.13	16.15
Heart	3.08	n/a	4.02	n/a	2.93	4.61	2.47	1.62	4.41	5.39
Kidneys	3.09	n/a	4.94	n/a	6.23	7.75	8.58	6.02	15.10	18.44
Liver	3.16	n/a	4.87	n/a	5.82	7.32	7.42	5.14	12.77	16.07
Lungs	2.99	n/a	3.29	n/a	2.24	3.44	1.91	1.24	3.57	4.27
Muscle	2.05	n/a	2.88	n/a	3.02	3.98	4.19	3.06	6.59	7.80
Ovaries	-	n/a	-	n/a	n/a	6.72	n/a	5.34	n/a	14.68
Pancreas	2.76	n/a	4.16	n/a	5.21	6.49	6.43	4.34	10.77	13.60
Red Marrow	1.10	n/a	1.56	n/a	2.14	2.89	3.39	2.46	6.12	7.35
Remainder_ICRP103	2.60	n/a	3.71	n/a	4.48	5.77	5.87	4.32	10.13	12.81
Remainder_ICRP60	1.82	n/a	2.57	n/a	2.96	5.71	4.84	4.03	10.03	13.04
Salivary Glands	0.01	n/a	0.01	n/a	0.01	0.01	0.00	0.00	0.01	0.01
Skeleton	5.06	n/a	5.84	n/a	4.43	6.02	5.81	4.16	8.60	10.03
Skin	1.93	n/a	2.80	n/a	2.54	3.42	3.60	2.61	5.79	6.39
Small Intestine	2.96	n/a	4.43	n/a	5.67	7.16	7.81	5.81	13.04	15.72
Spleen	3.03	n/a	4.80	n/a	5.75	7.27	7.44	5.08	12.98	16.14
Stomach	3.19	n/a	4.93	n/a	6.01	7.52	7.98	5.56	13.73	17.07
Testicles	3.53	n/a	6.25	n/a	6.99	-	9.68	n/a	7.76	n/a
Thymus	1.43	n/a	0.51	n/a	0.35	0.60	0.35	0.20	0.81	0.72
Thyroid	0.13	n/a	0.16	n/a	0.09	0.17	0.07	0.05	0.11	0.14
Upper Large Intestine	2.98	n/a	4.65	n/a	5.97	7.41	8.12	6.06	13.72	16.47
Urinary Bladder	3.06	n/a	4.71	n/a	6.03	7.53	8.44	6.42	13.62	16.74
Uterus	-	n/a	-	n/a	n/a	6.73	n/a	5.61	n/a	15.23

Table 4.10 shows the five highest organ doses for 0-yr patients that found in skeleton, testicles, gall bladder, stomach, and liver, with the values of 5.06, 3.53, 3.20, 3.19 and 3.16 mGy, respectively. For 1-yr, the highest organ doses were found in testicles, skeleton, kidneys, stomach and liver with the values of 6.25, 5.84, 4.94, 4.93 and 4.87 mGy, respectively, 5-yr patients were found on female in kidneys, urinary bladder, stomach, upper large intestine, and liver with the values of 7.75, 7.53, 7.52, 7.41 and 7.32 mGy, respectively, 10-yr patients were found on male in testicles, kidneys, urinary bladder, upper large intestine, and stomach with the values of 9.68, 8.58, 8.44, 8.12 and 7.98 mGy, respectively, for 15-yr patients were found on female

in kidneys, stomach, urinary bladder, upper large intestine and spleen, with the values of 18.44, 17.07, 16.74, 16.47 and 16.14 mGy, respectively.

Nine highest organ doses in all age groups were seen in gall bladder, kidneys, liver, skeleton, spleen stomach, testicles, upper large intestine, and urinary bladder, and we found that majority of organ doses were found in kidney, stomach, and urinary bladder (Figure 4.4).

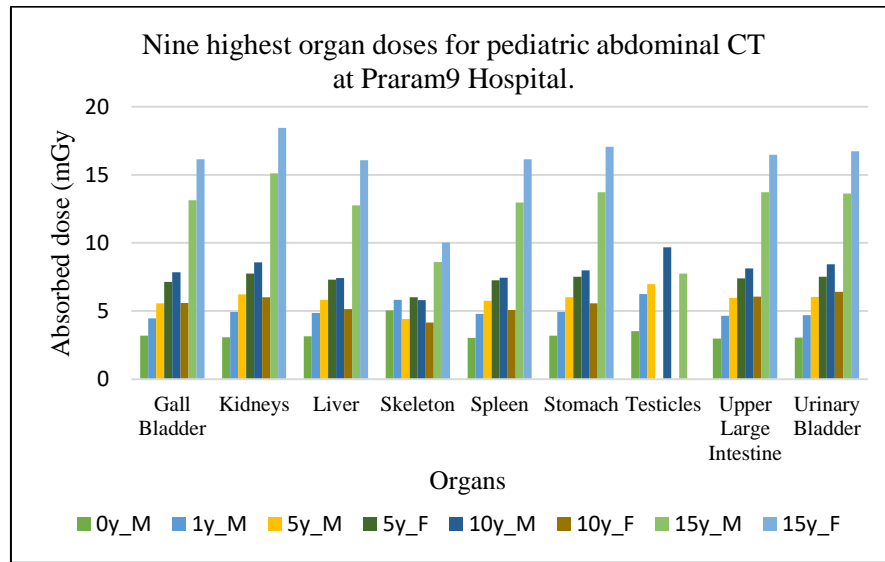


Figure 4.4 Nine highest organ doses found for pediatric abdominal CT at Praram9 Hospital.

When analyzing the organ doses for each CT scanner, it found that the radiation dose was high in 15-year-old female patients who examined the lower abdomen by Siemens CT scanner. The top five organs in this group were found in kidneys, urinary bladder, stomach, spleen, upper large intestine, with the values of 23.82, 22.08, 22.19, 21.02, 21.32 mGy, respectively (Table 4.12).

Table 4.11 Effective doses to pediatric for lower abdominal CT, Siemens.

Patient age	0y		1y		5y		10y		15y	
Gender	M=0	F=0	M=0	F=0	M=0	F=3	M=4	F=2	M=4	F=9
Effective dose(mSv) ICRP 103										
Min	n/a	n/a	n/a	n/a	n/a	5.13	5.09	1.96	4.11	10.07
25 th percentile	n/a	n/a	n/a	n/a	n/a	5.23	6.70	2.70	4.14	10.46
Median	n/a	n/a	n/a	n/a	n/a	5.33	8.67	3.43	4.27	13.04
75 th percentile	n/a	n/a	n/a	n/a	n/a	5.80	10.66	4.17	6.91	14.05
Max	n/a	n/a	n/a	n/a	n/a	6.28	12.34	4.90	14.46	16.61
mean	n/a	n/a	n/a	n/a	n/a	5.58	8.69	3.43	6.78	12.79
SD	n/a	n/a	n/a	n/a	n/a	0.62	3.19	2.08	5.12	2.48
body weight(kg)	n/a	n/a	n/a	n/a	n/a	19.00	46.00	28.40	39.00	54.80

Table 4.12 Organ doses to pediatric for lower abdominal CT, Siemens.

Patient age	0y		1		5y		10y		15y	
Gender	M=0	F=0	M=0	F=0	M=0	F=3	M=4	F=2	M=4	F=9
Organ dose (mGy) (29)										
Adrenals	n/a	n/a	n/a	n/a	n/a	7.32	7.17	4.96	9.84	18.28
Brain	n/a	n/a	n/a	n/a	n/a	0.01	0.01	0.00	0.01	0.01
Breasts	n/a	n/a	n/a	n/a	n/a	0.51	-	0.26	-	1.16
Colon	n/a	n/a	n/a	n/a	n/a	8.84	15.50	5.76	11.55	20.30
Esophagus	n/a	n/a	n/a	n/a	n/a	3.70	1.98	1.47	3.36	6.26
Eye Lenses	n/a	n/a	n/a	n/a	n/a	0.01	0.01	0.00	0.00	0.01
Gall Bladder	n/a	n/a	n/a	n/a	n/a	8.85	14.12	6.00	11.76	20.81
Heart	n/a	n/a	n/a	n/a	n/a	5.12	1.49	1.15	3.66	6.37
Kidneys	n/a	n/a	n/a	n/a	n/a	9.33	16.03	6.59	13.48	23.82
Liver	n/a	n/a	n/a	n/a	n/a	8.98	11.43	5.83	11.48	20.99
Lungs	n/a	n/a	n/a	n/a	n/a	3.76	1.23	0.99	2.93	5.30
Muscle	n/a	n/a	n/a	n/a	n/a	4.80	8.23	2.72	5.81	10.27
Ovaries	n/a	n/a	n/a	n/a	n/a	8.00	-	5.22	-	19.54
Pancreas	n/a	n/a	n/a	n/a	n/a	7.98	10.29	4.99	9.79	17.59
Red Marrow	n/a	n/a	n/a	n/a	n/a	3.56	6.42	2.27	5.43	9.67
Remainder_ICRP103	n/a	n/a	n/a	n/a	n/a	7.01	9.97	4.60	9.03	16.64
Remainder_ICRP60	n/a	n/a	n/a	n/a	n/a	6.88	8.68	4.59	9.57	16.92
Salivary Glands	n/a	n/a	n/a	n/a	n/a	0.01	0.01	0.00	0.01	0.01
Skeleton	n/a	n/a	n/a	n/a	n/a	7.14	11.08	3.54	7.38	13.09
Skin	n/a	n/a	n/a	n/a	n/a	4.04	7.11	2.26	4.83	8.63
Small Intestine	n/a	n/a	n/a	n/a	n/a	8.81	15.19	5.76	11.55	20.30
Spleen	n/a	n/a	n/a	n/a	n/a	8.95	11.98	5.83	11.66	21.02
Stomach	n/a	n/a	n/a	n/a	n/a	9.18	13.43	6.22	12.35	22.19
Testicles	n/a	n/a	n/a	n/a	n/a	-	21.45	-	7.46	-
Thymus	n/a	n/a	n/a	n/a	n/a	0.60	0.29	0.16	0.54	0.95
Thyroid	n/a	n/a	n/a	n/a	n/a	0.23	0.07	0.04	0.07	0.12
Upper Large Intestine	n/a	n/a	n/a	n/a	n/a	8.98	15.81	6.03	12.11	21.32
Urinary Bladder	n/a	n/a	n/a	n/a	n/a	9.15	16.70	6.28	12.63	22.08
Uterus	n/a	n/a	n/a	n/a	n/a	8.15	-	5.50	-	19.86

Table 4.13 Effective doses to pediatric lower abdominal CT TOSHIBA.

Patient age	0y		1y		5y		10y		15y	
Gender	M=0	F=0	M=0	F=0	M=11	F=3	M=12	F=4	M=25	F=10
Effective dose(mSv) ICRP 103										
Min	n/a	n/a	n/a	n/a	2.83	1.92	1.94	3.33	1.60	4.83
25 th percentile	n/a	n/a	n/a	n/a	1.57	2.39	2.59	3.55	4.80	7.03
Median	n/a	n/a	n/a	n/a	1.70	2.87	3.28	3.75	5.75	7.66
75 th percentile	n/a	n/a	n/a	n/a	2.87	3.75	4.89	3.94	7.42	9.68
Max	n/a	n/a	n/a	n/a	4.60	4.64	17.32	4.15	20.64	13.38
mean	n/a	n/a	n/a	n/a	3.59	3.14	4.76	3.74	7.18	8.30
SD	n/a	n/a	n/a	n/a	0.63	1.38	4.19	0.35	4.85	2.41
body weight(kg)	n/a	n/a	n/a	n/a	20.60	23.13	33.48	39.70	57.06	51.73

Table 4.14 Organ doses to pediatric lower abdominal CT TOSHIBA.

Patient age	0y		1y		5y		10y		15y	
Gender	M=0	F=0	M=0	F=0	M=11	F=3	M=12	F=4	M=25	F=10
Organ dose (mGy) (29)										
Adrenals	n/a	n/a	n/a	n/a	4.82	3.69	6.26	5.39	10.85	11.82
Brain	n/a	n/a	n/a	n/a	0.00	0.01	0.00	0.00	0.01	0.01
Breasts	n/a	n/a	n/a	n/a	-	0.53	-	0.40	-	0.58
Colon	n/a	n/a	n/a	n/a	5.73	5.01	8.36	5.88	13.26	13.71
Esophagus	n/a	n/a	n/a	n/a	2.12	1.77	2.01	2.07	3.28	3.59
Eye Lenses	n/a	n/a	n/a	n/a	0.01	0.01	0.01	0.00	0.01	0.01
Gall Bladder	n/a	n/a	n/a	n/a	5.42	4.90	8.41	6.28	13.40	14.22
Heart	n/a	n/a	n/a	n/a	2.31	2.58	1.73	3.02	2.95	3.02
Kidneys	n/a	n/a	n/a	n/a	6.11	5.56	9.04	6.62	15.44	16.28
Liver	n/a	n/a	n/a	n/a	5.75	4.87	7.75	6.15	12.78	13.65
Lungs	n/a	n/a	n/a	n/a	1.82	2.04	1.37	2.21	2.49	2.49
Muscle	n/a	n/a	n/a	n/a	2.89	2.69	3.84	3.08	6.30	6.44
Ovaries	n/a	n/a	n/a	n/a	-	4.70	-	5.10	-	12.87
Pancreas	n/a	n/a	n/a	n/a	5.14	4.15	6.68	5.34	10.74	11.67
Red Marrow	n/a	n/a	n/a	n/a	2.04	1.88	3.35	2.57	5.98	6.13
Remainder_ICRP103	n/a	n/a	n/a	n/a	4.40	3.91	6.06	4.82	10.16	11.10
Remainder_ICRP60	n/a	n/a	n/a	n/a	2.69	4.02	5.58	4.78	10.79	11.29
Salivary Glands	n/a	n/a	n/a	n/a	0.00	0.01	0.00	0.00	0.01	0.01
Skeleton	n/a	n/a	n/a	n/a	4.14	3.98	4.89	4.28	7.87	8.02
Skin	n/a	n/a	n/a	n/a	2.39	2.43	3.10	2.59	5.46	5.04
Small Intestine	n/a	n/a	n/a	n/a	5.55	4.99	8.38	5.86	13.48	13.99
Spleen	n/a	n/a	n/a	n/a	5.67	4.85	7.67	6.14	13.04	13.91
Stomach	n/a	n/a	n/a	n/a	5.92	5.13	8.37	6.44	13.86	14.77
Testicles	n/a	n/a	n/a	n/a	7.22	-	7.90	-	4.37	-
Thymus	n/a	n/a	n/a	n/a	0.28	0.34	0.25	0.33	0.52	0.43
Thyroid	n/a	n/a	n/a	n/a	0.07	0.09	0.05	0.07	0.09	0.11
Upper Large Intestine	n/a	n/a	n/a	n/a	5.88	5.21	8.67	6.12	14.20	14.61
Urinary Bladder	n/a	n/a	n/a	n/a	5.88	5.31	8.85	6.41	13.95	14.90

Patient age	0y		1y		5y		10y		15y	
Gender	M=0	F=0	M=0	F=0	M=11	F=3	M=12	F=4	M=25	F=10
Organ dose (mGy) (29)										
Uterus	n/a	n/a	n/a	n/a	-	4.77	-	5.51	-	13.65

Table 4.15 Effective doses to pediatric whole abdominal CT TOSHIBA.

Patient age	0y		1y		5y		10y		15y	
Gender	M=3	F=0	M=1	F=0	M=14	F=3	M=22	F=8	M=7	F=11
Effective dose(mSv) ICRP 103										
Min	2.16	n/a	3.23	n/a	2.44	3.71	1.89	2.70	4.24	5.90
25 th percentile	2.21	n/a	3.23	n/a	2.69	4.70	2.72	2.99	10.63	7.92
Median	2.25	n/a	3.23	n/a	3.86	5.69	3.06	3.15	9.81	8.32
75 th percentile	2.27	n/a	3.23	n/a	4.34	5.81	3.19	3.50	10.63	9.09
Max	2.29	n/a	3.23	n/a	6.01	5.92	6.12	5.14	11.80	9.42
mean	2.24	n/a	3.23	n/a	3.75	5.11	3.32	3.38	8.78	8.24
SD	0.07	n/a	n/a	n/a	1.09	1.22	1.16	0.77	2.46	1.21
body weight	3.89	n/a	13.00	n/a	17.10	21.00	28.05	35.61	62.06	52.56

Table 4.16 Organ doses to pediatric whole abdominal CT TOSHIBA.

Patient age	0y		1y		5y		10y		15y	
Gender	M=3	F=0	M=1	F=0	M=14	F=3	M=22	F=8	M=7	F=11
Organ dose (mGy) (29)										
Adrenals	2.84	n/a	4.03	n/a	4.79	5.94	4.55	3.66	11.56	11.92
Brain	0.01	n/a	0.01	n/a	0.01	0.01	0.00	0.00	0.01	0.01
Breasts	-	n/a	-	n/a	-	5.43	-	0.20	-	2.04
Colon	2.95	n/a	4.52	n/a	5.88	6.66	5.18	6.25	12.54	12.16
Esophagus	2.30	n/a	2.36	n/a	2.42	3.56	1.71	1.21	5.11	4.80
Eye Lenses	0.03	n/a	0.01	n/a	0.01	0.01	0.00	0.00	0.01	0.01
Gall Bladder	3.20	n/a	4.46	n/a	5.70	6.41	5.42	5.47	13.01	12.92
Heart	3.08	n/a	4.02	n/a	3.42	5.78	2.28	1.20	8.37	7.50
Kidneys	3.09	n/a	4.94	n/a	6.33	7.14	5.80	5.86	14.88	14.62
Liver	3.16	n/a	4.87	n/a	5.88	6.91	5.28	4.76	13.25	13.19
Lungs	2.99	n/a	3.29	n/a	2.56	4.28	1.73	0.93	6.54	5.48
Muscle	2.05	n/a	2.88	n/a	3.13	3.91	2.76	3.27	7.61	6.59
Ovaries	-	n/a	-	n/a	-	6.42	-	5.78	-	11.02
Pancreas	2.76	n/a	4.16	n/a	5.26	6.30	4.58	3.92	11.22	11.21
Red Marrow	1.10	n/a	1.56	n/a	2.22	2.75	2.28	2.60	6.74	6.11
Remainder_ICRP103	2.60	n/a	3.71	n/a	4.54	5.47	4.10	4.23	10.49	10.33
Remainder_ICRP60	1.82	n/a	2.57	n/a	3.17	5.37	3.12	3.67	8.33	10.53
Salivary Glands	0.01	n/a	0.01	n/a	0.01	0.01	0.00	0.00	0.01	0.01
Skeleton	5.06	n/a	5.84	n/a	4.67	6.27	3.89	4.42	10.90	8.98

Patient age	0y		1y		5y		10y		15y	
Gender	M=3	F=0	M=1	F=0	M=14	F=3	M=22	F=8	M=7	F=11
Organ dose (mGy) (29)										
Skin	1.93	n/a	2.80	n/a	2.65	3.40	2.34	2.78	7.00	5.42
Small Intestine	2.96	n/a	4.43	n/a	5.76	6.42	5.17	6.14	12.52	12.30
Spleen	3.03	n/a	4.80	n/a	5.82	6.77	5.30	4.62	13.35	13.04
Stomach	3.19	n/a	4.93	n/a	6.07	7.05	5.57	5.23	13.93	13.76
Testicles	3.53	n/a	6.25	n/a	6.80	-	6.09	-	16.35	-
Thymus	1.43	n/a	0.51	n/a	0.40	0.76	0.33	0.17	1.65	0.85
Thyroid	0.13	n/a	0.16	n/a	0.11	0.16	0.06	0.04	0.16	0.19
Upper Large Intestine	2.98	n/a	4.65	n/a	6.04	6.81	5.39	6.37	13.14	12.88
Urinary Bladder	3.06	n/a	4.71	n/a	6.12	6.90	5.58	6.80	13.19	12.49
Uterus	-	n/a	-	n/a	-	6.16	-	6.00	-	11.51

Table 4.17 Effective doses to pediatric whole abdominal CT Siemens.

Patient age	0y		1y		5y		10y		15y	
Gender	M=0	F=0	M=0	F=0	M=0	F=2	M=6	F=1	M=0	F=0
Effective dose(mSv) ICRP 103										
Min	n/a	n/a	n/a	n/a	n/a	4.61	7.69	1.86	n/a	n/a
25 th percentile	n/a	n/a	n/a	n/a	n/a	5.37	7.69	1.86	n/a	n/a
Median	n/a	n/a	n/a	n/a	n/a	6.13	7.76	1.86	n/a	n/a
75 th percentile	n/a	n/a	n/a	n/a	n/a	6.89	8.24	1.86	n/a	n/a
Max	n/a	n/a	n/a	n/a	n/a	7.64	8.54	1.86	n/a	n/a
mean	n/a	n/a	n/a	n/a	n/a	6.13	7.97	1.86	n/a	n/a
SD	n/a	n/a	n/a	n/a	n/a	2.14	0.39	0.00	n/a	n/a
body weight(kg)	n/a	n/a	n/a	n/a	n/a	24.20	46.20	37.60	n/a	n/a

Table 4.18 Organ doses to pediatric whole abdominal CT Siemens.

Patient age	0y		1y		5y		10y		15y	
Gender	M=0	F=0	M=0	F=0	M=0	F=2	M=6	F=1	M=0	F=0
Organ dose (mGy) (29)										
Adrenals	n/a	n/a	n/a	n/a	n/a	7.39	10.07	2.05	n/a	n/a
Brain	n/a	n/a	n/a	n/a	n/a	0.01	0.01	0.00	n/a	n/a
Breasts	n/a	n/a	n/a	n/a	n/a	4.19	-	0.07	n/a	n/a
Colon	n/a	n/a	n/a	n/a	n/a	9.07	11.71	3.32	n/a	n/a
Esophagus	n/a	n/a	n/a	n/a	n/a	3.66	3.96	0.49	n/a	n/a
Eye Lenses	n/a	n/a	n/a	n/a	n/a	0.01	0.02	0.49	n/a	n/a
Gall Bladder	n/a	n/a	n/a	n/a	n/a	9.05	11.45	3.08	n/a	n/a
Heart	n/a	n/a	n/a	n/a	n/a	5.12	5.27	0.32	n/a	n/a
Kidneys	n/a	n/a	n/a	n/a	n/a	9.61	12.90	3.80	n/a	n/a
Liver	n/a	n/a	n/a	n/a	n/a	9.11	11.89	2.83	n/a	n/a
Lungs	n/a	n/a	n/a	n/a	n/a	3.81	4.09	0.28	n/a	n/a

Patient age	0y		1y		5y		10y		15y	
Gender	M=0	F=0	M=0	F=0	M=0	F=2	M=6	F=1	M=0	F=0
Organ dose (mGy) (29)										
Muscle	n/a	n/a	n/a	n/a	n/a	4.77	7.44	2.08	n/a	n/a
Ovaries	n/a	n/a	n/a	n/a	n/a	8.28	-	2.98	n/a	n/a
Pancreas	n/a	n/a	n/a	n/a	n/a	8.06	10.12	2.38	n/a	n/a
Red Marrow	n/a	n/a	n/a	n/a	n/a	3.61	5.50	1.33	n/a	n/a
Remainder_ICRP103	n/a	n/a	n/a	n/a	n/a	7.17	9.27	2.48	n/a	n/a
Remainder_ICRP60	n/a	n/a	n/a	n/a	n/a	7.00	7.11	2.88	n/a	n/a
Salivary Glands	n/a	n/a	n/a	n/a	n/a	0.01	0.01	0.00	n/a	n/a
Skeleton	n/a	n/a	n/a	n/a	n/a	7.03	11.21	2.91	n/a	n/a
Skin	n/a	n/a	n/a	n/a	n/a	3.97	6.86	2.01	n/a	n/a
Small Intestine	n/a	n/a	n/a	n/a	n/a	9.08	11.44	3.19	n/a	n/a
Spleen	n/a	n/a	n/a	n/a	n/a	9.11	11.76	3.00	n/a	n/a
Stomach	n/a	n/a	n/a	n/a	n/a	9.34	12.42	3.26	n/a	n/a
Testicles	n/a	n/a	n/a	n/a	n/a	-	18.59	-	n/a	n/a
Thymus	n/a	n/a	n/a	n/a	n/a	0.76	0.65	0.05	n/a	n/a
Thyroid	n/a	n/a	n/a	n/a	n/a	0.24	0.12	0.01	n/a	n/a
Upper Large Intestine	n/a	n/a	n/a	n/a	n/a	9.26	11.93	3.40	n/a	n/a
Urinary Bladder	n/a	n/a	n/a	n/a	n/a	9.35	12.59	3.74	n/a	n/a
Uterus	n/a	n/a	n/a	n/a	n/a	8.39	-	3.10	n/a	n/a

4.4 Factors affecting organ doses in pediatric patients.

4.4.1 Correlation between age and patient-specific organ dose

A higher organ dose was found with older age groups, because the average sizes of patient were increased. (Figure 4.5)

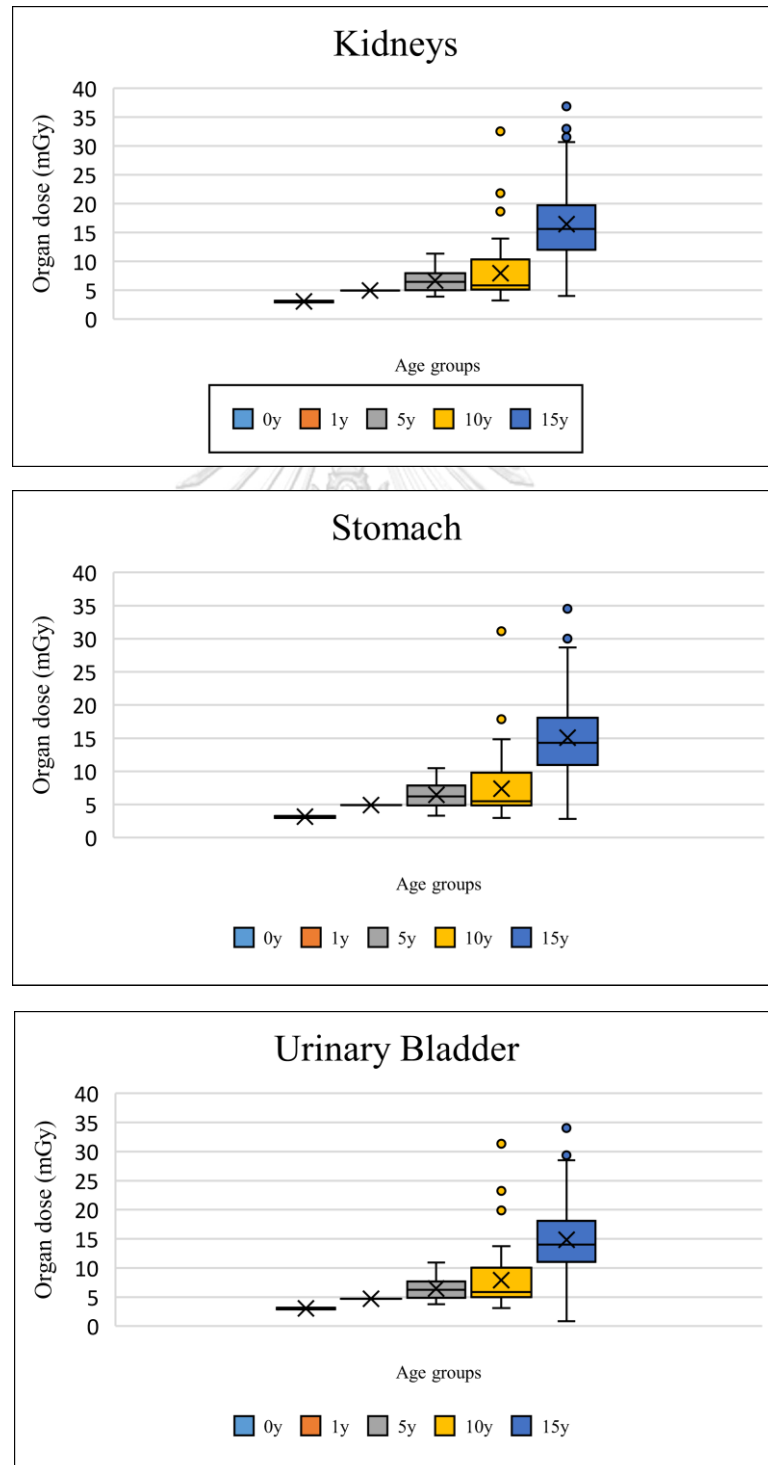


Figure 4.5 The highest organ doses for pediatric abdominal CT.

4.4.2 Correlation between body weight and patient-specific organ dose

Plot graph for the relationship between $CTDI_{vol}$ and body weight, and the correlation between $CTDI_{vol}$ and age, the results are shown in figure 4.6-4.9 and the correlation between SSDE and body weight, and the relationship between $CTDI_{vol}$ and age, the results are shown in figure 4.10-4.13

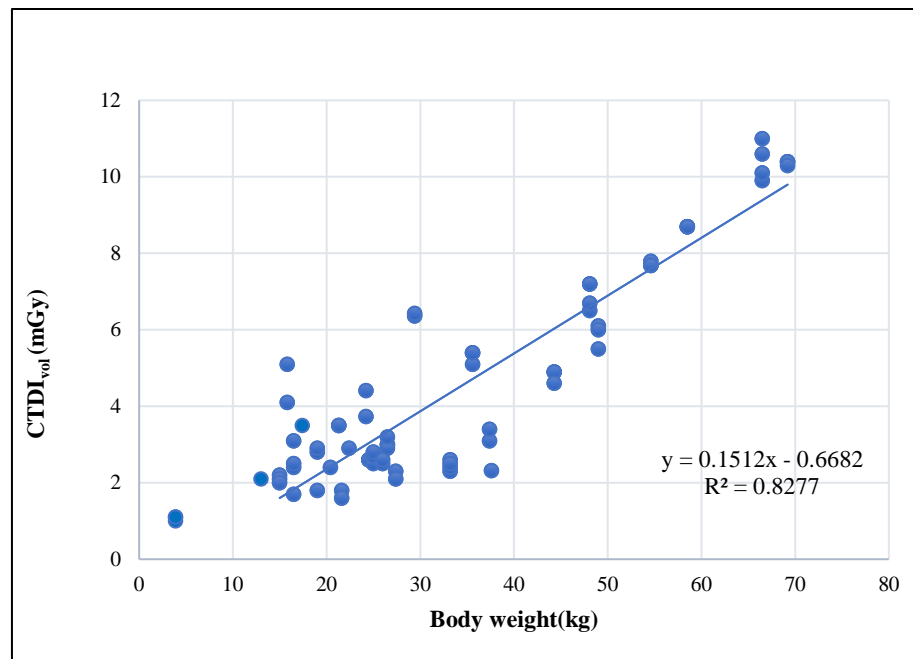


Figure 4.6 Correlation between $CTDI_{vol}$ and body weight for CT whole abdomen

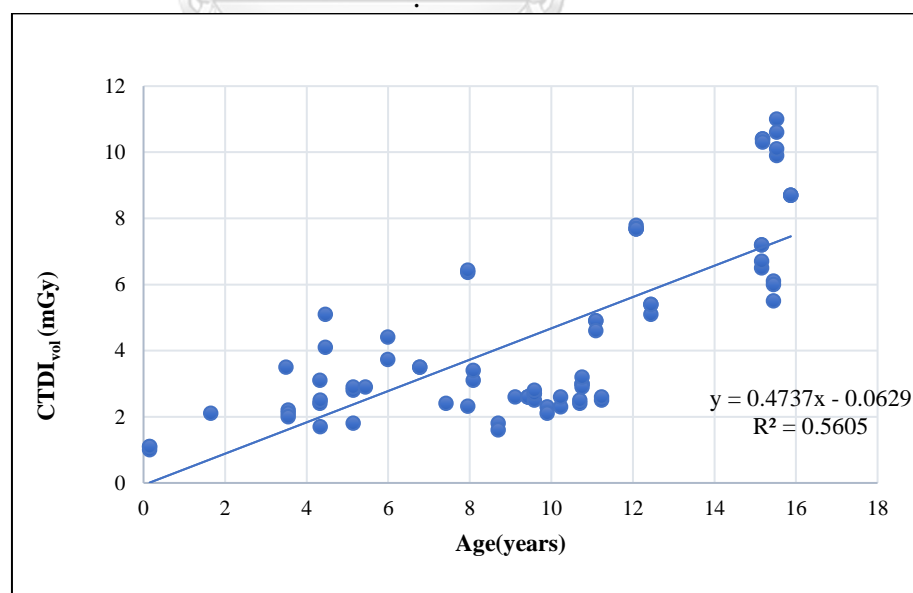


Figure 4.7 Correlation between $CTDI_{vol}$ and patient age for CT whole abdomen.

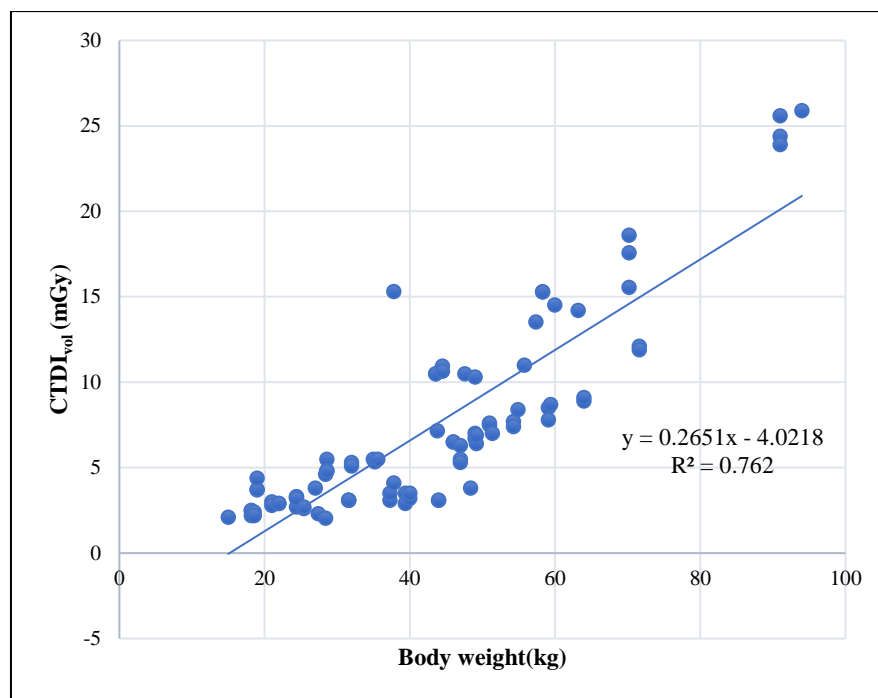


Figure 4.8 Correlation between CTDI_{vol} and body weight for CT lower abdomen.

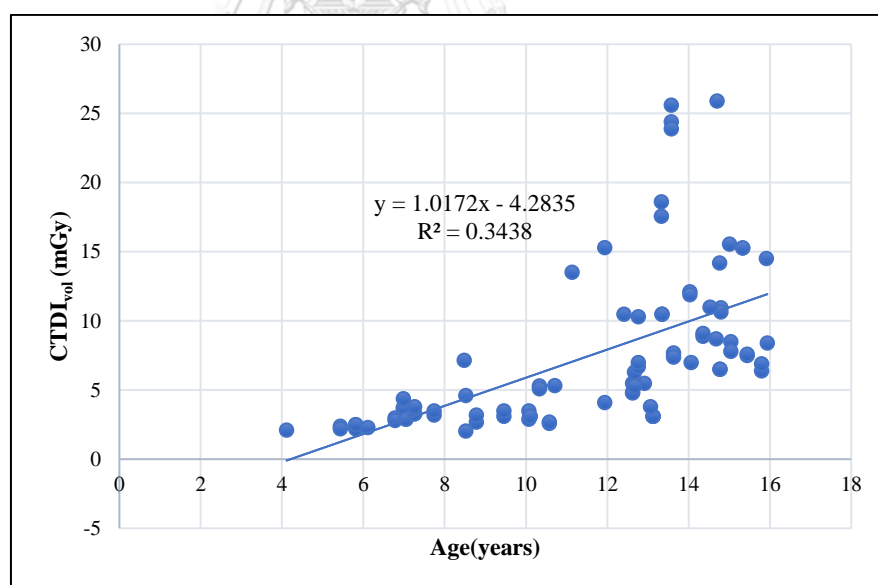


Figure 4.9 Correlation between CTDI_{vol} and patient age for CT lower abdomen.

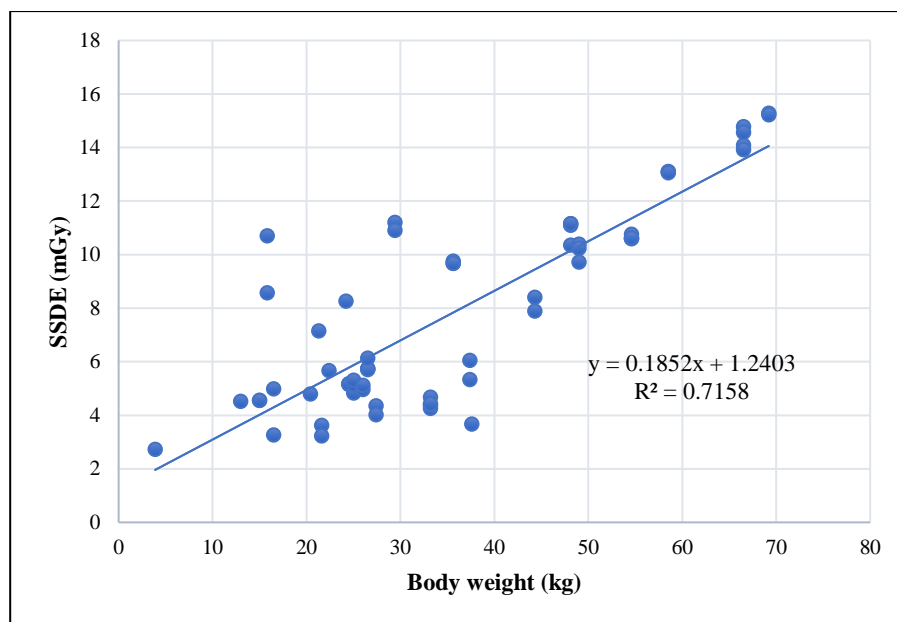


Figure 4.10 Correlation between SSDE and body weight for CT whole abdomen.

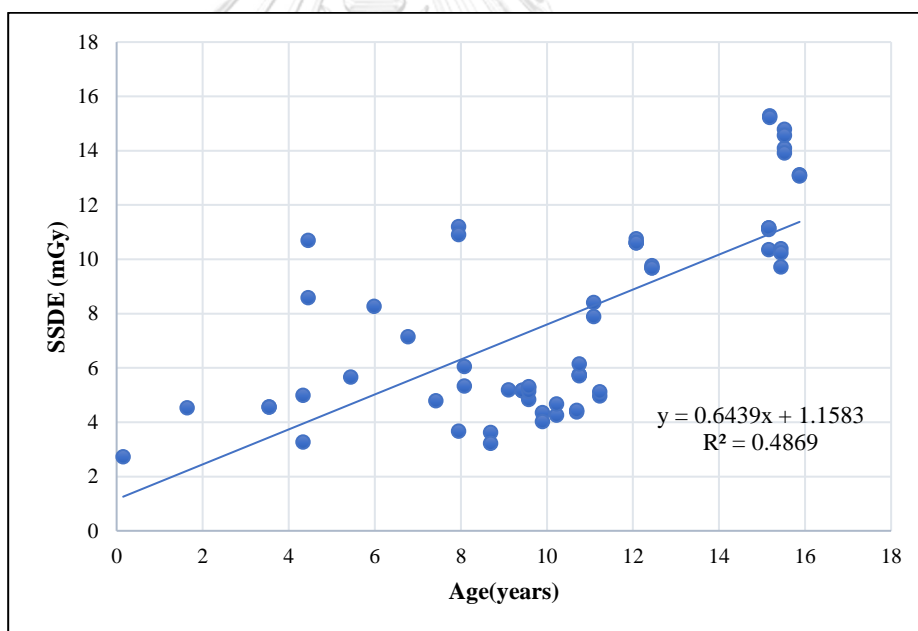


Figure 4.11 Correlation between SSDE and patient age for CT whole abdomen.

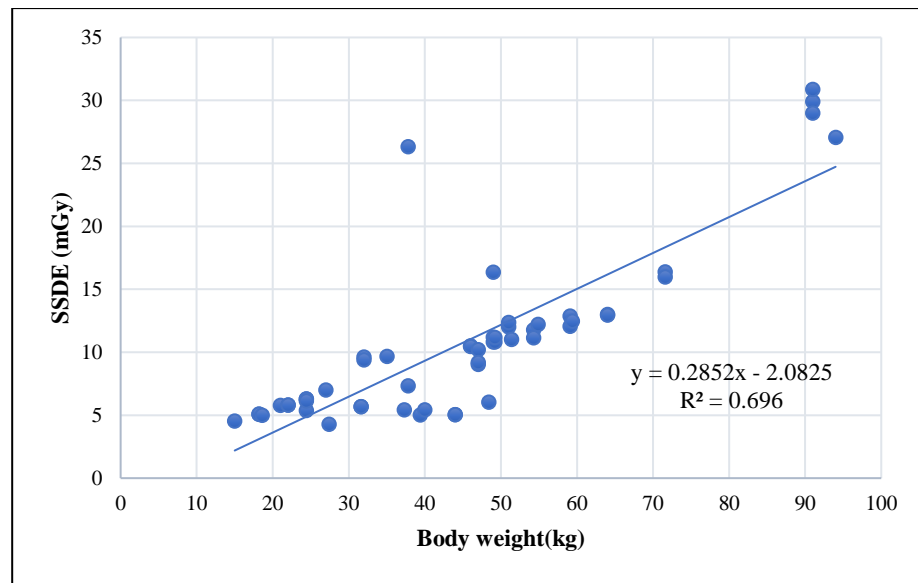


Figure 4.12 Correlation between SSDE and body weight for CT lower abdomen.

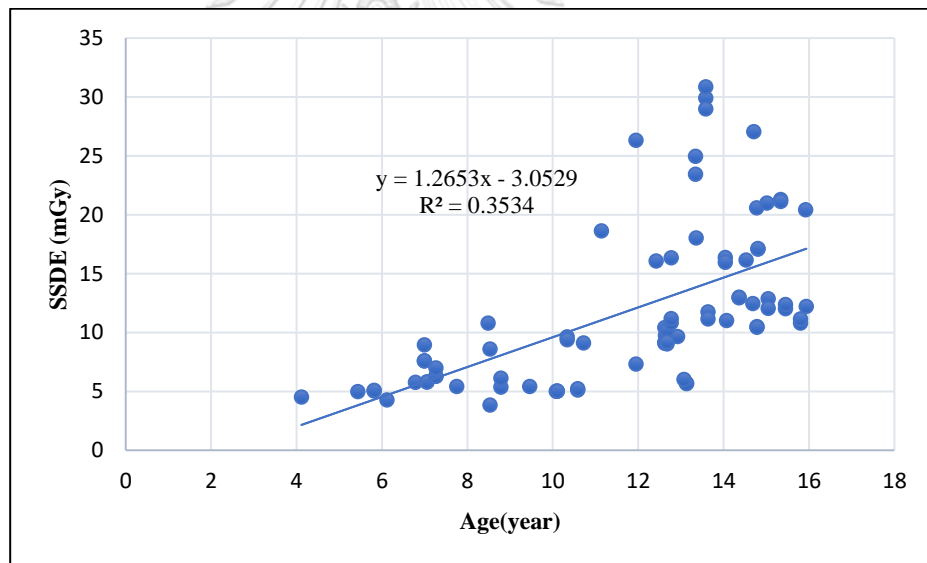


Figure 4.13 Correlation between SSDE and patient age for CT lower abdomen.

Strong correlation was found between $CTDI_{vol}$ and body weight, whereas moderate correlation was found between $CTDI_{vol}$ and age. When consider in SSDE, strong correlation was found between SSDE and body weight, whereas moderate correlation was found between SSDE and age.

4.4.3 Correlation between gender and patient-specific organ dose

The figure 4.14-4.17 showed correlation between gender and absorbed organ dose, it was found that in the most of age groups, female patients tended to have higher radiation dose than male patients except for age group 10 years.

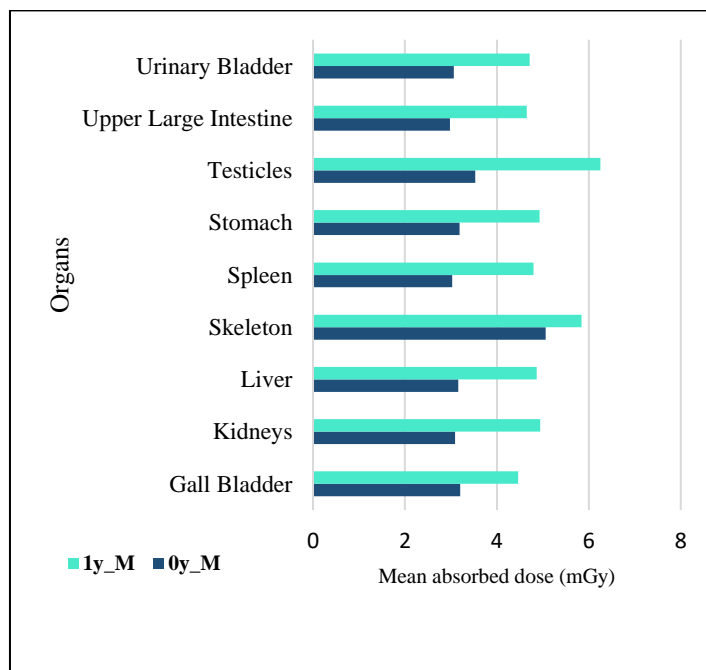


Figure 4.14 Nine organ doses for 0-1 yrs pediatric abdominal CT.

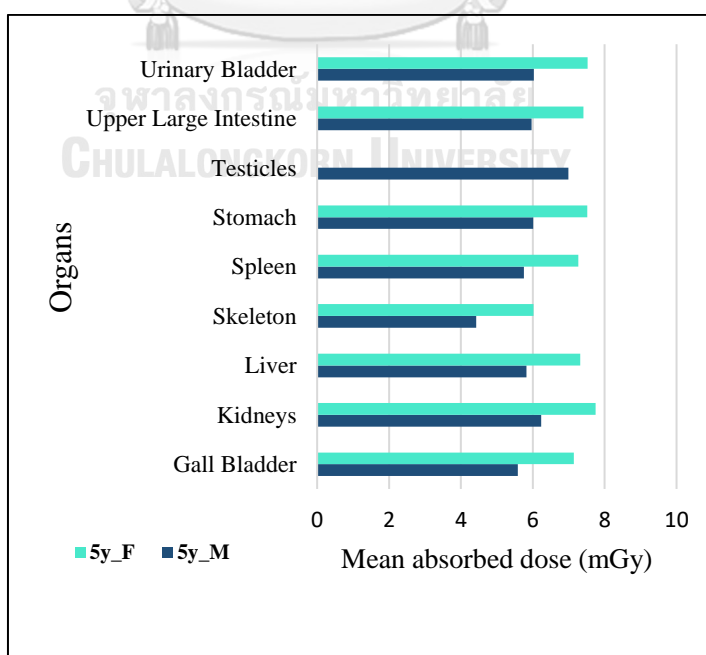


Figure 4.15 Nine organ doses for 5 yrs pediatric abdominal CT.

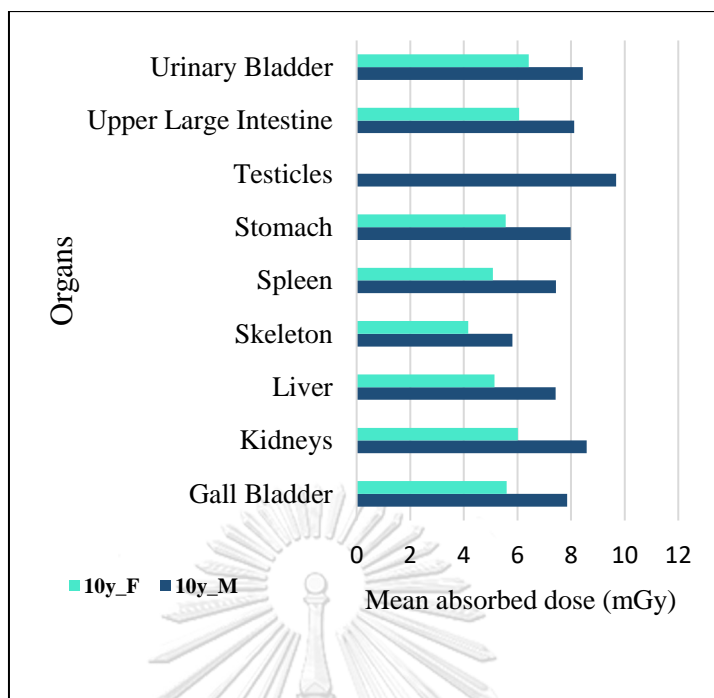


Figure 4.16 Nine organ doses for 10-yrs pediatric abdominal CT.

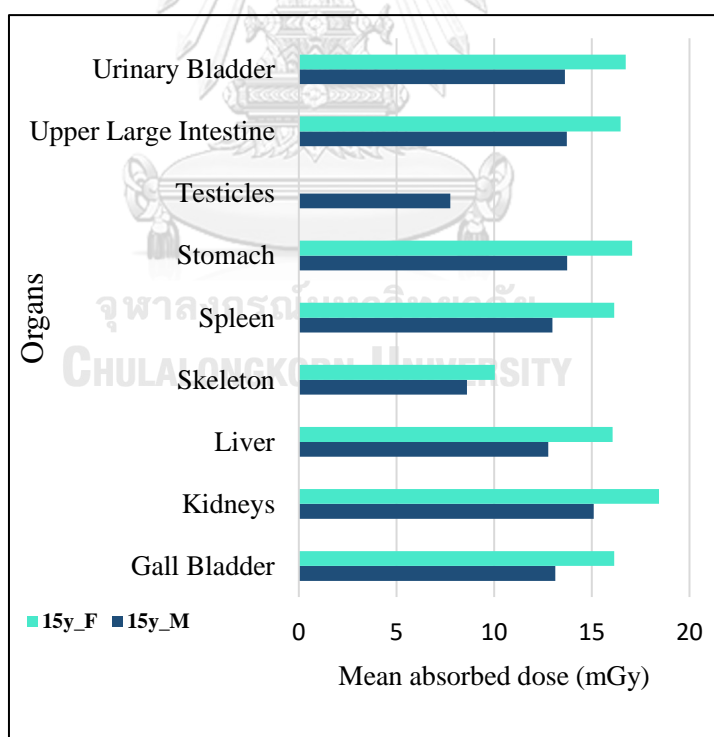


Figure 4.17 Nine organ doses for 15-yrs pediatric abdominal CT.

4.5 Local diagnostic reference level (LDRL) for pediatrics abdominal CT at Praram9 Hospital

In descriptive statistics, a boxplot was used in explanatory data analysis. Box plots visually show the distribution of numerical data and skewness through displaying the data quartiles (or percentiles) and averages. A box plot is constructed from five values: The minimum value is the lowest score, excluding outliers (shown at the end of the bottom whisker). The first quartile is 25 percent of scores fall below the lower quartile value (also known as the first quartile). The median is the mid-point of the data and is shown by the line that divides the box into two parts (sometimes known as the second quartile). The third quartile is 75 percent of the scores fall below the upper quartile value (also known as the third quartile). Thus, 25% of data are above this value. The maximum value is the highest score, excluding outliers (shown at the end of the top whisker). The two whiskers extend from the first quartile to the smallest value and from the third quartile to the largest value.

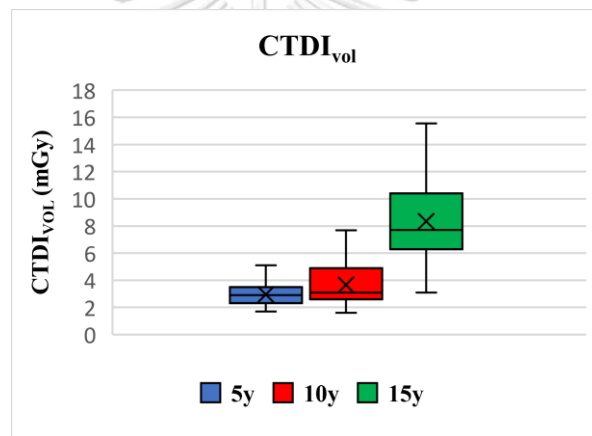


Figure 4.18 Comparisons of median and 75th percentile of CTDI_{vol} for various pediatric age groups.

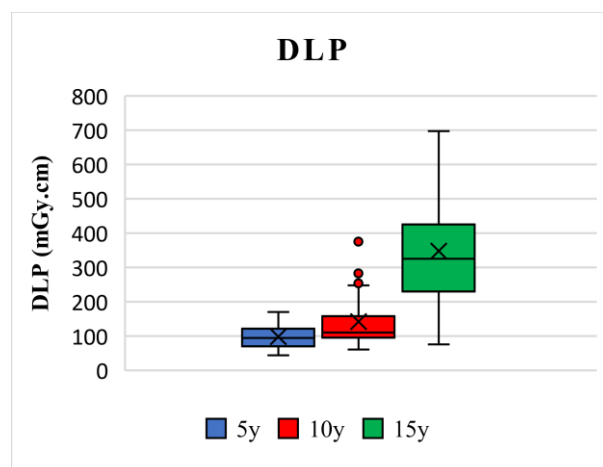


Figure 4.19 Comparisons of median and 75th percentile of DLP for various pediatric age groups.

The range, and distribution of CTDI_{vol} and DLP for 5 to 15-yrs were compared. We observed that there was a greater variability for CTDI_{vol} and DLP as well as larger outliers with older patients. For 5-yrs, CTDI_{vol} and DLP at the minimum value were 1.70 mGy and 44.10 mGy.cm, the first quartile were 2.38 mGy and 69.78 mGy.cm, the median were 2.90 mGy and 94.15 mGy.cm, the third quartile were 3.50 mGy and 117.25 mGy.cm, and the maximum value were 5.10 mGy and 170.00 mGy.cm, respectively. For 10-yrs, CTDI_{vol} and DLP at the minimum value were 1.60 mGy and 61.00 mGy.cm, the first quartile were 2.60 mGy and 92.20 mGy.cm, the median were 3.10 mGy and 109.74 mGy.cm, the third quartile were 4.76 mGy and 152.80 mGy.cm, and the maximum value were 7.68 mGy and 376.00 mGy.cm, respectively. For 15-yrs, CTDI_{vol} and DLP at the minimum value were 3.10 mGy and 75.50 mGy.cm, the first quartile were 6.35 mGy and 235.98 mGy.cm, the median were 7.70 mGy and 325.21 mGy.cm, the third quartile were 10.40 mGy and 423.49 mGy.cm, and the maximum value were 15.55 mGy and 697.00 mGy.cm, respectively (Figure 4.18-4.19).

In order to establish the local diagnostic reference level for CT examination in pediatric patients at Praram9 Hospital, the median and 75th percentile of CTDI_{vol}, DLP and SSDE of age groups between 5-15 years were determined as shown in Table 4.19.

Table 4.19 Median and 75th percentile of CTDI_{vol}, DLP, and SSDE of 5-15 yrs.

Age group	No.	CTDI _{vol} (mGy)				DLP (mGy.cm)				SSDE (mGy)			
		Percentile											
		25 th	50 th	75 th	90 th	25 th	50 th	75 th	90 th	25 th	50 th	75 th	90 th
5-yrs	36	2.38	2.96	3.50	3.95	69.78	94.15	121.55	134.90	4.94	5.80	7.26	8.48
10-yrs	55	2.60	3.10	4.76	5.98	95.20	109.74	152.8	251.52	4.98	5.32	8.28	10.35
15-yrs	59	6.35	7.70	10.40	11.94	235.98	325.21	423.49	588.82	10.40	12.05	15.23	18.04
Sum	150												

CHAPTER IV

DISCUSSION AND CONCLUSIONS

5.1 Discussion

Monitoring the amount of radiation to the human body received during CT examination is very important. The use of CT in pediatric patients has been increasing rapidly. However, since the potential for increased radiation exposure to children undergoing these scans, pediatric CT is a public health concern. Currently, several dose monitoring software tools are available to track and control dose distribution during CT examinations. Some software tools include Monte Carlo Simulation (MCS) and enables effective doses and organ dose calculations.

5.1.1 Measurement of CTDI

Quality control of CT system should be firstly performed prior to research data collection. The results of dose measurement are verified for accuracy and reproducibility. All the measured CT dosimetry was evaluated following the IAEA Human Health No.19 protocol.

CTDI₁₀₀ in air was measured using head and body protocols in all kVp and slice collimation. CTDI_{100, air} values decrease when slice collimation increases. When tube voltage increased from 80 kVp to 135 kVp in each slice collimation, CTDI_{100, air} values were increased for both head and body protocols. CTDI_{vol} displayed on the CT monitor was verified by the comparison of the measurements at the same kVp, mAs and slice collimation. The difference between measured CTDI_{vol} in Toshiba in body phantom was 10.39% of the CTDI display monitor. The discrepancy between the measurement and the CT monitor resulted from the uncertainty of chamber type, chamber position and measurement scenario such as the precision of reading, tube loading, the phantom construction, over scan phenomenon, the chamber response in phantoms and the inaccuracy on laser beam alignment. Additional sources of uncertainty arise from the effect of scattered radiation inside the phantom, beam hardening and other effects which may affect the chamber response for measurements in phantom (28).

5.1.2 Verification of organ doses: Radimetrics Program

The verification of the radiation dose assessed by a dose monitoring software tool based on MCS is a very important step to ensure that the software can calculate the organ doses correctly. In this study, we performed the measurements in the Rando phantom inserted with the glass dosimeters to confirm the agreement in the abdominal CT protocol between the measurement and the calculation using dose monitoring software.

In clinical, many types of dosimeters are applied in the procedures to verify dose accuracy, to obtain dose to critical areas or organs, and to verify machine output for QA purposes. For TLD, OSLD, and RPLGD, when radiation interacts with the medium in the dosimeters, part of the absorbed energy is first stored in a metastable energy state of the medium. Then some of this energy can be recovered later as visible light after proper physical process, such as heating.

Nowadays, TLD is still the major radiation dosimeter widely used for dose verification in diagnostic radiology and in radiotherapy. However, the major problem with TLD is its non-repeatable readout for the measurements. But for RPLGD, the luminescence signal does not disappear after readout, therefore, repeated readout for a single exposure is possible. Hsu SM et al (29) reported the dosimetric properties of RPLGD were superior to TLD regarding energy response, fading effect, and readout reproducibility. The component of RPLGD is fabricated from high melting point material which contributes to small variation among RPLGDs (16).

Twelve organs were measured for the organ dose verification, in which these organs were fully irradiated. Because the phantom is completely homogeneous, organ separation is quite difficult, so the phantom was compared with real patient CT image at similar body size and weight to evaluate position of each organ.

The difference of organ doses ranges from 8.88-51.85%, with the highest difference was uterus with the values of 51.85%. The large difference values cause by the uncertainty of MC simulation results is estimated 5–10% (30), including the uncertainty of measurement scenario such as the precision of reading, tube loading, the phantom construction, over scan phenomenon, the effect of scattered radiation inside the phantom, beam hardening and other effects which may affect the glass dosimeter response for measurements in Rando phantom (20). Tabulations of organ dose conversion coefficients for use in CT have been provided by the GSF and the NRPB. Both sets of tabulations provide conversion coefficients for a series of CT slices that cover the length of the patient. The conversion coefficients have been provided by the GSF and the NRPB may be make the organ dose calculations based on our research inaccurate. Determination of the conversion coefficients to convert the symptomatic absorbable dose for RPLGD in pediatric patients to the absorbed dose. It is therefore interesting to study in detail in the future.

5.1.3 Patient data and radiation dose determined from abdominal CT examination.

This study aimed to estimate the effective and organ doses for pediatric patients who were undergoing abdominal scans with AEC using patient-specific scan parameters from CT images and individual patient size data. Complex validated Monte Carlo dosage with realistic pediatric phantoms facilitate patient specific organs. The estimation of patient-specific organ sizes, the Radimetrics not only received a longitudinal AEC from the DICOM header of the patient image, it also automatically

selects a phantom that is closest to the patient based on age and gender, weight, and diameter.

All pediatric patients undergoing abdominal CT were divided into five groups according to the Radimetrics program. Pediatric patient geometry was modeled based on the Christy-Eckerman stylized phantoms where organs are represented by simple geometric shapes described by mathematical equations (23) (31). There was a small number for 0 and 1-yrs group, because the clinician intended to reduce the risk of radiation exposure for this group of children, other options of imaging were recommended for examination.

One very large pediatric patient was included into 15-year-olds age group by age (94 kg body weight), this may be considered as adult patients instead or exclude for outlier data due to unusual body weight.

Table 5.1 Mean and 75th percentile of CTDI_{vol} compared with national data by age group for abdominal CT scans.

Age groups (yr.)	No	CTDI _{vol} (mGy)						
		This study	Gao Y et al. (22) (2018)	Galanski M et al. (32) (2005)	Shrimpton P et al. (33) (2003)	Matsunaga Y et al (34) (2018)	Verdun FR et al. (35) (2008)	ACR (36) 2011 (2001-2004)
5	36	2.9(3.5)	6.0(7.0)	4.1(4.7)	n/a	8.6(11.2)	7.2(9.0)	15.5(20.0)
10	59	4.2(5.1)	8.0(10.0)	5.6(7.4)	11.0(13.0)		10.0(13.0)	
15	65	9.7(10.7)	11.0(12.0)	8.3(10.1)	11.0(13.0)		13.0(16.0)	

(22) (32) (33) (34) Age is classified as follows: 1= \leq 1 years 5=1-5years 10=5-10 years 15=10-15 years.

The mean value and 75th percentile of CTDI_{vol} were lower than the reference values from all previous literatures (22) (33) (35) (35) (34) (36), Only the CTDI_{vol} of the 15 -year-olds group is greater Galanski M et al (32). The difference less than 20%. Using AEC systems is an important aspect of CT scanners in optimizing and reducing patient dose as well as obtaining useful quality images for patient management and care especially in pediatric. However, the data collected in this study differed from those obtained by surveys conducted in other studies in terms of population size, scanner types, examination techniques, and patients' weights especially the 15-year-old patient with a relatively large body size.

Table 5.2 Mean and 75th percentile of DLP compared with national data by age group for abdominal CT scans.

Age Groups (yr.)	No	DLP (mGy.cm)						
		This study	Gao Y et al. (22) (2018)	Galanski M et al. (32) (2005)	Shrimpton P et al. (33) (2003)	Matsunaga Y et al. (34) (2018)	Verdun FR et al. (35) (2008)	Tap NHM et al. (37). 2017 (mean)
0	3	25(26)	43(43)	39(45)	n/a	n/a	n/a	234
1	1	60(60)	162(220)	79(82)	n/a	n/a	107(130)	230
5	36	98(117)	247(293)	115(147)	n/a	257.1(343.9)	238(300)	216
10	59	162(177)	438(502)	180(227)	473(534)	n/a	308(380)	303
15	65	401(499)	611(719)	328(402)	473(534)	n/a	398(500)	418
Total	164							

(22) (32) (33) (34) Age is classified as follows: 1=<1 years 5=1-5years 10=5-10 years 15=10-15 years.

In this study, the DLP were no greater than the reference values from all previous literatures. Only the DLP of the 15-year-olds group is greater than Galanski M et al (32). and Verdun FR et al (35). The differences were less than 20% and 1% respectively, it may be the result of the length of the examination, which depends on the height of the patient. In the 15-year-olds group, the maximum height was 172 cm. This study classified age groups differently from other studies, the authors can only use information that the patients are close to for the comparison (22, 33) (35). The scanning parameters will change as the patient size changes. The patient's body size increases, the scanning parameter will also increase due to the use of AEC.

Organ dose in each organ was found that there was a higher radiation dose in patients with older age groups, because the increased average size may increase the organ doses. When separated by gender and machines, it was demonstrated that the highest average organ doses also found in female 15 years.

Average organ doses were found higher in older age groups because the average sizes of patients were increased. Average sizes of patients increased, resulting in the AEC increasing the radiation dose automatically. It is the nature of auto mA modulation. CTDI_{vol} at each slice increased, resulting in higher organ dose in older age groups (Figure 4.4). We also found that the majority of organ doses were seen in the kidney, stomach, and urinary bladder.

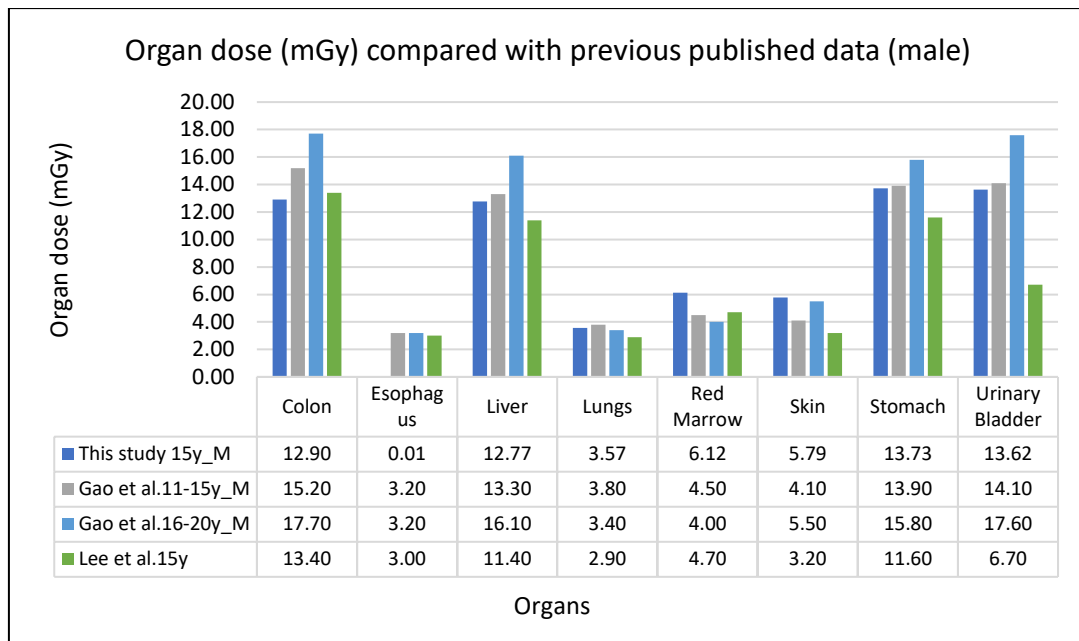


Figure 5.1 Organ dose (mGy) compared with previous published data in male pediatric patients 15y.

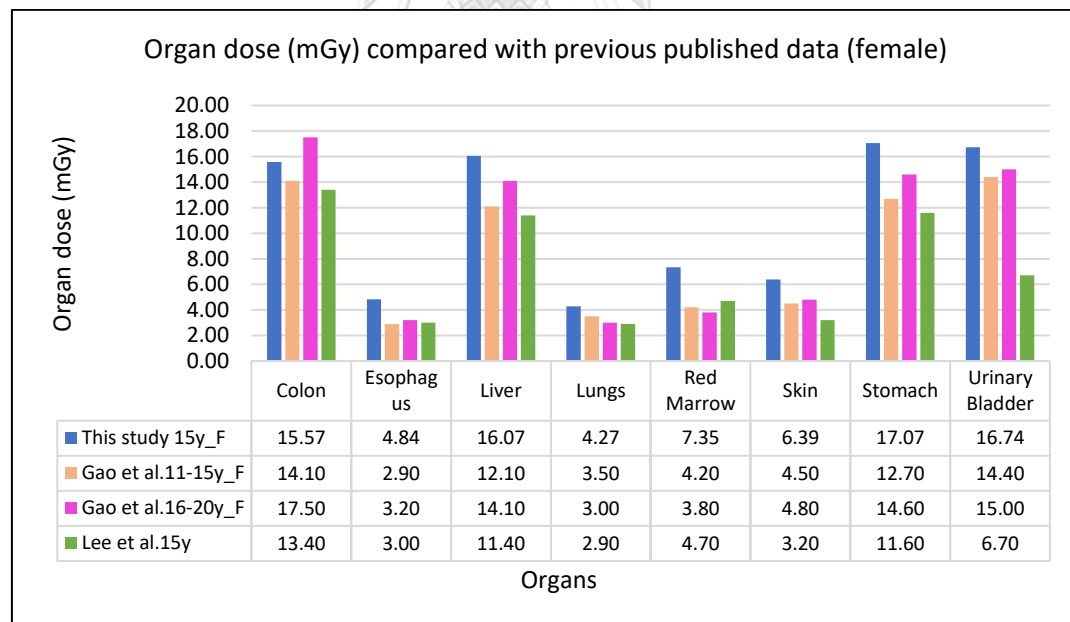


Figure 5.2 Organ dose (mGy) compared with previous published data in female pediatric patients 15y.

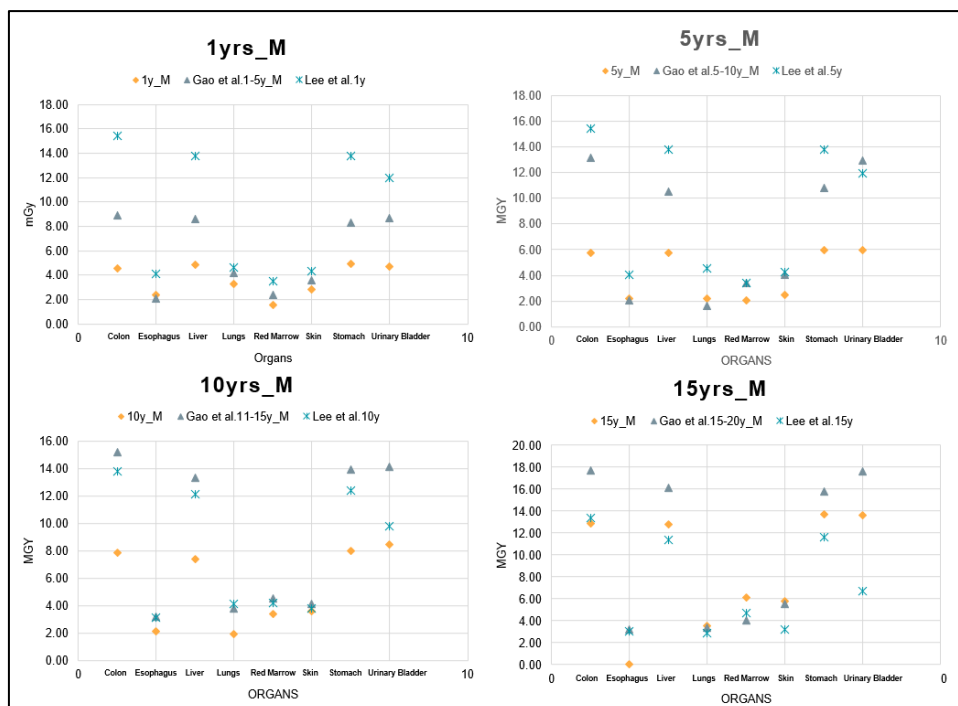


Figure 5.3 Organ dose (mGy) compared with previous published data in male pediatric patients.

In addition, when comparing the organ doses at each age group with other studies, the Figure 5.3 shows organ doses of male pediatric patients in each age group. Orange square in the graph represents the patient in this study. When comparing the organ doses with other studies, it was found that most of the organ doses were lower than literatures, except for organ doses 15 years. When looking at the group 15-yr old male, organ doses in this study were greater than Gao et al. (22) and Lee et al. (21) in red bone marrow, and skin.

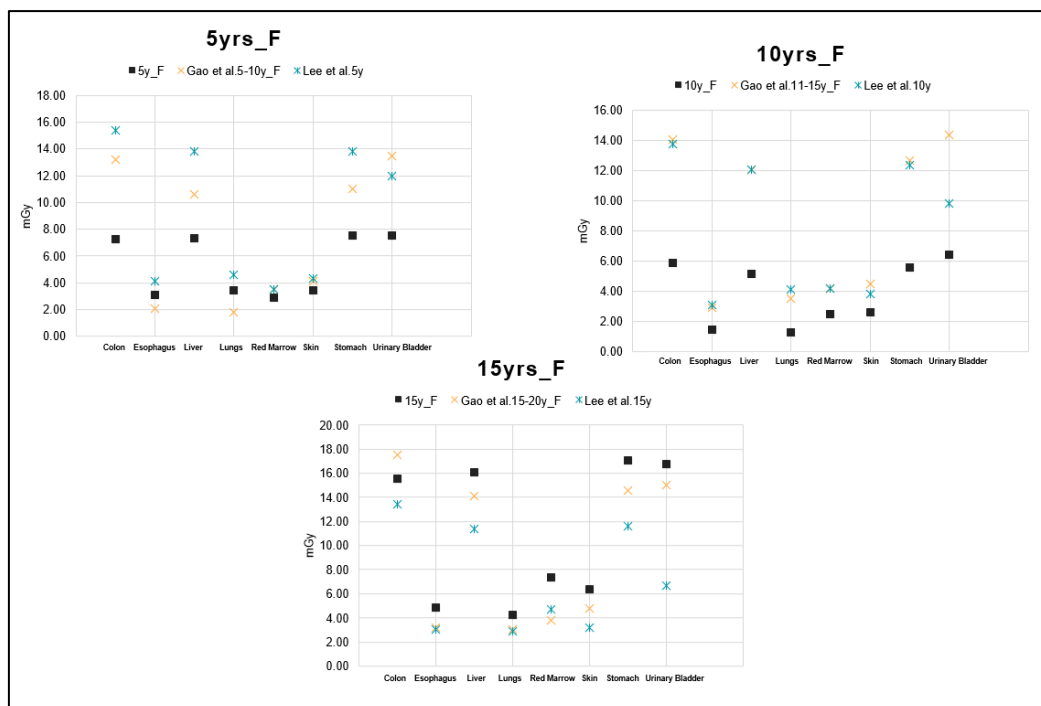


Figure 5.4 Organ dose (mGy) compared with previous published data in female pediatric patients.

The Figure 5.4 shows organ doses of female pediatric patients in each age group. Black square in the graph represents the patient in this study. When comparing the organ doses with other studies, it was found that most of the absorbed doses were lower than literature, except for organ doses of 15 years. Organ doses of this group in this study were much greater than Gao et al. and Lee et al. in all organs except in the colon.

Organ doses estimated by this study were large differences with other studies especially for Gao et al. as they have the difference of patient age classification, and body part examined matched to the body region of the phantoms, with the start and end of scans defined as from top of the liver through the symphysis, while our study started at 2 cm above of the liver through the ischial tuberosity. For the study of Lee et al., the organ doses were calculated by normalizing to the product of 100 mAs, while our study was based on AEC.

When considering the high-radiation dose of female patients, it was found that they underwent CT lower abdomen from Siemens SOMATOM Sensation 64 detector-row. The top five organs were found in kidneys, urinary bladder, stomach, spleen, upper large intestine, with the mean values of 23.82, 22.08, 22.19, 21.02, 21.32 mGy, respectively (Table 4.8). The main reason for the high radiation dose was due to the body weight of the patients. Organ doses of this group were very high since most of them have the tendency of high body weight, resulting in higher scanning parameters and higher patient doses. As a result, tube current modulation was increased to 203-

247 mAs in each patient. Poor positioning also directly affected the AEC in adjusting the radiation dose. In addition, improper positioning results in larger FOV opening in order to cover the organs of interest, which increases the radiation dose as well. From this reason can be applied for clinical benefits in the matter of focusing on positioning.

The calculated mean ED and SSDE for CT scans of the abdomen CT showed that the highest dose was in the age group 15 yrs, which was estimated to be 8.46 mSv and 14.21 mGy, respectively. The ED for this age group ranged from 1.60 to 20.64 mSv, and the SSDE ranged 5.56 to 30.87 mGy (Table 4.6). A review of the data shows that for some of the 15 years, an adult abdomen protocol was utilized; this, coupled with some patients with extended scan length above the diaphragm, contributed to additional dose from abdomen scans in this age group. Large variations in the scanner output were found to accommodate the variations in patient sizes. In our study, the large variations in scan parameters accommodating variations in patient weight and size led to variations in organ doses.

The quantity assumed to be related to the stochastic radiation risk is the mean organ equivalent dose, H_T . It is derived from the mean organ absorbed dose, D_T , i.e., the total amount of energy deposited in an organ (or tissue), T , per mass of the organ, by multiplying with a radiation weighting factor, W_R . Accurately and quickly calculated organ absorbed doses can reflect the relative biological efficiency of incident radiation (38).

There were relatively small number of pediatric patients age less than 1-yr for organ dose estimation. Thus, comparing the information on organ doses with other previous studied could not be applied as only four pediatric patients were collected. The results of organ doses for these age group may not reflect the findings toward these patients due to limited number of patient data. This was the limitation in this study.

5.1.4 Correlation

When looking at the subject of $CTDI_{vol}$ and SSDE, the results showed good correlation between $CTDI_{vol}$, SSDE and body weight rather than the relationship between $CTDI_{vol}$, SSDE and age with R-square were 0.83, 0.72 respectively in CT whole abdomen and R-square were 0.76, 0.70 respectively in CT lower abdomen. Therefore, the patient's weight or body size influences the dose calculation.

In relation between gender and radiation dose, it was found that in all age groups, female patients tended to have higher radiation dose than male patients except for 10 years age group. The amount of radiation is significantly lower. This may be due to the 10-year-old female population was relatively low in weight or size compared to males for our collected data in this study. Thus, the patient's weight and size had a significant effect on the radiation dose. In addition, selecting inappropriate

scanning technique by CT technologist was also another reason that may increase the amount of radiation to the patient.

5.1.5 Local diagnostic reference level (LDRL)for pediatrics abdominal CT at Praram9 hospital

By collecting the data for this study, $CTDI_{vol}$ and DLP values were obtained in the calculation of cases where local DRL values can be analyzed for 5-yrs, 10-yrs and 15-yrs. Pediatric patients over 80 kg of body weight were excluded (10). The resulting median values for 5y, $CTDI_{vol} = 2.90$ mGy, $DLP = 94.15$ mGy.cm, for 10y, $CTDI_{vol} = 3.10$ mGy, $DLP = 109.74$ mGy.cm, for 15y $CTDI_{vol} = 7.70$ mGy, $DLP = 325.98$ mGy.cm. The median value of the on-site DRL will be compared with the national DRL to identify whether the data for the location are substantially higher or lower than might be anticipated.

For 75th percentile 5y, $CTDI_{vol} = 3.50$ mGy, $DLP = 117.25$ mGy.cm, for 10y, $CTDI_{vol} = 4.76$ mGy, $DLP = 152.80$ mGy.cm, and for 15y, $CTDI_{vol} = 10.40$ mGy, $DLP = 423.49$ mGy.cm. Typically, the 75th percentile of the collecting data will be used to set up for the local DRL. Therefore, the obtained values can be used for reference data at Praram9 Hospital to improve the working protocol for the radiation safety and optimization of pediatric patients. Also, it can be used as a database for further study of radiation dose in pediatric patients in private hospital in Thailand.

When compared the median value of $CTDI_{vol}$ of our study to DRL of the American College of Radiology (ACR) in the 5,10 and 15-year patient age group found that in our study was lower than the ACR DRL. Effective since January 1, 2008, the ACR program implemented United States-specific diagnostic reference levels of 20 mGy for the $CTDI_{vol}$ of pediatric abdominal CT scans which routine pediatric abdominal were instructed to report their techniques assuming a 5-year-old patient (32).

A diagnostic reference level or DRL is a model of the level used as a tool to optimize and prevent of patient medical exposure for diagnostic and intervention procedures. It is used in medical imaging with ionizing radiation to indicate whether, in routine conditions, the amount of radiation used for a specified procedure is unusually high or low for that procedure. Both $CTDI_{vol}$ and DLP are the metrics commonly used for DRL in CT to determine radiation dose to the patients.

Local DRL settings may be available for procedures without national DRLs or where there is a national value. However, local equipment or techniques enable a higher level of optimization, so that the values less than the relevant national DRL can be used. According to the International Commission on Radiological Protection (ICRP) guideline, the DRL value should not be used as a dose limit, as the dose limit does not apply to the patient's medical exposure. However, the DRL procedure is

intended to optimize radiation protection for a group of patients and is based on standard patients. It is not an individual patient (27).

5.2 Conclusions

Patient-specific organs and effective doses from 0 through 15-years-old can be determined effectively using dose tracking software. The high organ doses from abdominal CT in pediatric patients aged 0-15-yrs at Praram9 Hospital were found in gallbladder, kidneys, urinary bladder, and stomach, respectively. As the various sizes of pediatrics, the patient ED and SSDE were correlated with the patient's body weight rather than the patient age according to earlier results reported by the ICRP classification. The local DRL of $CTDI_{vol}$ of pediatric patients who underwent abdominal CT scan at Praram9 Hospital were 3.5, 5.10 and 7.70 mGy for patient 5y, 10y and 15y, respectively. The median value of $CTDI_{vol}$ of pediatric patients who underwent abdominal CT scan at Praram9 Hospital was lower than the ACR DRL. The organ doses and local DRL investigated in this study can be used as a reference data for the radiation dose obtained from abdominal CT in pediatric patients in private hospital using the dose monitoring software.

REFERENCES

1. Chodick G, Kim KP, Shwarz M, Horev G, Shalev V, Ron E. Radiation risks from pediatric computed tomography scanning. *Pediatr Endocrinol Rev.* 2009;7(2):29-36.
2. American Association of Physicists in Medicine Task Group 204. Size-Specific Dose Estimates (SSDE) in Pediatric and Adult Body Examination. American Association of Physicists in Medicine (AAPM), Report No204. 2011.
3. Kost SD, Fraser ND, Carver DE, Pickens DR, Price RR, Hernanz-Schulman M, et al. Patient-specific dose calculations for pediatric CT of the chest, abdomen and pelvis. *Pediatric Radiology.* 2015;45(12):1771-80.
4. Moore BM, Brady SL, Mirro AE, Kaufman RA. Size-specific dose estimate (SSDE) provides a simple method to calculate organ dose for pediatric CT examinations. *Med Phys.* 2014;41(7):071917.
5. Parakh A, Kortensniemi M, Schindera ST. CT Radiation Dose Management: A Comprehensive Optimization Process for Improving Patient Safety. *Radiology.* 2016;280(3):663-73.
6. Computed Tomography (CT) - National institute of biomedical imaging and bioengineering. (online) 2013.
7. Kalender WA. Computed tomography: fundamentals, system technology, image quality, applications: John Wiley & Sons; 2011.
8. Dance D, Christofides S, Maidment A, McLean I, Ng K. Diagnostic radiology physics: A handbook for teachers and students. Endorsed by: American Association of Physicists in Medicine, Asia-Oceania Federation of Organizations for Medical Physics, European Federation of Organisations for Medical Physics. 2014.
9. Bushberg JT, Boone JM. The essential physics of medical imaging: Lippincott Williams & Wilkins; 2011.
10. Dendy PP, Heaton B. Physics for diagnostic radiology: CRC press; 2011.
11. McCollough CH, Leng S, Yu L, Cody DD, Boone JM, McNitt-Gray MF. CT dose index and patient dose: they are not the same thing. *Radiology.* 2011;259(2):311-6.
12. Protection R. ICRP publication 103. *Ann ICRP.* 2007;37(2.4):2.
13. Children's (Pediatric) CT (Computed Tomography). (online). *RadiologyInfo.org.* 2021.
14. Berland LL. The American College of Radiology strategy for managing incidental findings on abdominal computed tomography. *Radiologic Clinics of North America.* 2010;49(2):237-43.
15. Oonsiri P, Kingkaew S, Vannavijit C, Suriyapee S. Investigation of the dosimetric characteristics of radiophotoluminescent glass dosimeter for high-energy photon beams. *Journal of Radiation Research and Applied Sciences.* 2019;12(1):65-71.
16. Huang DY, Hsu S-M. Radio-Photoluminescence Glass Dosimeter (RPLGD): INTECH Open Access Publisher; 2011.
17. Alikhani B, Getzin T, Kaireit TF, Ringe KI, Jamali L, Wacker F, et al. Correlation of size-dependent conversion factor and body-mass-index using size-specific dose estimates formalism in CT examinations. *European journal of*

- radiology. 2018;100:130-4.
18. Tsujiguchi T, Obara H, Ono S, Saito Y, Kashiwakura I. Consideration of the usefulness of a size-specific dose estimate in pediatric CT examination. *Journal of radiation research*. 2018;59(4):430-5.
 19. Moore BM, Brady SL, Mirro AE, Kaufman RA. Size-specific dose estimate (SSDE) provides a simple method to calculate organ dose for pediatric CT examinations. *Medical physics*. 2014;41(7):071917.
 20. Guberina N, Suntharalingam S, Naßenstein K, Forsting M, Theysohn J, Wetter A, et al. Verification of organ doses calculated by a dose monitoring software tool based on Monte Carlo simulation in thoracic CT protocols. *Acta Radiologica*. 2018;59(3):322-6.
 21. Lee C, Kim KP, Long DJ, Bolch WE. Organ doses for reference pediatric and adolescent patients undergoing computed tomography estimated by Monte Carlo simulation. *Medical physics*. 2012;39(4):2129-46.
 22. Gao Y, Quinn B, Pandit-Taskar N, Behr G, Mahmood U, Long D, et al. Patient-specific organ and effective dose estimates in pediatric oncology computed tomography. *Physica medica*. 2018;45:146-55.
 23. HealthCare B. Radimetrics enterprise platform [Internet]. Whippany: Bayer HealthCare [cited 2015 Sep 22].
 24. IAEA. Human Health Series No. 19. Quality Assurance Programme for Computed Tomography: Diagnostic and Therapy Applications (IAEA, Marketing and Sales Unit, Publishing Section, International Atomic Energy Agency, Vienna International Centre, PO Box 100, 1400 Vienna, Austria, 2012). 2011:13-7.
 25. Agency IAE. Dosimetry in Diagnostic Radiology: An International Code of Practice, Technical reports series no.457: International Atomic Energy Agency; 2007.
 26. Zankl M, Panzer W, Drexler G. The calculation of dose from external photon exposures using reference human phantoms and Monte Carlo methods. Pt. 6. GSF-Forschungszentrum fuer Umwelt und Gesundheit GmbH; 1991.
 27. Vañó E, Miller D, Martin C, Rehani M, Kang K, Rosenstein M, et al. ICRP publication 135: diagnostic reference levels in medical imaging. *Annals of the ICRP*. 2017;46(1):1-144.
 28. Agency IAE. Dosimetry in Diagnostic Radiology: International Atomic Energy Agency; 2007.
 29. Hsu S-M, Yeh S-H, Lin M-S, Chen W-L. Comparison on characteristics of radiophotoluminescent glass dosimeters and thermoluminescent dosimeters. *Radiation protection dosimetry*. 2006;119(1-4):327-31.
 30. Guberina N, Suntharalingam S, Naßenstein K, Forsting M, Theysohn J, Wetter A, et al. Clinical evaluation of a dose monitoring software tool based on Monte Carlo simulation in assessment of eye lens doses for cranial CT scans. *Neuroradiology*. 2016;58(10):955-9.
 31. Cristy M, Eckerman K. Specific absorbed fractions of energy at various ages from internal photon sources: 3, Five-year-old. Oak Ridge National Lab., TN (USA); 1987.
 32. Galanski M, Nagel H, Stamm G. Paediatric CT exposure practice in the Federal Republic of Germany. Results of a nation-wide survey in. 2005;6:2006.

33. Shrimpton P, Hillier M, Lewis M, Dunn M. Doses from computed tomography (CT) examinations in the UK-2003 review: NRPB Chilton; 2005.
34. Matsunaga Y, Chida K, Kondo Y, Kobayashi K, Kobayashi M, Minami K, et al. Diagnostic reference levels and achievable doses for common computed tomography examinations: results from the Japanese nationwide dose survey. The British journal of radiology. 2019;92(1094):20180290.
35. Verdun FR, Gutierrez D, Vader JP, Aroua A, Alamo-Maestre LT, Bochud F, et al. CT radiation dose in children: a survey to establish age-based diagnostic reference levels in Switzerland. European radiology. 2008;18(9):1980-6.
36. McCollough C, Branham T, Herlihy V, Bhargavan M, Robbins L, Bush K, et al. Diagnostic reference levels from the ACR CT accreditation program. Journal of the American College of Radiology. 2011;8(11):795-803.
37. Tap NHM, Sidek MAJ, Ridzwan SFM, Selvarajah SE, Zaki FM, Hamid HA. Computed Tomography dose in paediatric care: simple dose estimation using dose length product conversion coefficients. The Malaysian journal of medical sciences: MJMS. 2018;25(4):82.
38. Fisher DR, Fahey FH. Appropriate use of effective dose in radiation protection and risk assessment. Health physics. 2017;113(2):102.



APPENDICES

จุฬาลงกรณ์มหาวิทยาลัย
CHULALONGKORN UNIVERSITY

Appendix A: Data record form

Table A 1 Data collection sheet for patient information.

Patient data	Mean \pm SD	Minimum	Maximum
Age (year)			
Body weight (kg)			
BMI (kg/m ²)			
Height (cm)			

Table A 2 Data collection volume pediatric CT Examinations by age

Age		Body weight (kg)	Examination type		
Groups (year)	Mean(min-max)		MDCT whole abdomen	MDCT lower abdomen	Total
0					
1					
5					
10					
15					
Overall					

Table A 4 Data collection for patient specific organ dose of pediatric abdominal CT data form.

Organ	Age groups				
	0	1	5	10	15
	(Body weight)	(Body weight)	(Body weight)	(Body weight)	(Body weight)
Adrenals					
Brain					
Breasts					
Colon					
Esophagus					
Eye Lenses					
Gall Bladder					
Heart					
Kidneys					
Liver					
Lungs					
Muscle					
Pancreas					
Red Marrow					
Remainder ICRP103					
Remainder ICRP60					
Salivary Glands					
Skeleton					
Skin					
Small Intestine					
Spleen					
Stomach					
Testicles					
Thymus					
Thyroid					
Upper Intestine Large					
Urinary Bladder					

Table A 5 Effective dose (mSv) of pediatric CT examinations by age and gender

Age (years)	kVp	mAs	CTDI _{vol} (mGy)	DLP* (mGy.cm)	SSDE* (mGy)	ED* (mSv)
0						
1						
5						
10						
15						

Table A 6 Data collection dose indexes by age group for abdominal CT scans data form

Age Groups (yr.)	CTDI _{vol} (mGy)					DLP (mGy.cm)					SSDE (mGy.cm)				
	No	Mean	25th	Median	75th	No	Mean	25th	Median	75th	No	Mean	25th	Median	75th
0															
1															
5															
10															
15															
Total															

Table A 7 Median and 75th percentile of CTDI_{vol} and DLP of various age groups at Praram9 Hospital data form

Age group	Median		75 th percentile	
	CTDI _{vol} (mGy)	DLP (mGy.cm)	CTDI _{vol} (mGy)	DLP (mGy.cm)
0-yrs				
1-yrs				
5-yrs				
10-yrs				
15-yrs				

Appendix B: Quality Control of MDCT system

1. MDCT system TOSHIBA Aquilion ONE 320 detectors

Location: X-ray department at Praram9 Hospital Floor.2

Manufacturer: TOSHIBA Model: AQUILION ONE

Installed: 2017

Date: 4 April 2021

Pass	Scan Localization Light Accuracy
Pass	Alignment of Table to Gantry
Pass	Table Increment Accuracy
Pass	Slice Increment Accuracy
Pass	Reproducibility of CT Numbers
Pass	mAs Linearity
Pass	Linearity of CT Numbers
Pass	Accuracy of Distance Measurement
Pass	High Contrast Resolution
Pass	Low Contrast Detectability
Pass	Slice thickness accuracy
Pass	Image uniformity

1.1 Scan Localization Light Accuracy

Purpose: To test congruency of scan localization light and scan plane.

Method:

1. Place the tape measurement vertically along the midline the couch aligned with the longitudinal axis.
2. Set external light align with the reference point on the tape measurement.
3. Set table position to zero. Move table by monitor scanner, the table position move from external to internal localization light. Measure and record deviation position.

Tolerance: The center of the irradiation field from the pin pricks should be less than 2 mm

Results: Measured Deviation External70...mm Internal70...mm

Comment: Pass



Figure B 1 Localization light accuracy setting on the tape measurement.

1.2 Alignment of Table to Gantry

Purpose: To ensure that long axis of the table is horizontally aligned with a vertical line passing through the rotational axis of the scanner.

Method:

1. Locate the table midline using a ruler and mark it on a tape affixed to the table. With the gantry untitled, extend the tabletop into gantry to tape position.
2. Measure the horizontal deviation between the gantry aperture center and the table midline.

Tolerance: The Deviation should be within 5 mm

Results:

Table B 1 Alignment of table to gantry

	Table	Bore
Distance from Right to Centre (mm)	390	390
Distance from Centre to Left (mm)	390	390
Measured Deviation	0	0

*Measured deviation = (Distance from right to center – Distance from center to Left)/2

Comment: Pass

1.3 Table increment Accuracy.

Purpose: To determine accuracy and reproducibility of table longitudinal motion.

Method:

1. Tape a measuring tape at the foot end of the table.
2. Place a paper clip at the center of the tape to function as an indicator.
3. Load the table uniformly with 150 lbs. From the initial position move the table 300, 400 and 500 mm.

4. Record the relative displacement of the pointer on the ruler. Reverse the direction of motion and repeat.

5. Repeat the measurements four times.

Tolerance: Positional errors should be less than 3 mm at 300 mm position.

Result:

Table B 2 Table increment Accuracy.

Indicated (mm)	Measured (mm)	Deviation (mm)
300	300	0
400	400	0
500	500	0
-300	-300	0
-400	-402	2
-500	-500	0

*Deviation = | Indicated – Measured|

Comment: Pass

1.4 Position dependence and S/N ratio of C.T. numbers

Method:

1. Position the C.T. head phantom centered in the gantry.
2. Using 1 cm slice thickness obtain one scan using typical head technique.
3. Select a circular region of interest of approximately 400 sq. mm.
4. Record the mean C.T. number and standard deviation for each of the positions 1 through 5.

Technique: 120 kV, 300 mA, 1 second, 250 mm. FOV

Tolerance: The coefficient of variation of mean CT numbers of the four scans should be less than 0.2.

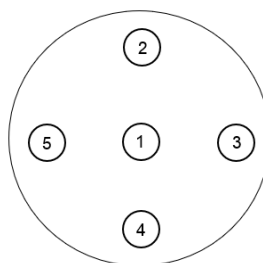


Figure B 2 Draw region of interest for each of the positions 1 through 5.

Results:**Table B 3** Position dependence and S/N ratio of C.T. numbers

Position	Mean C.T.	S.D.	C.V.
1	51.14	2.23	0.043
2	51.40	1.92	0.037
3	51.71	2.04	0.039
4	52.44	2.27	0.043
5	51.29	2.07	0.040

*CV = Standard deviation/mean CT number

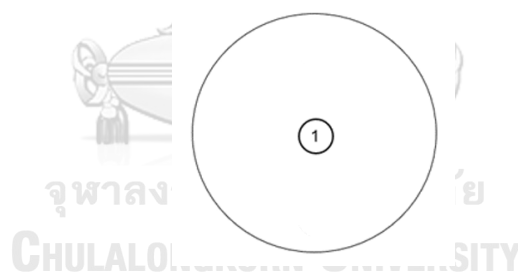
Comment: Pass

1.5 Reproducibility of C.T. Numbers.

Method:

1. Using the same set up and technique as position dependence, obtain three scans.
2. Using the same ROI as position dependence in location 1, which is the center of the phantom, obtain mean C.T. numbers for each of the four scans

Tolerance: The coefficient of variation of mean C.T. numbers of the four scans should be less than 0.002

**Figure B 3** Draw region of interest of the positions 5.**Results:****Table B 4** Reproducibility of C.T. numbers

Run Number	1	2	3	4
C. T Number	51.14	51.34	51.29	51.19
Mean Global C.T Number	51.24			
Standard Deviation	0.08			
Coefficient of variation	0.001			

Comment: Pass

1.6 mAs Linearity

Method:

1. Set up the same as position dependence and insert 10 cm long pencil chamber in the center slot of the C.T. dose head phantom.
2. Select the same kVp and time as used for head scan. Obtain four scans in each of the mA stations normally used in the clinic. For each mA station record the exposure in mGy for each scan. Scans should be performed in the increasing order of mA. Compute mGy/mAs for each mA setting.

Technique: 120 kVp, 1 second, 240 mm. FOV, slice collimation 8 mm varying mA

Results:

Table B 5 mAs linearity

mA	Exposure in mGy				mGy/mAs	C.V.
	Run 1	Run 2	Run 3	Run 4		
50	0.48	0.47	0.47	0.47	0.01	
100	0.97	1.01	0.93	0.96	0.01	0.012
200	1.9	1.95	1.87	2.02	0.01	0.000
300	2.96	2.95	2.81	2.99	0.01	0.004
400	5.13	5.1	5.21	5.22	0.01	0.139
500	6.44	6.4	6.52	6.39	0.01	0.001

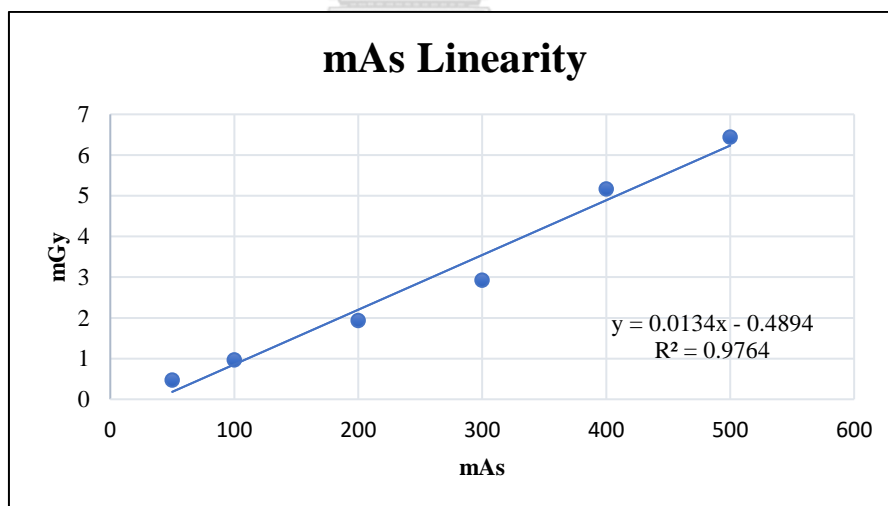


Figure B 4 The relationship of mGy and mAs.

Comment: Pass

1.7 Linearity of C.T. Numbers

Method:

1. Set up the Catphan phantom as described in beam alignment.
2. Select the section containing the test objects of different C.T. numbers.
3. Select the head technique and perform a single transverse scan.
4. Select a region of interest (ROI) of sufficient size to cover the test objects.
5. Place the ROI in the middle of each test object and record the mean C.T. number.

Technique: 120 kVp 300 mA 1.0 sec, FOV 240 mm, Slice thickness 8 mm

Tolerance: R-square between measured CT number and linear attenuation coefficient (μ) more than 0.9

Results:

Table B 6 Linearity of CT Number

Material	Expected CT Number	Measured CT Number
Air (Superior)	-1000	-955.53
Air (Inferior)	-1000	-1008.3
PMP	-200	-186.95
LDPE	-100	-102.39
Polystyrene	-35	-45.20
Acrylic	120	116.36
Delrin™	340	353.38
Teflon	990	999.40

1.8 Slice thickness accuracy

Purpose: To Determine the accuracy of the slice thickness.

Method:

1. Set up the catphan phantom as described in beam alignment set up as you would for beam profile measurement.
2. Select the section containing the accuracy of the slice thickness test objects (CTP682)
3. Select the head technique, 120 kVp, 300 mAs, smallest slit width.
4. Perform several scans with different programmed slice thicknesses under auto control.
5. Perform scan following catphan manual in each slice collimation.
6. Calculate the real slice thickness.

Tolerance: Deviation should be $< 1\text{mm}$

Result:**Table B 7** Slice thickness accuracy

Slice thickness (mm)	1	4	8
Peak	577.20	195.67	157.75
BG	101.42	95.53	97.09
Net peak (NP)	475.78	100.14	60.66
50% NP	237.89	50.07	30.33
HM (50%NP+BG)	339.31	145.60	127.42
FWHM L1	2.55	9.82	19.71
FWHM L2	2.78	10.28	19.33
FWHM L3	2.65	9.79	19.50
FWHM L4	2.68	9.93	19.70
Average FWHM	2.665	9.955	19.56
SL=Avg FWHMx0.42	1.119	4.181	8.215
%Diff (set vs calculate)	0.119	0.181	0.215

Slice Thick in mm	Measured Thick in mm	Deviation (mm)
1	1.119	0.119
4	4.181	0.181
8	8.215	0.215

*Deviation = |Slice thickness – Measured thickness|

Comment: Pass

1.9 High Contrast Resolution

Purpose: To test resolution sections ranging from 1 to 21 lines pairs per cm. This radial design pattern eliminates the possibility of streaking artifacts from other test objects.

Method:

1. Set up the Catphan phantom in beam alignment.
2. Select the section containing the high-resolution test object. (CTP714 line pair high resolution Module).
3. Select the head technique and perform a single transverse scan.
4. Select the area containing the high-resolution test objects.
5. Select appropriate window and level for the best visualization of the test objects.

Technique: kVp: 120 mA: 300Seconds: 1.0 FOV: 300 mm Slice

Technique: 120kVp, 300mA, 1.0 sec, FOV 240 mm

Tolerance: > 5 lp/cm visible

Table B 8 High contrast resolution

Slice Thickness in mm	Resolution	Gap size
4 mm	8-line pair/cm	0.063 cm
8 mm	8-line pair/cm	0.063 cm
12 mm	8-line pair/cm	0.063 cm

Comment: Pass

1.10 Low contrast resolution

Purpose: To determine the actual target contrasts before testing specific contrast performance specifications.

Method:

1. Set up the Catphan 700 phantom in beam alignment.
2. Select the section containing the low-resolution test object CTP515 Sub-slice and supra-slice low contrast Module).
3. Select the head technique and perform a single transverse scan.
4. Select the area containing the low-resolution test objects.
5. Select appropriate window and level for the best visualization of the test objects.
6. Record the smallest test object visualized.

Technique: 120 kVp, 300 mA, 1.0 sec, FOV 240 mm slice collimation 8 mm.

Tolerance: should see 4 spokes at Supra- slice 0.5% nominal target contrast level

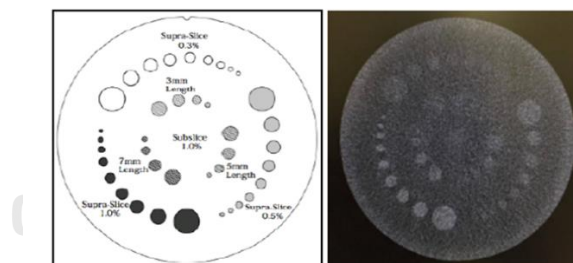


Figure B 5 Low contrast detectability

Result:

Table B 9 Low contrast resolution

Slice thickness in mm	Smallest target(spokes) diameter (mm) should be seen					
	Contrast level of supra-slice			Length of sub-slice 1.0%		
	1.00%	0.50%	0.30%	7 mm	5 mm	3 mm
4	8	5	4	3	2	1.5
8	9	6.5	4.5	3	2	1.5
12	9	8	6	3	2	2

Comment: Pass

1.11 Image uniformity

Method:

1. Set up the Catphan phantom as described in beam alignment.
2. Select the CTP712 image uniformity module.
3. Select the head technique and perform a single transverse scan.
4. Select a region of interest (ROI) of sufficient size to cover the test objects.
5. Place the ROI in the middle of each test object and record the mean C.T. number

Technique: 120kVp, 300 mA, 1sec, 250mm FOV, slice collimation 1 mm

Tolerance: Less than 5 HU

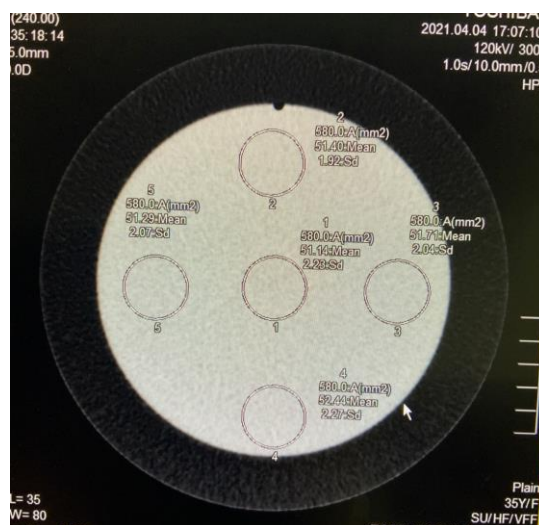


Figure B 6 Image Uniformity

Results:

Table B 10 Image uniformity

Position	Mean C.T Number	S.D.	Difference (HU)
1	51.14	2.23	
2	51.40	1.92	0.26
3	51.71	2.04	0.56
4	52.44	2.27	1.3
5	51.29	2.07	0.15

Different = |CT number center – CT number peripheral|

Comment: Pass

2.Verification of Computed Tomography Dose Index (CTDI)

2.1. Measurement CTDI₁₀₀ in air (C_{air} or CTDI_{air})

CTDI₁₀₀ in air was measured using 100 mm pencil ion chamber set at the isocenter of the CT bore. The scan parameters were 100 mA tube current, 1 sec scan time and small focal spot size setting for all measurements at tube potential setting of 80, 100, 120 and 135. The results of CTDI₁₀₀ measurement are shown as in Table B 11

Table B 11 The measured Ca,100 in air for head protocols for each kVp and slice collimations.

kVp	CTDI ₁₀₀ (mGy) in air in Head protocol							
	Slice Collimation in mm (NT)							
	1(1x1)	2(0.5x4)	4(1x4)	8(2x4)	12(3x4)	16(4x4)	20(5x4)	32(8x4)
80	8.68	5.93	4.99	4.05	3.11	2.16	1.7	1.46
100	14.52	9.94	8.37	6.8	5.2	3.66	2.88	2.5
120	21.58	14.81	12.48	10.16	7.83	5.5	4.34	3.75
135	27.64	19.02	16.05	13.08	10.1	7.13	5.64	4.89

CTDI₁₀₀ in air using head techniques 100 mAs, 240 mm. FOV all Slice Collimations are plotted in Figure B 7

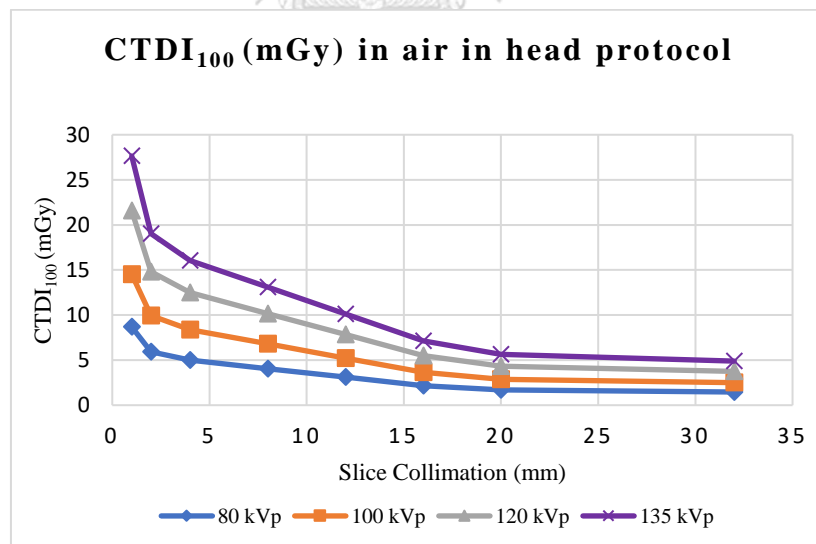


Figure B 7 CTDI₁₀₀ in air, head protocol as the function of kVp and slice collimation are plotted in blue, orange, gray, and violet colors at kVp of 80, 100, 120 and 135, respectively.

Table B 12 The measured CTDI₁₀₀ in air for body protocol for each kVp and slice collimation.

kVp	CTDI ₁₀₀ (mGy) in air in body protocol							
	Slice Collimation in mm (NT)							
	1(1x1)	2(0.5x4)	4(1x4)	8(2x4)	12(3x4)	16(4x4)	20(5x4)	32(8x4)
80	6.83	4.67	3.94	3.20	2.46	1.72	1.35	1.16
100	12.11	8.29	6.99	5.67	4.37	3.07	2.41	2.08
120	18.67	12.81	10.81	8.81	6.79	4.78	3.80	3.27
135	24.44	16.81	14.40	11.59	8.95	6.30	5.01	4.36

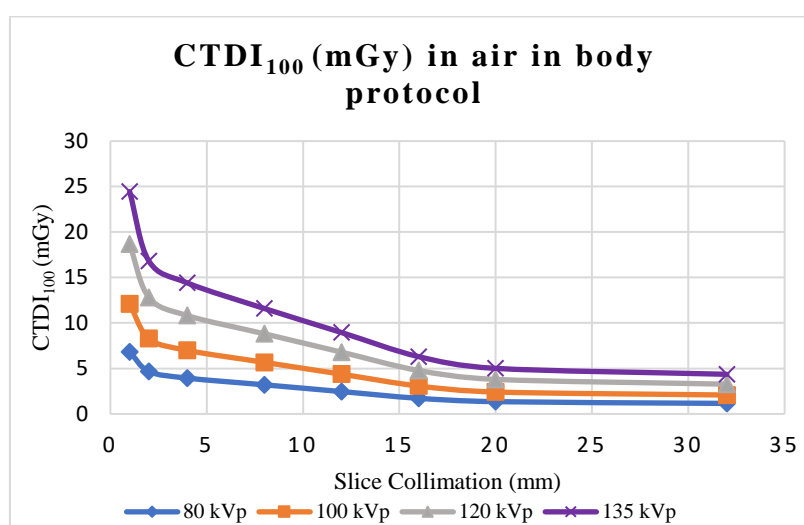


Figure B 8 CTDI₁₀₀ in air, body protocol as the function of kVp and slice collimation are plotted in blue, orange, gray, and violet colors at kVp of 80, 100, 120 and 135, respectively.

2.2 Measurement of CTDI₁₀₀ in PMMA phantom

2.2.1 CTDI₁₀₀ in phantom

Purpose: To verification of Computed Tomography Dose Index (CTDI)

Method:

1. The CTDI₁₀₀ in head and body PMMA phantom by using a 100 mm pencil chamber place in each hole of 16(32) cm diameter PMMA phantom at the iso-center of C.T. bore.
2. Using head and body protocols.
3. The scan parameters were 100 mA, 1 sec scan time, 180 and 500 mm FOV for all measurements at each kVp setting of 80, 100, 120 and 135 in axial volume mode.
4. Record C.T. dose in unit of mGy.
5. Calculate CTDI_w and _nCTDI_w following

$$\text{CTDI}_w = 1/3 \text{ CTDI}_{100, \text{center}} + 2/3 \text{ CTDI}_{100, \text{periphery}}$$

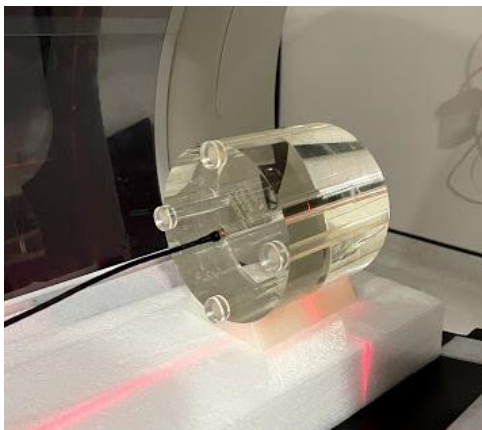


Figure B 9 CTDI₁₀₀ measurement in head PMMA phantoms using 100 mm. pencil ion chamber.

Table B 13 The measured CTDI₁₀₀ at each position of head phantom for each kVp, CTDI_w and _nCTDI_w in unit of mGy/mAs.

kVp	CTDI ₁₀₀ in head phantom (mGy)						
	At center	At peripheral				CTDI _w or C _w (mGy@100mAs)	_n CTDI _w or _n C _w (mGy/mAs)
		12 o'clock	3 o'clock	6 o'clock	9 o'clock		
80	0.72	0.92	0.88	0.73	1	10.3125	0.1031
100	1.38	1.74	1.59	1.3	1.68	18.8958	0.1889
120	2.21	2.70	2.4	2.12	2.65	29.7708	0.2977
135	3.4	3.7	3.5	3.2	3.8	43.7500	0.4375

Table B 14 The measured CTDI₁₀₀ at each position of body phantom for each kVp, CTDI_w and _nCTDI_w in unit of mGy/mAs.

kVp	CTDI ₁₀₀ in body phantom (mGy)						
	At center	At peripheral				CTDI _w or C _w (mGy@100mAs)	_n CTDI _w or _n C _w (mGy/mAs)
		12 o'clock	3 o'clock	6 o'clock	9 o'clock		
80	0.15	0.43	0.43	0.29	0.41	3.875	0.03875
100	0.34	0.82	0.80	0.54	0.80	7.6458	0.07645
120	0.93	1.4	1.32	1.15	1.54	15.1458	0.15145
135	1.33	1.97	1.85	1.59	2.0	20.9791	0.2097

2.2.2 CTDI_{vol} on monitor and calculated CTDI_w

Purpose: To compare the CTDI_{vol} displayed on CT monitor with calculated CTDI_w.

Method:

1. Determine the CTDI_w by using the results in Table B13 and B14.
2. The CTDI_{vol} displayed on CT monitor were recorded to compare percentage difference with the calculated values as shown in Table 5 for CTDI_{vol} in head phantom, and table 6 for CTDI_{vol} in body phantom.

Tolerance: The difference between measured CTDI_w and display should be less than $\pm 10\%$

Results:

Table B 15 CTDI_{vol} displayed on monitor and calculated CTDI_w using head techniques 100 mAs and 240 mm FOV, slice collimation 2x4 mm.

kVp	CTDI _{vol} in head phantom(mGy)		
	Calculated	Displayed	% Difference
80	10.3291	11.30	-8.98
100	18.8958	19.4	-2.63
120	29.7708	31	-4.05
135	43.7500	48	-9.26

Comment: Pass

Table B16 CTDI_{vol} displayed on monitor and calculated CTDI_w using body techniques 100 mAs and 240 mm FOV, slice collimation 2x4 mm.

kVp	CTDI _{vol} in head phantom(mGy)		
	Calculated	Displayed	% Difference
80	3.875	4.3	-10.39
100	7.6458	8.2	-6.99
120	15.1458	16.4	-7.95
135	20.9791	23.1	-9.62

Comment: Pass

Appendix C: Quality Control of MDCT system

1. MDCT system SIEMENS SOMATOM Sensation

Location: X-ray department at Praram9 Hospital Floor.2

Manufacturer: SIEMENS Model: SOMATOM Sensation 64 slice

Installed: 17 January 2013

Date: 4 April 2021

Pass	Scan Localization Light Accuracy
Pass	Alignment of Table to Gantry
Pass	Table Increment Accuracy
Pass	Slice Increment Accuracy
Pass	Reproducibility of CT Numbers
Pass	mAs Linearity
Pass	Linearity of CT Numbers
Pass	Accuracy of Distance Measurement
Pass	High Contrast Resolution
Pass	Low Contrast Detectability
Pass	Slice thickness accuracy
Pass	Image uniformity

1.1 Scan Localization Light Accuracy

Purpose: To test congruency of scan localization light and scan plane.

Method:

1. Place the tape measurement vertically along the midline the couch aligned with the longitudinal axis.
2. Set external light align with the reference point on the tape measurement.
3. Set table position to zero. Move table by monitor scanner, the table position move from external to internal localization light. Measure and record deviation position.

Tolerance: The center of the irradiation field from the pin pricks should be less than 2 mm

Results: Measured Deviation External50...mm Internal50...mm

Comment: Pass

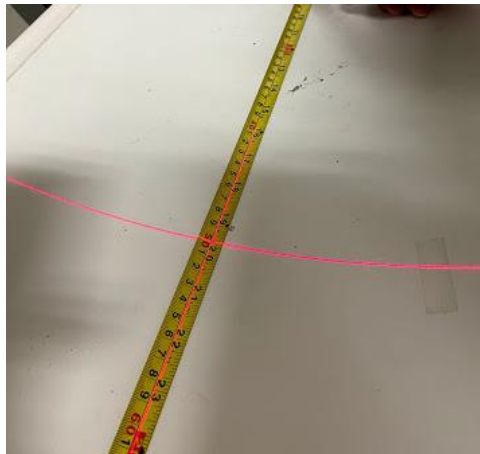


Figure C 1 Localization light accuracy setting on the tape measurement.

1.2 Alignment of Table to Gantry

Purpose: To ensure that long axis of the table is horizontally aligned with a vertical line passing through the rotational axis of the scanner.

Method:

1. Locate the table midline using a ruler and mark it on a tape affixed to the table. With the gantry untitled, extend the tabletop into gantry to tape position.
2. Measure the horizontal deviation between the gantry aperture center and the table midline.

Tolerance: The Deviation should be within 5 mm

Results:

Table C 1 Alignment of table to gantry

	Table	Bore
Distance from Right to Centre (mm)	347	347.5
Distance from Centre to Left (mm)	348	347.5
Measured Deviation	0.5	0

*Measured deviation = (Distance from right to center – Distance from center to Left)/2

Comment: Pass

1.3 Table increment Accuracy.

Purpose: To determine accuracy and reproducibility of table longitudinal motion.

Method:

1. Tape a measuring tape at the foot end of the table.
2. Place a paper clip at the center of the tape to function as an indicator.
3. Load the table uniformly with 150 lbs. From the initial position move the table 300, 400 and 500 mm.

4. Record the relative displacement of the pointer on the ruler. Reverse the direction of motion and repeat.
5. Repeat the measurements four times.

Tolerance: Positional errors should be less than 3 mm at 300 mm position.

Result:

Table C 2 Table increment Accuracy.

Indicated (mm)	Measured (mm)	Deviation (mm)
300	300	0
400	400	0
500	500	0
-300	-300	0
-400	-402	2
-500	-500	0

*Deviation = | Indicated – Measured|

Comment: Pass

1.4 Position dependence and S/N ratio of C.T. numbers

Method:

1. Position the C.T. head phantom centered in the gantry.
2. Using 1 cm slice thickness obtain one scan using typical head technique.
3. Select a circular region of interest of approximately 400 sq. mm.
4. Record the mean C.T. number and standard deviation for each of the positions 1 through 5.

Technique: 120 kV, 300 mA, 1 second, 250 mm. FOV

Tolerance: The coefficient of variation of mean CT numbers of the four scans should be less than 0.2.

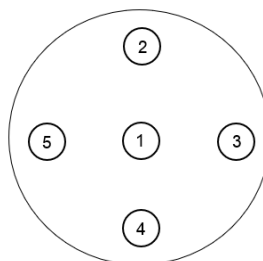


Figure C 2 Draw region of interest for each of the positions 1 through 5.

Results:

Table C 3 Position dependence and S/N ratio of C.T. numbers

Position	Mean C.T.	S.D.	C.V.
1	12.8	3.1	0.24
2	13.9	2.9	0.21
3	13.4	2.9	0.22
4	13.4	2.9	0.22
5	13.7	2.9	0.22

*CV = Standard deviation/mean CT number

Comment: Pass

1.5 Reproducibility of C.T. Numbers.

Method:

1. Using the same set up and technique as position dependence, obtain three scans.
2. Using the same ROI as position dependence in location 1, which is the center of the phantom, obtain mean C.T. numbers for each of the four scans

Tolerance: The coefficient of variation of mean C.T. numbers of the four scans should be less than 0.002

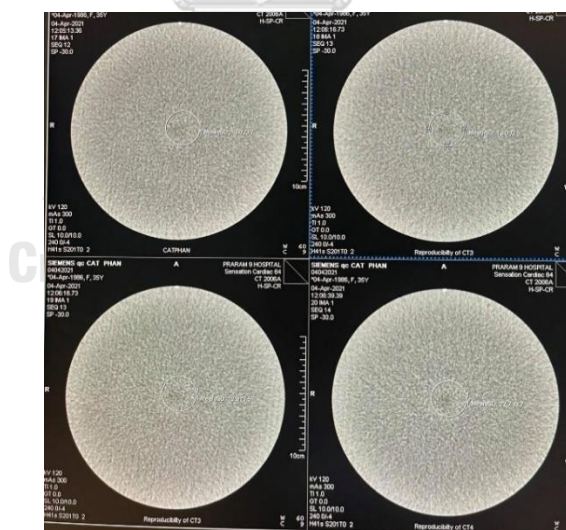


Figure C 3 Draw region of interest of the positions 5.

Results:**Table C 4** Reproducibility of C.T. numbers

Run Number	1	2	3	4
C. T Number	43	43	42.9	42.8
Mean Global C.T Number	42.93			
Standard Deviation	0.095			
Coefficient of variation	0.002			

Comment: Pass**1.6 mAs Linearity****Method:**

1. Set up the same as position dependence and insert 10 cm long pencil chamber in the center slot of the C.T. dose head phantom.
2. Select the same kVp and time as used for head scan. Obtain four scans in each of the mA stations normally used in the clinic. For each mA station record the exposure in mGy for each scan. Scans should be performed in the increasing order of mA. Compute mGy/mAs for each mA setting.

Technique: 120 kVp, 1 second, 240 mm. FOV, slice collimation 8 mm varying mA**Results:****Table C 5** mAs linearity

mA	Exposure in mGy				mGy/mAs	C.V.
	Run 1	Run 2	Run 3	Run 4		
50	0.55	0.5	0.63	0.49	0.01	
100	1.02	1.23	1.11	1.09	0.01	0.013
200	2.04	1.99	2.1	1.98	0.01	0.046
250	2.56	2.49	2.53	2.5	0.01	0.003
300	3.08	3.04	3.1	3.06	0.01	0.008
400	4.13	4.1	3.97	4.2	0.01	0.001
500	5.6	5.68	5.7	5.83	0.01	0.053

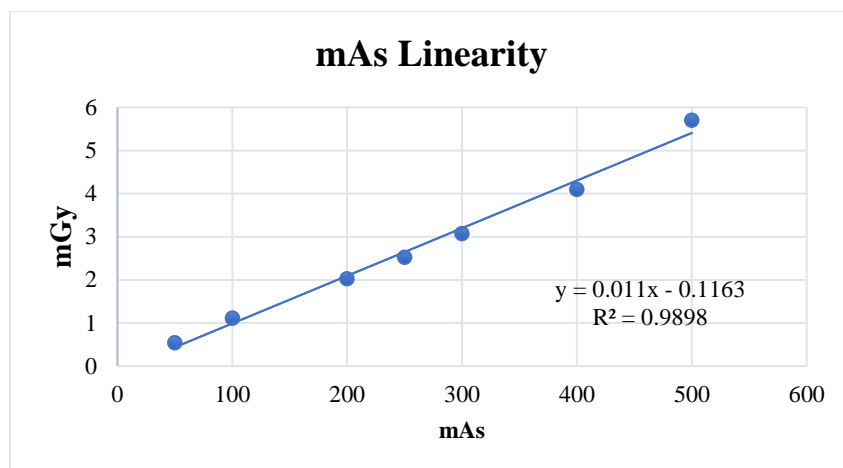


Figure C 4 The relationship of mGy and mAs.

Comment: Pass

1.7 Linearity of C.T. Numbers

Method:

- 1 Set up the Catphan phantom as described in beam alignment.
- 2 Select the section containing the test objects of different C.T. numbers.
- 3 Select the head technique and perform a single transverse scan.
- 4 Select a region of interest (ROI) of sufficient size to cover the test objects.
- 5 Place the ROI in the middle of each test object and record the mean C.T. number.

Technique: 120 kVp 300 mA 1.0 sec, FOV 240 mm, Slice thickness 8 mm

Tolerance: R-square between measured CT number and linear attenuation coefficient (μ) more than 0.9

Results:

Table C 6 Linearity of CT Number

Material	Expected CT Number	Measured CT Number
Air (Superior)	-1000	-1022.2
Air (Inferior)	-1000	-1008.3
PMP	-200	-185.5
LDPE	-100	-93.7
Polystyrene	-35	-36
Acrylic	120	121
Delrin™	340	353.38
Teflon	990	999.40

1.8 Slice thickness accuracy

Purpose: To Determine the accuracy of the slice thickness.

Method:

1. Set up the Catphan phantom as described in beam alignment set up as you would for beam profile measurement.
2. Select the section containing the accuracy of the slice thickness test objects (CTP672)
3. Select the head technique, 120 kVp, 300 mAs, smallest slit width.
4. Perform several scans with different programmed slice thicknesses under auto control.
5. Perform scan following Catphan manual in each slice collimation.
6. Calculate the real slice thickness.

Tolerance: Deviation should be $< 1\text{mm}$

Result:

Table C 7 Slice thickness accuracy

Slice thickness (mm)	1	4	8
Peak	200.4	129.3	92.2
BG	58	59.2	59
Net peak (NP)	142.4	70.1	33.2
50% NP	71.2	35.05	16.59
HM (50%NP+BG)	129.2	94.25	75.6
FWHM L1	0.78	1.10	2.40
FWHM L2	0.82	1.17	2.42
FWHM L3	0.79	1.20	2.51
FWHM L4	0.71	1.11	2.45
Average FWHM	0.78	1.15	2.45
SL=Avg FWHMx0.42	0.33 cm	0.48 cm	1.10 cm
Calculated Slice thickness (mm)	3.3	4.8	11.0

Slice Thick in mm	Measured Thick in mm	Deviation (mm)
3	3.3	0.3
5	4.8	0.2
10	11	1

*Deviation = |Slice thickness – Measured thickness|

Comment: Pass

1.9 High Contrast Resolution

Purpose: To test resolution sections ranging from 1 to 21 lines pairs per cm. This radial design pattern eliminates the possibility of streaking artifacts from other test objects.

Method:

1. Set up the Catphan phantom in beam alignment.
2. Select the section containing the high-resolution test object (CTP714 line pair high resolution Module).
3. Select the head technique and perform a single transverse scan.
4. Select the area containing the high-resolution test objects.
5. Select appropriate window and level for the best visualization of the test objects.

Technique: kVp: 120 mA: 300Seconds: 1.0 FOV: 300 mm Slice

Technique: 120kVp, 300mA, 1.0 sec, FOV 240 mm

Tolerance: > 5 lp/cm visible

Table C 8 High contrast resolution

Slice Thickness in mm	Resolution	Gap size
3 mm	8-line pair/cm	0.063 cm
5 mm	8-line pair/cm	0.063 cm
10 mm	8-line pair/cm	0.063 cm

Comment: Pass

1.10 Low contrast resolution

Purpose: To determine the actual target contrasts before testing specific contrast performance specifications.

Method:

1. Set up the Catphan 700 phantom in beam alignment.
2. Select the section containing the low-resolution test object CTP515 Sub-slice and supra-slice low contrast Module).
3. Select the head technique and perform a single transverse scan.
4. Select the area containing the low-resolution test objects.
5. Select appropriate window and level for the best visualization of the test objects.
6. Record the smallest test object visualized.

Technique: 120 kVp, 300 mA, 1.0 sec, FOV 240 mm slice collimation 8 mm.

Tolerance: should see 4 spokes at Supra- slice 0.5% nominal target contrast level

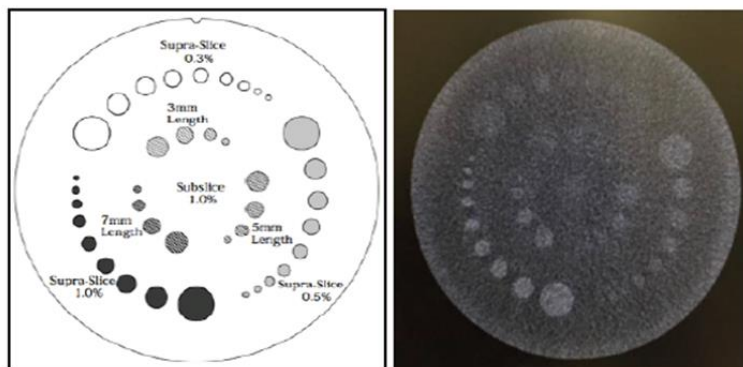


Figure C 5 Low contrast detectability

Result:

Table C 9 Low contrast resolution

Slice thickness in mm	Smallest target(spokes) diameter (mm) should be seen					
	Contrast level of supra-slice			Length of sub-slice 1.0%		
	1.00%	0.50%	0.30%	7 mm	5 mm	3 mm
1	7	5	2	2	2	1
5	8	6	2	3	2.5	1
10	8	6	2	3	2.5	1

Comment: Pass

1.11 Image uniformity

Method:

1. Set up the Catphan phantom as described in beam alignment.
2. Select the CTP712 image uniformity module.
3. Select the head technique and perform a single transverse scan.
4. Select a region of interest (ROI) of sufficient size to cover the test objects.
5. Place the ROI in the middle of each test object and record the mean C.T. number

Technique: 120kVp, 300 mA, 1sec, 250mm FOV, slice collimation 1 mm

Tolerance: Less than 5 HU

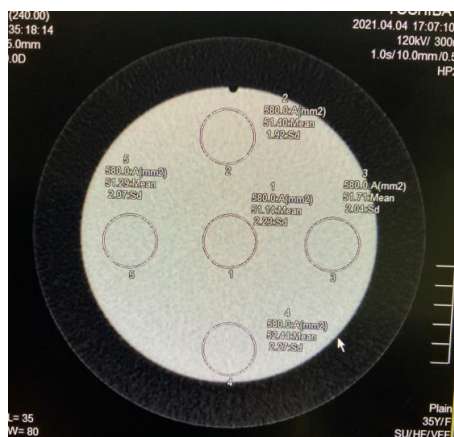


Figure C 6 Image Uniformity

Results:

Table C 10 Image uniformity

Position	Mean C.T Number	S.D.	Difference (HU)
1	12.8	3.1	
2	13.9	2.9	1.1
3	13.4	2.9	1.4
4	13.4	2.9	0.6
5	13.7	2.9	0.9

Different = |CT number center – CT number peripheral|

Comment: Pass

2.Verification of Computed Tomography Dose Index (CTDI)

2.1. Measurement CTDI₁₀₀ in air (C_{air} or CTDI_{air})

CTDI₁₀₀ in air was measured using 100 mm pencil ion chamber set at the isocenter of the CT bore. The scan parameters were 100 mA tube current, 1 sec scan time and small focal spot size setting for all measurements at tube potential setting of 80, 100, 120 and 135. The results of CTDI₁₀₀ measurement are shown as in Table 4.11.

Table C 11 The measured Ca,100 in air for head protocols for each kVp and slice collimations.

kVp	CTDI ₁₀₀ (mGy) in air in Head protocol		
	Slice Collimation 10 mm		
	run1	run2	run3
80	0.45	0.45	0.45
100	0.92	0.91	0.92
120	1.54	1.53	1.54
140	2.42	2.43	2.43

CTDI₁₀₀ in air using head techniques 100 mAs, 240 mm.FOV all Slice Collimations are plotted in Figure B 7, B 8

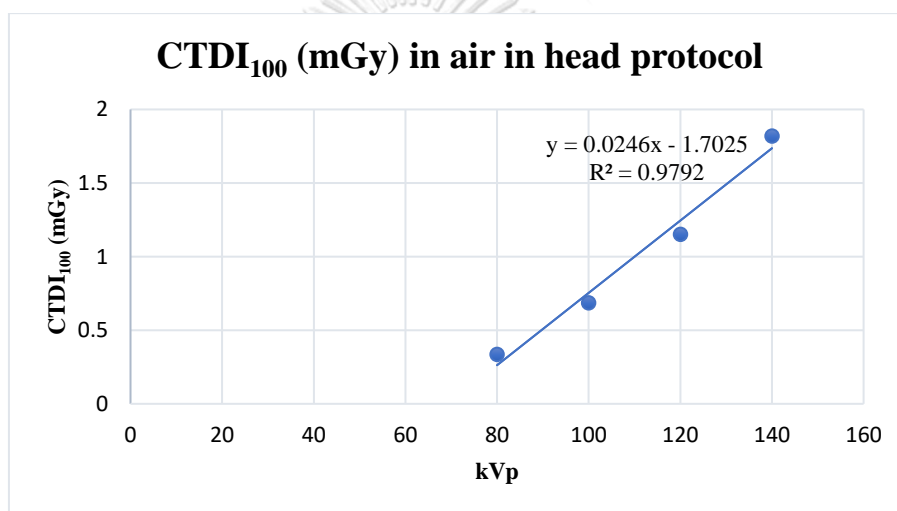


Figure C 7 CTDI₁₀₀ in air, head protocol as the function of kVp and slice collimation are plotted in blue, orange, gray, and violet colors at kVp of 80, 100, 120 and 135, respectively.

Table C 12 The measured CTDI₁₀₀ in air for body protocol for each kVp and slice collimation.

kVp	CTDI ₁₀₀ (mGy) in air in body protocol		
	Slice Collimation 10 mm		
	run1	run2	run3
80	0.50	0.51	0.51
100	0.92	0.91	0.93
120	1.54	1.54	1.55
150	2.42	2.43	2.42

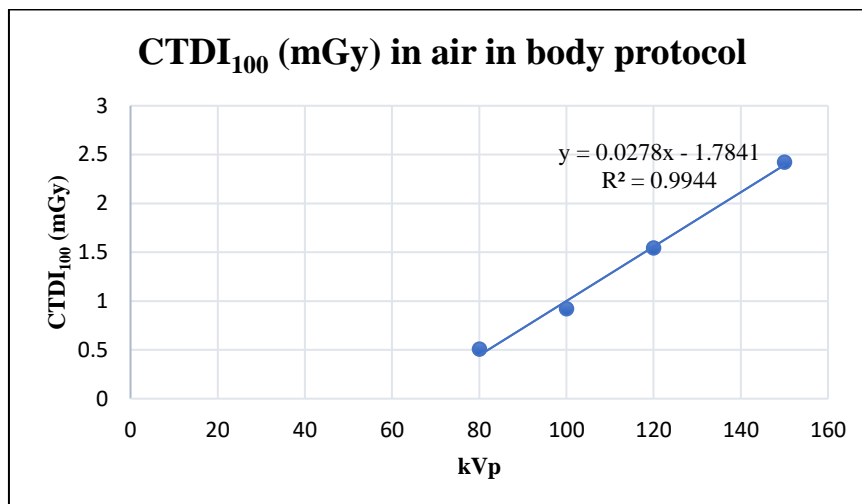


Figure C 8 CTDI₁₀₀ in air, body protocol as the function of kVp and slice collimation are plotted in blue, orange, gray, and violet colors at kVp of 80, 100, 120 and 135, respectively.

2.2 Measurement of CTDI₁₀₀ in PMMA phantom

2.2.1 CTDI₁₀₀ in phantom

Purpose: To verification of Computed Tomography Dose Index (CTDI)

Method:

1. The CTDI₁₀₀ in head and body PMMA phantom by using a 100 mm pencil chamber place in each hole of 16(32) cm diameter PMMA phantom at the iso-center of C.T. bore.
2. Using head and body protocols.
3. The scan parameters were 100 mA, 1 sec scan time, 180 and 500 mm FOV for all measurements at each kVp setting of 80, 100, 120 and 135 in axial volume mode.
4. Record C.T. dose in unit of mGy.
5. Calculate C_w and _nC_w following

$$CTDI_w = 1/3 CTDI_{100, \text{center}} + 2/3 CTDI_{100, \text{periphery}}$$

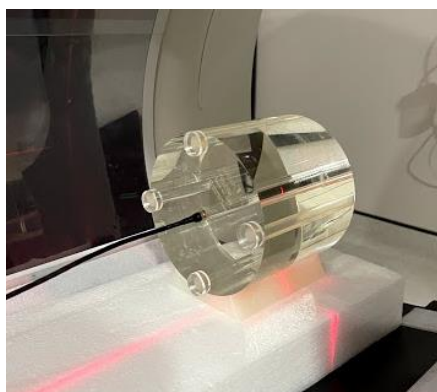


Figure C 9 CTDI₁₀₀ measurement in head PMMA phantoms using 100 mm. pencil ion chamber.

Table C 13 The measured CTDI₁₀₀ at each position of head phantom for each kVp, CTDI_w and _nCTDI_w in unit of mGy/mAs.

kVp	CTDI ₁₀₀ in head phantom (mGy)						
	At center	At peripheral				CTDI _w or C _w (mGy@100mAs)	_n CTDI _w or _n C _w (mGy/mAs)
		12o'clock	3 o'clock	6 o'clock	9 o'clock		
120	1.11	1.25	1.20	1.06	1.18	11.5166	0.1151

Table C 14 The measured CTDI₁₀₀ at each position of body phantom for each kVp, CTDI_w and _nCTDI_w in unit of mGy/mAs.

kVp	CTDI ₁₀₀ in body phantom (mGy)						
	At center	At peripheral				CTDI _w or C _w (mGy@100mAs)	_n CTDI _w or _n C _w (mGy/mAs)
		12o'clock	3 o'clock	6 o'clock	9 o'clock		
120	0.32	0.66	0.63	0.55	0.60	5.1166	0.05116

2.2.2 CTDI_{vol} on monitor and calculated CTDI_w

Purpose: To compare the CTDI_{vol} displayed on CT monitor with calculated CTDI_w.

Method:

1. Determine the CTDI_w by using the results in Table B 13 and B 14.
2. The CTDI_{vol} displayed on CT monitor were recorded to compare percentage difference with the calculated values as shown in Table B 15 for CTDI_{vol} in head phantom.

and Table B 16 for CTDI_{vol} in body phantom.

Tolerance: The difference between measured CTDI_w and display should be less than $\pm 10\%$

Results:

Table C 15 CTDI_{vol} displayed on monitor and calculated CTDI_w using head techniques 100 mAs and 240 mm FOV, slice collimation 10 mm.

kVp	CTDI _{vol} in head phantom(mGy)		
	Calculated	Displayed	% Difference
120	11.5166	12.12	-5.10

Comment: Pass

Table C 16 CTDI_{vol} displayed on monitor and calculated CTDI_w using body techniques 100 mAs and 240 mm FOV, slice collimation 10 mm.

kVp	CTDI _{vol} in head phantom(mGy)		
	Calculated	Displayed	% Difference
120	5.1166	5.112	0.09

Comment: Pass

Appendix D: The Approval of Institutional Review Board



COA No. 875/2020

IRB No. 455/63

INSTITUTIONAL REVIEW BOARD

Faculty of Medicine, Chulalongkorn University

1873 Rama 4 Road, Patumwan, Bangkok 10330, Thailand, Tel 662-256-4493

Certificate of Approval

The Institutional Review Board of the Faculty of Medicine, Chulalongkorn University, Bangkok, Thailand, has approved the following study which is to be carried out in compliance with the International guidelines for human research protection as Declaration of Helsinki, The Belmont Report, CIOMS Guideline and International Conference on Harmonization in Good Clinical Practice (ICH-GCP)

Study Title : Patient-specific organ dose calculated by dose tracking software based on Monte Carlo simulation in pediatric abdominal CT

Study Code : -

Principal Investigator : Miss Yuparak Innan

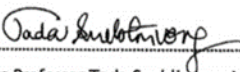
Affiliation of PI : Department of Radiology,
Faculty of Medicine, Chulalongkorn University.


Review Method : Expedited

Continuing Report : At least once annually or submit the final report if finished.

Document Reviewed :

1. Research Proposal Version 2 Date 6 July 2020
2. Protocol Synopsis Version 2 Date 6 July 2020
3. Case record form Version 2 Date 6 July 2020
4. Curriculum Vitae and GCP Training
 - Miss Yuparak Innan
 - Assist.Prof. Kitiwat Khamwan, Ph.D.

Signature 
(Emeritus Professor Tada Sueblinvong MD)
Chairperson
The Institutional Review Board

Signature 
(Associate Professor Supeecha Wittayalerpanya)
Member and Assistant Secretary, Acting Secretary
The Institutional Review Board

Date of Approval : July 13, 2020

Approval Expire Date : July 12, 2021

Approval granted is subject to the following conditions: (see back of this Certificate)

All approved investigators must comply with the following conditions:

1. Strictly conduct the research as required by the protocol;
2. Use only the information sheet, consent form (and recruitment materials, if any), interview outlines and/or questionnaires bearing the Institutional Review Board's seal of approval ; and return one copy of such documents of the first subject recruited to the Institutional Review Board (IRB) for the record;
3. Report to the Institutional Review Board any serious adverse event or any changes in the research activity within five working days;
4. Provide reports to the Institutional Review Board concerning the progress of the research upon the specified period of time or when requested;
5. If the study cannot be finished within the expire date of the approval certificate, the investigator is obliged to reapply for approval at least one month before the date of expiration.
6. If the research project is completed, the researcher must be form the Faculty of Medicine, Chulalongkorn University.

* A list of the Institutional Review Board members (names and positions) present at the meeting of Institutional Review Board on the date of approval of this study has been attached. All approved documents will be forwarded to the principal investigator.



COA No. 875/2020

IRB No. 455/63

คณะกรรมการพิจารณาจริยธรรมการวิจัย

คณะแพทยศาสตร์ จุฬาลงกรณ์มหาวิทยาลัย

1873 ถ.พระราม 4 เขตปทุมวัน กรุงเทพฯ 10330 โทร. 0-2256-4493

เอกสารรับรองโครงการวิจัย

คณะกรรมการจริยธรรมการวิจัยในคน คณะแพทยศาสตร์ จุฬาลงกรณ์มหาวิทยาลัย ดำเนินการให้การรับรองโครงการวิจัยตามแนวทางหลักจริยธรรมการวิจัยในคนที่เป็นมาตรฐานสากลได้แก่ Declaration of Helsinki, The Belmont Report, CIOMS Guideline และ International Conference on Harmonization in Good Clinical Practice หรือ ICH-GCP

ชื่อโครงการ : การคำนวณปริมาณรังสีจำเพาะต่ออวัยวะด้วยวิธีมอนติคาร์โลจากโปรแกรมติดตามปริมาณรังสีในการตรวจเอกซเรย์คอมพิวเตอร์ช่องท้องของผู้ป่วยเด็ก

เลขที่โครงการวิจัย : -

ผู้วิจัยหลัก : นางสาวยุพารักษ์ อินแนน

สังกัดหน่วยงาน : ภาควิชารังสีวิทยา คณะแพทยศาสตร์ จุฬาลงกรณ์มหาวิทยาลัย

วิธีบทวน : แบบเร่งด่วน

รายงานความก้าวหน้า : ส่งรายงานความก้าวหน้าอย่างน้อย 1 ครั้ง/ปี หรือส่งรายงานฉบับสมบูรณ์หากดำเนินการโครงการเสร็จสิ้นก่อน 1 ปี

เอกสารรับรอง

1. โครงร่างการวิจัย Version 2 Date 6 July 2020
2. โครงการวิจัยฉบับย่อ Version 2 Date 6 July 2020
3. Case record form Version 2 Date 6 July 2020
4. Curriculum Vitae and GCP Training
 - Miss Yuparak Innan
 - Assist.Prof. Kitiwat Khamwan, Ph.D.

ลงนาม

(ศาสตราจารย์กิตติคุณแพทย์หญิงชดาศ สืบหลินวงศ์)

ประธาน

คณะกรรมการพิจารณาจริยธรรมการวิจัย

วันที่รับรอง : 13 กรกฎาคม 2563

วันหมดอายุ : 12 กรกฎาคม 2564

ลงนาม

(รศ.สุพิชา วิทย์เลิศปัญญา)

กรรมการและผู้ช่วยเลขานุการปฏิบัติหน้าที่แทน
เลขานุการคณะกรรมการพิจารณาจริยธรรมการวิจัย

ทั้งนี้ การรับรองนี้มีเงื่อนไขดังที่ระบุไว้ด้านหลังทุกข้อ (ดูด้านหลังของเอกสารรับรองโครงการวิจัย)

นักวิจัยทุกท่านที่ผ่านการรับรองจริยธรรมการวิจัยต้องปฏิบัติดังต่อไปนี้

1. ดำเนินการวิจัยตามที่ระบุไว้ในโครงร่างการวิจัยอย่างเคร่งครัด
2. ใช้เอกสารแนะนำอาสาสมัคร ใบยินยอม (และเอกสารเชิญเข้าร่วมวิจัยหรือใบโฆษณาถ้ามี) แบบสัมภาษณ์ และหรือ แบบสอบถาม เฉพาะที่มีตราประทับของคณะกรรมการพิจารณาจริยธรรมเท่านั้น และส่งสำเนาเอกสารดังกล่าวให้กับผู้เข้าร่วมวิจัยจริงรายแรกมาที่ฝ่ายวิจัย คณะแพทยศาสตร์ เพื่อเก็บไว้เป็นหลักฐาน
3. รายงานเหตุการณ์ไม่พึงประสงค์ร้ายแรงที่เกิดขึ้นหรือการเปลี่ยนแปลงกิจกรรมวิจัยใดๆ ต่อคณะกรรมการพิจารณาจริยธรรมการวิจัย ภายใน 5 วันทำการ
4. ส่งรายงานความก้าวหน้าต่อคณะกรรมการพิจารณาจริยธรรมการวิจัย ตามเวลาที่กำหนดหรือเมื่อได้รับการร้องขอ
5. หากการวิจัยไม่สามารถดำเนินการเสร็จสิ้นภายในกำหนด ผู้วิจัยต้องยื่นขออนุมัติใหม่ก่อน อย่างน้อย 1 เดือน
6. หากการวิจัยเสร็จสมบูรณ์ ผู้วิจัยต้องแจ้งปิดโครงการตามแบบฟอร์มของคณะแพทยศาสตร์ จุฬาลงกรณ์มหาวิทยาลัย

* รายชื่อของคณะกรรมการจริยธรรมการวิจัยในคน (ชื่อและตำแหน่ง) ที่อยู่ในที่ประชุมวันที่รับรองโครงการวิจัยได้แนบมาด้วย เอกสารที่รับรองทั้งหมดจะถูกส่งไปยังผู้วิจัยหลัก



ที่อา 64.13 5829

คณะแพทยศาสตร์ จุฬาลงกรณ์มหาวิทยาลัย
ถนนพระรามที่ 4 เขตปทุมวัน
กรุงเทพฯ 10330

11 สิงหาคม 2563

เรื่อง ขออนุญาตเก็บรวบรวมข้อมูลเพื่อทำวิทยานิพนธ์

เรียน กรรมการผู้อำนวยการ โรงพยาบาลพระรามเก้า

- สิ่งที่ส่งมาด้วย 1. โครงร่างวิทยานิพนธ์ฉบับเต็ม, โครงร่างวิทยานิพนธ์ฉบับย่อ, Case Record Form และ CV
2. สำเนาเอกสารรับรองโครงการวิจัย จากคณะกรรมการพิจารณาจริยธรรมการวิจัยในมนุษย์
คณะแพทยศาสตร์ จุฬาลงกรณ์มหาวิทยาลัย

เนื่องด้วย นางสาวภากรภรณ์ อินแนน ตำแหน่งนักรังสีเทคนิคผู้เชี่ยวชาญพิเศษ แผนกเอกซเรย์ โรงพยาบาลพระรามเก้า ซึ่งเป็นบุคลากรในสังกัดของท่าน ปัจจุบันกำลังศึกษาในหลักสูตรวิทยาศาสตรมหาบัณฑิต สาขาวิชาฟิสิกส์การแพทย์ ชั้นปีที่ 2 ภาควิชารังสีวิทยา คณะแพทยศาสตร์ จุฬาลงกรณ์มหาวิทยาลัย มีความประสงค์จะทำวิทยานิพนธ์ เรื่อง การคำนวณปริมาณรังสีจำเพาะต่ออวัยวะด้วยวิธีมอนติคาร์โล จากโปรแกรมติดตามปริมาณรังสี ในการตรวจเอกซเรย์คอมพิวเตอร์ช่องท้องของผู้ป่วยเด็ก (Patient-specific organ dose calculated by dose tracking software based on Monte Carlo simulation in pediatric abdominal CT) โดยมี ผศ.ดร.กิตติวัฒน์ คำวัน เป็นอาจารย์ที่ปรึกษาวิทยานิพนธ์ และมีวัตถุประสงค์เพื่อประเมินค่าปริมาณรังสีจำเพาะต่ออวัยวะจากการคำนวณโดยซอฟต์แวร์ติดตามปริมาณรังสีของผู้ป่วยโดยใช้การจำลองแบบมอนติคาร์โลในการตรวจวินิจฉัยเอกซเรย์คอมพิวเตอร์ช่องท้องในผู้ป่วยเด็กมีค่าเท่าใด จะขออนุญาตเก็บรวบรวมข้อมูลผู้ป่วยที่แผนกเอกซเรย์ โรงพยาบาลพระรามเก้า ตั้งแต่ เดือน มกราคม พ.ศ. 2560 ถึง เดือนพฤษภาคม พ.ศ. 2563 ซึ่งวิทยานิพนธ์เรื่องนี้ได้ผ่านการรับรองจากคณะกรรมการพิจารณาจริยธรรมการวิจัย คณะแพทยศาสตร์ จุฬาลงกรณ์มหาวิทยาลัย เรียบร้อยแล้ว และได้แนบสำเนาเอกสารดังกล่าวมาให้ด้วยแล้ว

ในการนี้ คณะแพทยศาสตร์ จุฬาลงกรณ์มหาวิทยาลัย จึงขอความอนุเคราะห์ให้หนังสือดังกล่าว ไปเก็บรวบรวมข้อมูลเพื่อทำวิทยานิพนธ์ที่โรงพยาบาลพระรามเก้า และหลังจากจบการศึกษาแล้ว จะขอมอบวิทยานิพนธ์นี้เพื่อใช้ประโยชน์ในองค์กรของท่าน จำนวน 1 เล่ม ซึ่งการศึกษานี้จะไม่นำชื่อและข้อมูลส่วนตัวของผู้ป่วยไปวิเคราะห์หรือเผยแพร่โดยเด็ดขาด

จึงเรียนมาเพื่อโปรดพิจารณาอนุมัติ และดำเนินการต่อไปด้วย จักเป็นพระคุณยิ่ง

ขอแสดงความนับถือ

(ศาสตราจารย์ นายแพทย์สุเทพ กลชาญวิทย์)

รองคณบดีฝ่ายบัณฑิตศึกษา

ปฏิบัติการแทนคณบดี

ภาควิชารังสีวิทยา คณะแพทยศาสตร์ จุฬาฯ
โทรศัพท์ 02-2564000 ต่อ 60848

VITA

NAME Yuparak Innan

DATE OF BIRTH 15 February 1986

PLACE OF BIRTH Phetchabun, Thailand

HOME ADDRESS 890/463 LPN Park Rama9-Ratchada, Chaturathit Rd.,
Huai Khwang, Bangkok, Thailand, 10310

PUBLICATION Innan Y, Khamwan k, Patient-specific organ dose
calculated using dose tracking software based on Monte
Carlo simulation in pediatric abdominal CT. Proceeding of
the 20th AOCMP & 18th SEACOMP, Phuket, Thailand.,
2020

